Doctoral Dissertation (Shinshu University)

Study on the dynamic behavior of stimulus-responsive hydrogel microspheres by means of nanoscale visualization

(ナノスケール可視化技術による刺激応答性ハイドロゲル微粒子の動的挙動に関する研究)

March 2019

Shusuke Matsui

Graduate School of Textile Science & Technology

Table of Contents

3. Chapter II

"Monitoring the thermoresponsive behavior of individual microgels"

3.1. Introduction

3.2. Experimental section

3.3. Results and discussion

3.3.1. Synthesis and characterization of thermoresponsive microgels

3.3.2. Observation of the thermoresponsive behavior of microgels using HS-AFM

3.3.3. Relationship between the height of the microgels on the substrate and D_h

3.3.4. Magnified time-lapse HS-AFM images of an individual N5 microgel

3.4. Conclusions

3.5. References

4. Chapter III

"Development of fast-driven autonomously oscillating microgels"

4.1. Introduction

4.2. Experimental section

4.3. Results and discussion

4.3.1. Synthesis of poly(NIPAm-*co*-AAm-*co*-Ru(bpy)$_3$) microgels

4.3.2. Evaluation of the critical flocculation temperature of microgels

4.3.3. Optimization of the BZ reaction conditions

4.3.4. Characterization of oscillation waveforms

4.3.5. Arrhenius dependence of the oscillation frequency

4.3.6. Preparation of fast-oscillating macrogels

5. Summary

6. Acknowledgements

1. Introductory remarks

1.1. Background

"Stimulus-responsiveness" is an essential feature for the development of advanced functional materials that exhibit desired functions at specific times. In particular, in nature, living organisms have evolved advanced systems to flexibly adapt to the external environment through such stimulus-responsiveness.[1–4] Inspired by these natural systems, the development of stimulus-responsive artificial materials has rapidly progressed.[1–16] Stimulus-responsive materials show dramatic changes in their structure/shape and physicochemical properties in response to changes in the environment, and hence, they are referred to as "intelligent materials" or "smart materials".[4–16] Until now, a wide variety of stimulus-responsive or smart materials have been developed based on e.g. metal alloys or inorganic compounds, carbon, and polymers.[16,17] In the context of "hard matter", such as metal alloys or inorganic compounds, shape-memory alloys and ceramics have been extensively used to fabricate actuators.[17] On the other hand, in terms of "soft matter", polymer-based materials, hydrogels, shape-memory polymers, and liquid crystal elastomers have been extensively developed owing to their broad advantages, such as good elasticity, light weight, low cost, and high transparency.[17] In particular, polymeric hydrogels have received much attention owing to the significant tunability of their physicochemical properties in response to a variety of stimuli.[4] The key factors and requirements for stimulus-responsive materials are for the changes to be fast, reversible, complex, and robust in response to the external stimuli.[4] The response speed of hydrogels is dominated by their dimensions, and thus they may show slow response rates arising from limited water diffusion into or out of the hydrogel network,[4] as described by the Tanaka–

Fillmore equation.[18]

By downsizing hydrogels to the colloidal size scale, they can be stably dispersed in water while exhibiting behavior that is distinctly different from that of the corresponding bulk hydrogel.[19] Hydrogel microspheres (microgels) are stimulus-responsive materials with great potential to fulfill the aforementioned requirements. Microgels are very soft colloidal microspheres composed of cross-linked hydrophilic polymer networks that are swollen in aqueous media, with typical sizes in the range from several tens of nanometers to several micrometers.[19–31] In contrast to bulk hydrogels, microgels exhibit rapid stimulus-responsiveness, i.e., their physicochemical properties such as hydrophilicity/hydrophobicity and surface-charge density can be quickly tuned by applying external stimuli such as e.g. changes in temperature or pH value, biomolecular interactions, or irradiation with light.[19–21,24–33] Poly(*N*-isopropyl acrylamide) (pNIPAm) microgels (or other acrylamide-derived microgels) exhibit a volume phase transition temperature (VPTT) in pure water resulting from the lower critical solution temperature (LCST) of the polymer chain.[20–23] PNIPAm-based microgels can be synthesized by aqueous free-radical precipitation polymerization, resulting in microgels with uniform size.[20,21] In addition, by adding surfactants or suitable co-monomers, the size, surface charge density, and charge distribution of the microgels can be fine-tuned.[34–37] Furthermore, multi-responsive microgels can be obtained by co-polymerization of functional co-monomers, i.e., by introducing pH-responsive, biomolecular-responsive,[38] or photo-responsive moieties in the microgels.[39] Based on these many advantages, pNIPAm-based microgels have been extensively investigated not only as model systems for crystals and glasses in fundamental colloid research,[38–42] but also for potential applications in e.g. molecular separations, drug-delivery carriers, sensors, and actuators.[43–50]

In contrast to the aforementioned external stimulus-responsive microgels, Suzuki et al. have developed “autonomously oscillating microgels” as a new class of stimulus-responsive microgels that show periodical and reversible changes in size and assembly state following a chemical redox oscillation, i.e., the Belousov–Zhabotinsky (BZ) reaction,[53–55] within the microgels.[56–64] Ruthenium(II) (4-vinyl-4’-methyl-2,2’-bipyridine)bis(2,2’-bipyridine)bis(hexafluorophosphate) ($Ru(bpy)_3$), which is the metal catalyst for the BZ reaction, is covalently bound to a thermoresponsive microgel such as the pNIPAm main chain.[56–64] As the BZ reaction proceeds, the volume or colloidal stability of the microgels changes periodically under the redox oscillation of $Ru(bpy)_3$ in the absence of any external stimulus.[56] Up to now, control

over such oscillatory behavior[56] and the effects of the cross-linking density,[57] initial substrate concentration,[58] viscosity changes,[59,60] introduction of a core–shell structure,[61] and the construction of oscillating soft autonomously actuators[62] have been investigated. Therefore, autonomously oscillating microgels present great potential as the next generation of stimulus-responsive nanomaterials.

As mentioned above, microgels are swollen in water and dispersed in aqueous media, and thus, they exhibit dynamic functions at the nanoscale in aqueous solution. Therefore, the evaluation and understanding of the dynamic properties of microgels in aqueous solution are essential for the further development of novel smart materials. So far, the structure and physical properties of microgels have been evaluated by ensemble techniques such as scattering methods,[65–87] spectroscopy,[88–113] calorimetry,[114–120] sensors[121–130] (**Table 1.1**). Scattering techniques allow the quantitative determination of the size and internal structure of water-swollen microgels, and are thus frequently used. In particular, small-angle X-ray (SAXS) or neutron scattering (SANS) methods are suitable for the investigation of the internal nanoscopic structure of microgels in aqueous solution. However, the obtained data provide "static" information. In contrast, "time-resolved" techniques are powerful methods to evaluate dynamic structural changes in microgels with high temporal resolution. In this context, time-resolved SAXS is able to monitor microgel-to-particle transition processes with high temporal resolution.[79] This transition is a two-stage process, where very fast collapsed clusters form at the periphery, leading to hollowish core–shell structures that slowly transform into globules.[79]

Spectroscopy is usually used to analyze the properties of microgels, including e.g. the structure, phase transition behavior, and molecular uptake behavior.[88–113] For instance, the combination of UV-vis spectroscopy and a stopped-flow instrument allows the detection of phase-transition kinetics of the order of milliseconds.[91,93] Dielectric spectroscopy is able to detect dipole and charge motions within microgels and also to determine the structural and dynamic properties of polymers.[110–113] It has been reported that the swelling ability and dehydration dynamics are affected by the charge and cross-linking density distributions in the microgels,[110] where two-phase transition processes exist, i.e., colloidal crystal-to-liquid transitions.[113]

Differential scanning calorimetry (DSC) has been widely employed to characterize swelling in pNIPAm gels by detecting endothermic or exothermic events induced by phase transitions,[21,114–117] while isothermal titration calorimetry (ITC) has been applied to determine the

thermo-dynamical parameters of protein binding on colloidal microspheres.[118–120] Surface plasmon resonance (SPR) or quartz crystal microbalance (QCM) techniques can be used to monitor the phase transition dynamics of microgels coated on a substrate in real time.[121–130] Li et al. have investigated the phase-transition behavior of p(NIPAm-*co*-acrylic acid) microgel assemblies coated on an Au electrode via quartz-crystal microbalance with dissipation (QCM-D) measurements.[130] They revealed that the changes in the solution temperature and pH value depend dramatically on the viscosity of the microgels, the water content in the microgel network, and the Au overlayer.[130]

Table 1.1. Classification of ensemble techniques for the evaluation of microgels

Classification	Technique	Information	References
Scattering	Dynamic light scattering (DLS)	Hydrodynamic diameter	66, 68, 69, 71, 72, 74, 75, 76, 77, 82
	Electrophoretic light scattering (ELS)	Electrophoretic mobility	77, 83, 84, 85, 86, 87
	Static light scattering (SLS)	Radius of gyration	80, 81, 82
	Small-angle neutron scattering (SANS)	Scattering intensity	65, 66, 67, 68, 69, 70, 71, 72, 74, 75, 76
	Small-angle X-ray scattering (SAXS)	Scattering intensity	67, 73, 74, 77, 78, 79
Spectroscopy	UV-vis spectroscopy	Optical transmittance	88, 89, 90, 91, 92, 93
	Fluorescent spectroscopy	Fluorescent intensity	94, 95, 96, 97, 98
	Nuclear magnetic resonance (NMR) spectroscopy	NMR spectra	99, 100, 101
	Infrared (IR) spectroscopy	Absorption spectrum	102, 103, 104, 105
	X-ray photoelectron spectroscopy (XPS)	Photoelectron energy	106, 107, 108, 109
	Dielectric spectroscopy	Dielectric relaxation	110, 111, 112, 113
Calorimetry	Differential scanning calorimetry (DSC)	Exothermic/Endothermic	114, 115, 116, 117
	Isothermal titration calorimetry (ITC)	Exothermic/Endothermic	118, 119,120
Sensors	Surface plasmon resonance (SPR)	Dielectric Refractive index	121, 122, 123, 124
	Quartz crystal microbalance (QCM)	Resonant frequency	121, 125, 126, 127, 128, 129, 130

Although these ensemble techniques present advantages by providing ensemble-averaged information of the system, the distribution and inhomogeneities in individual samples are always averaged. However, microgels synthesized by free-radical precipitation polymerization present an inhomogeneous internal structure,[21] implying that the individual properties of the microgels will also be averaged and thus overlooked. To overcome these limitations and to gain more reliable information on the microgels, a combination of ensemble techniques and single-particle measurements (such as imaging techniques) is highly desirable. In this context, various types of microscopy techniques, such as optical or fluorescence microscopy,[131–140,142,143] electron microscopy,[144–149] and scanning probe microscopy (SPM),[150–158] have been employed to directly gain morphological information (**Table 1.2**).

Optical or fluorescence microscopy can be used to directly observe the dynamic behavior of microgels both in the swollen and dispersed state, such as Brownian motion and interfacial

behavior.[131–134] Minato et al. have visualized the dynamic deformation behavior of a single microgel using a fluorescence microscope equipped with a high-speed camera with high temporal resolution.[136] However, despite the many advantages of optical microscopy, the effective spatial resolution remains limited to the wavelength of the light source, i.e., in the visible region, implying that the nanoscopic structure of microgels cannot be observed. To overcome this limitation, super-resolution fluorescence microscopy (SRFM) was developed in order to analyze the nanoscopic structure of biomolecules such as proteins with nanoscale spatial resolution.[142,143] Conley et al. have employed SRFM to visualize the three-dimensional structure of individual microgels and determine their internal density profiles.[142] Nevertheless, the samples must be labeled with fluorescent species and real-time observation remains difficult.

SEM is a commonly used method for the visualization of the surface morphology of microgels. However, the observation must be performed under high-vacuum conditions, i.e., the observation of solvent-swollen microgels is difficult.[146] To overcome this limitation, Horigome et al. have realized the visualization of "swollen" microgels by SEM using ionic liquids, which are conductive and nonvolatile even under high-vacuum conditions.[146] TEM is also frequently used for microgel morphology imaging with high spatial resolution under high-vacuum conditions. Cryo-tomography TEM techniques have been employed to reveal the three-dimensional structure and morphology of individual composite microgels in the swollen state.[148] Liquid-cell *in-situ* TEM allows monitoring microgels in real time in aqueous solution; however, the previous literature reports indicate that the spatial resolution is worse than that of cryo-TEM, and that high-contrast sample are required.[149]

AFM is an SPM technique that allows the visualization of the surface morphology of microgels in any environment, e.g., vacuum, air, and liquid conditions, with high spatial resolution.[150–158] Indeed, many reports exist on the characterization of the stimulus-responsiveness of microgels by AFM. For example, temperature-induced volume and microscopic structural changes in single microgels have been visualized by *in-situ* AFM,[150] and the time-dependent erosion of degradable single microgels under physiological conditions has been observed by in-liquid AFM.[154] However, tip–sample interactions cannot be neglected and the temporal resolution of AFM measurements remains low (about 1 min is typically required to capture an image),[163] and thus real-time observation cannot be performed.

On the other hand, a new type of microscopy based on an SPR sensor called single-

nanoparticle SPR microscopy allows monitoring polypeptide or protein binding to individual microgels,[159,160] although the detailed morphological changes in individual microgels at the nanoscale still cannot be visualized. In summary, despite the considerable progress on the above measurement techniques, to the best of the author's knowledge, the visualization of the dynamic behavior of individual microgels in aqueous solution at the nanoscale in real-time has not been reported to date.

Table 1.2. Classification of single-particle techniques for the evaluation of microgels

Technique	Source	Condition	References
Optical microscopy (OM)	Light	Dry, Liquid	131, 132, 133, 134
Fluorescent microscopy (FM)	Fluorescence	Dry, Liquid, Fluorescence-labeled	135, 136, 137
Confocal laser scanning microscopy (CLSM)			137, 138, 139, 140
Super-resolution fluorescence microscopy (SRFM)		Dry, Liquid, Fluorescence-labeled	142, 143, 149
Scanning electron microscopy (SEM)	Electron beam	Dry, High vacuum, Sputtering	144, 145, 146, 147, 148
Transmission electron microscopy (TEM)		Dry, Liquid, High vacuum	145, 147, 148, 149
Atomic force microscopy (AFM)	Probe	Dry, Liquid	150, 151, 152, 153, 154, 155, 156, 157, 158
Surface plasmon resonance microscopy (SPRM)	Surface plasmon polariton	Liquid	159, 160

Against this background, the author has focused on high-speed atomic force microscopy (HS-AFM) to visualize the dynamics of microgels in aqueous solution at the nanoscale. HS-AFM has been developed by Ando et al. to directly monitor the structural dynamics of active biomolecules (such as proteins) in motion, while retaining their physiological function in aqueous solution.[161-163] In contrast to conventional AFM, the image acquisition speed and sample invasiveness are improved by optimizing the feedback and force control. Such significant progress allows to greatly reduce the tip–sample interaction without sacrificing the imaging rate.[162-164] On the other hand, a few studies exist in the literature on the use of HS-AFM for the evaluation of artificial polymeric materials, for instance, the micro-Brownian motion of single polymer chains,[165] the time-dependent dissolution behavior of photoresists,[166] and the dynamic surfactant aggregation behavior on mica substrates.[167] Although a few reports are available on the use of HS-AFM to evaluate the dynamics of artificial polymeric materials, to the best of the author's knowledge, the study of artificial polymeric colloidal microspheres, especially microgels, remains unexplored.

In the present thesis, the author employed HS-AFM to study the dynamic behavior, including the stimulus-responsive behavior, of individual microgels with high spatio-temporal resolution in aqueous solution, aiming also at the establishment of a new design concept for stimulus-responsive microgels. In particular, the importance of combining ensemble-averaged measurements and real-time single-particle visualization using HS-AFM to understand the real behavior of these systems is demonstrated. Finally, as an improvement to conventional stimulus-responsive microgels, a novel design for autonomously oscillating microgels with enhanced oscillating properties, i.e., driving-speed, is proposed. The outlines are described in the following section.

1.2. Outlines

This thesis covers four research topics. In **Chapter I**, the dynamic adsorption behavior of microgels and other polymeric microspheres, such as elastomers and rigid microspheres, at the solid–liquid interface is evaluated by means of HS-AFM analysis. The author demonstrates that the deformability of microspheres at the solid–liquid interface is crucial for their adsorption kinetics. In **Chapter II**, the thermoresponsive behavior of pNIPAm microgels with different cross-

linking densities is discussed by means of temperature-controlled HS-AFM data. Temperature-induced morphological changes in individual microgels were investigated by combining a light-scattering method with direct nanoscopic visualization. Finally, in **Chapter III**, a new design for autonomously oscillating microgels that exhibit high-frequency oscillation is described.

1.3. References

1. Hanlon, R. Cephalopod dynamic camouflage. *Curr. Biol.* **2007**, *17*, R400−R404.
2. Capadona, J. R.; Shanmuganathan, K.; Tyler, D. J.; Rowan, S. J.; Weder, C. Stimuli-responsive polymer nanocomposites inspired by the sea cucumber dermis. *Science* **2008**, *319*, 1370−1374.
3. Forterre, Y.; Skotheim, J. M.; Dumais, J.; Mahadevan, L. How the Venus flytrap snaps. *Nature* **2005**, *433*, 421−425.
4. Ko, H.; Javey, A. Smart actuators and adhesives for reconfigurable matter. *Acc. Chem. Res.* **2017**, *50*, 691−702.
5. Gil, E. S.; Hudson, S. M. Stimuli-responsive polymers and their bioconjugates. *Prog. Polym. Sci.* **2004**, 29, 1173–1222.
6. Roy, D.; Cambre, J. N.; Sumerlin, B. S. Future perspectives and recent advances in stimuli-responsive materials. *Prog. Polym. Sci.* **2010**, *35*, 278–301.
7. Hoffman, A. S. Stimuli-responsive polymers: Biomedical applications and challenges for clinical translation. *Adv. Drug Deliv. Rev.* **2013**, *65*, 10–16.
8. Islam, M. R.; Lu, Z.; Li, X.; Sarker, A. K.; Hu, L.; Choi, P.; Li, X.; Hakobyan, N.; Serpe M. J., Responsive polymers for analytical applications: A review. *Anal. Chim. Acta* **2013**, *789*, 17–32.
9. Roy, D.; Brooks, W. L. A.; Sumerlin, B. S. New directions in thermoresponsive polymers. *Chem. Soc. Rev.* **2013**, *42*, 7214–7243.
10. Jiang, S.; Liu, F.; Lerch, A.; Ionov, L.; Agarwal, S. Unusual and superfast temperature-triggered actuators. *Adv. Mater.* **2015**, *27*, 4865–4870.
11. Wei, M.; Gao, Y.; Li, X.; Serpe, M. J. Stimuli-responsive polymers and their applications. *Polym. Chem.* **2017**, *8*, 127–143.

12. Montero de Espinosa, L.; Meesorn, W.; Moatsou, D.; Weder, C. Bioinspired polymer systems with stimuli-responsive mechanical properties. *Chem. Rev.* **2017**, *117*, 12851−12892.
13. Lu, C.; Urban, M. W. Stimuli-responsive polymer nano-science: shape anisotropy, responsiveness, applications. *Prog. Polym. Sci.* **2018**, *78*, 24–46.
14. Isapour, G.; Lattuada, M. Bioinspired stimuli-responsive color-changing systems. *Adv. Mater.* **2018**, *30*, 1707069.
15. Mirvakili, S. M.; Hunter, I. W. Artificial muscles: mechanisms, applications, and challenges. *Adv. Mater.* **2018**, *30*, 1704407.
16. Baughman, R. H.; Cui, C.; Zakhidov, A. A.; Iqbal, Z.; Barisci, J. N.; Spinks, G. M.; Wallace, G. G.; Mazzoldi, A.; Rossi, D. D.; Rinzler, A. G.; Jaschinski, O.; Roth, S.; Kertesz, M. Carbon nanotube actuators. *Science* **1999**, *284*, 1340–1344.
17. Yu, X.; Cheng, H.; Zhang, M.; Zhao, Y.; Qu, L.; Shi, G. Graphene-based smart materials. *Nat. Rev. Mater.* **2017**, *2*, 17046.
18. Tanaka, T.; Fillmore, D. J. Kinetics of swelling of gels. *J. Chem. Phys.* **1979**, *70*, 1214−1218.
19. Suzuki, D.; Horigome, K.; Kureha, T.; Matsui, S.; Watanabe, T. Polymeric hydrogel microspheres: design, synthesis, characterization, assembly and applications. *Polym. J.* **2017**, *49*, 695–702.
20. Pelton, R. H.; Chibante, P. Preparation of aqueous latices with *N*-isopropylacrylamide. *Colloids Surf.* **1986**, *20*, 247–256.
21. Pelton, R. Temperature-sensitive aqueous microgels. *Adv. Colloid Interface Sci.* **2000**, *85*, 1–33.
22. Heskins, M.; Guillet, J. E. Solution properties of poly(*N*-isopropylacrylamide). *J. Macromol. Sci., Chem.* **1968**, *A2*, 1441−1455.
23. Schild, H. G. Poly(*N*-isopropylacrylamide): experiment, theory and application. *Prog. Polym. Sci.* **1992**, *17*, 163−249.
24. Saunders, B. R.; Vincent, B. Microgel particles as model colloids: theory, properties and applications. *Adv. Colloid Interface Sci.*, **1999**, *80*, 1–25.
25. Nayak, S.; Lyon, L. A. Soft nanotechnology with soft nanoparticles. *Angew. Chem., Int. Ed.*, **2005**, *44*, 7686–7708.
26. Hoare, T.; Pelton, R. Characterizing charge and crosslinker distributions in polyelectrolyte microgels. *Curr. Opin. Colloid Interface Sci.*, **2008**, *13*, 413–428.

27. Pich, A.; Richtering, W. Microgels by precipitation polymerization: synthesis, characterization, and functionalization. *Adv. Polym. Sci.*, **2010**, *234*, 1–37.
28. Lu, Y.; Ballauff, M. Thermosensitive core–shell microgels: from colloidal model systems to nanoreactors. *Prog. Polym. Sci.*, **2011**, *36*, 767–792.
29. Lyon, L. A.; Fernandez-Nieves, A. The polymer/colloid duality of microgel suspensions. *Annu. Rev. Phys. Chem.*, **2012**, *63*, 25–43.
30. Hellweg, T. Responsive core–shell microgels: synthesis, characterization, and possible applications. *J. Polym. Sci. Part B: Polym. Phys.* **2013**, *51*, 1073–1083.
31. Kawaguchi, H. Thermoresponsive microhydrogels: preparation, properties and applications. *Polym. Int.* **2014**, *63*, 925–932.
32. Anselmo, A. C.; Mitragotri, S. Impact of particle elasticity on particle-based drug delivery systems. *Adv. Drug Deliv. Rev.* **2017**, *108*, 51–67.
33. Plamper, F. A.; Richtering, W. Functional microgels and microgel systems. *Acc. Chem. Res.* **2017**, *50*, 131–140.
34. Wu, X.; Pelton, R. H.; Hamielec, A. E.; Woods, D. R.; McPhee, W. The kinetics of poly(*N*-isopropylacrylamide) microgel latex formation. *Colloid Polym. Sci.* **1994**, *272*, 467−477.
35. Daly, E.; Saunders, B. R. Temperature−dependent electrophoretic mobility and hydrodynamic radius measurements of poly(*N*-isopropylacrylamide) microgel particles: structural insights. *Phys. Chem. Chem. Phys.* **2000**, *2*, 3187−3193.
36. Hoare, T.; Pelton, R. Highly pH and Temperature responsive microgels functionalized with vinylacetic acid. *Macromolecules* **2004**, *37*, 2544−2550.
37. Watanabe, T.; Kobayashi, C.; Song, C.; Murata, K.; Kureha, T.; Suzuki, D. Impact of spatial distribution of charged groups in core poly(*N*-isopropylacrylamide)-based microgels on the resultant composite structures prepared by seeded emulsion polymerization of styrene. *Langmuir* **2016**, *32*, 12760−12773.
38. Nayak, S.; Lyon, L. A. Photoinduced phase transitions in poly(*N*-isopropylacrylamide) microgels. *Chem. Mater.* **2004**, *16*, 2623−2627.
39. Kim, J.; Nayak, S.; Lyon, L. A. Bioresponsive hydrogel microlenses. *J. Am. Chem. Soc.* **2005**, *127*, 9588−9592.
40. Hellweg, T.; Dewhurst, C. D.; Bruckner, E.; Kratz, K.; Eimer, W. Colloidal crystals made of poly(*N*-isopropylacrylamide) microgel particles. *Colloid Polym. Sci.* **2000**, *278*, 972−978.

41. Lyon, L. A.; Debord, J. D.; Debord, S. B.; Jones, C. D.; McGrath, J. G.; Serpe, M. J. Microgel colloidal crystals. *J. Phys. Chem. B* **2004**, *108*, 19099−19108.
42. Mattsson, J.; Wyss, H. M.; Fernandez-Nieves, A.; Miyazaki, K.; Hu, Z.; Reichman, D. R.; Weitz, D. A. Soft colloids make strong glasses. *Nature* **2009**, *462*, 83−86.
43. Okubo, T.; Suzuki, D.; Yamagata, T.; Katsuno, A.; Sakurai, M.; Kimura, H.; Tsuchida, A. Colloidal crystallization of thermo-sensitive gel spheres of poly (*N*-isopropyl acrylamide). *Colloid Polym. Sci.* **2011**, *289*, 291−299.
44. Urayama, K.; Saeki, T.; Cong, S.; Uratani, S.; Takigawa, T.; Murai, M.; Suzuki, D. A simple feature of yielding behavior of highly dense suspensions of soft micro-hydrogel particles. *Soft Matter* **2014**, *10*, 9486−9495.
45. Kureha, T.; Aoki, D.; Hiroshige, S.; Iijima, K.; Aoki, D.; Takata, T.; Suzuki, D. Decoupled thermo- and pH-responsive hydrogel microspheres cross-linked by rotaxane networks. *Angew. Chem., Int. Ed.* **2017**, *56*, 15393–15396.
46. Kureha, T.; Suzuki, D. Nanocomposite microgels for the selective separation of halogen compounds from aqueous solution. *Langmuir* **2018**, *34*, 837–846.
47. Hoare, T.; Pelton, R. Impact of microgel morphology on functionalized microgel-drug interactions. *Langmuir* **2008**, *24*, 1005−1012.
48. Zhang, Q. M.; Xu, W.; Serpe, M. J. Optical devices constructed from multiresponsive microgels. *Angew. Chem., Int. Ed.* **2014**, *53*, 4827−4831.
49. Smith, M. H.; Lyon, L. A. Tunable encapsulation of proteins within charged microgels. *Macromolecules* **2011**, *44*, 8154–8160.
50. Tahara, Y.; Akiyoshi, K. Current advances in self-assembled nanogel delivery systems for immunotherapy. *Adv. Drug Deliv. Rev.* **2015**, *95*, 65–76.
51. Sigolaeva, L. V.; Gladyr, S. Y.; Mergel, O.; Gelissen, A. P. H.; Noyong, M.; Simon, U.; Pergushov, D. V.; Kurochkin, I. N.; Plamper, F. A.; Richtering, W. Easy-preparable butyrylcholinesterase/microgel construct for facilitated organophosphate biosensing. *Anal. Chem.* **2017**, *89*, 6091−6098.
52. Li, X.; Serpe, M. J. Understanding and controlling the self-folding behavior of poly (*N*-isopropylacrylamide) microgel-based devices. *Adv. Funct. Mater.* **2014**, *24*, 4119–4126.
53. Zaikin, A. N.; Zhabotinsky, A. M. Concentration wave propagation in two-dimensional liquid-phase self-oscillating system. *Nature* **1970**, *225*, 535−537.

54. Zhabotinsky, A. M.; Zaikin, A. N. Autowave processes in a distributed chemical system. *J. Theor. Biol.* **1973**, *40*, 45−61.
55. Field, R. J.; Burger, M. *Oscillations and Travelling Waves in Chemical Systems*; John Wiley & Sons, Inc.: New York, **1985**.
56. Suzuki, D.; Sakai, T.; Yoshida, R. Self-flocculating/self-dispersing oscillation of microgels. *Angew. Chem., Int. Ed.* **2008**, *47*, 917–920.
57. Suzuki, D.; Yoshida, R. Temporal control of self-oscillation for microgels by cross-linking network structure. *Macromolecules* **2008**, *41*, 5830–5838.
58. Suzuki, D.; Yoshida, R. Effect of initial substrate concentration of the Belousov−Zhabotinsky reaction on self-oscillation for microgel system. *J. Phys. Chem. B* **2008**, *112*, 12618–12624.
59. Suzuki, D.; Taniguchi, H.; Yoshida, R. Autonomously oscillating viscosity in microgel dispersions. *J. Am. Chem. Soc.* **2009**, *131*, 12058–12059.
60. Taniguchi, H.; Suzuki, D.; Yoshida, R. Characterization of autonomously oscillating viscosity induced by swelling/deswelling oscillation of the microgels. *J. Phys. Chem. B* **2010**, *114*, 2405–2410.
61. Suzuki, D.; Yoshida, R. Self-oscillating core/shell microgels: effect of a crosslinked nanoshell on autonomous oscillation of the core. *Polym. J.* **2010**, *42*, 501–508.
62. Suzuki, D.; Kobayashi, T.; Yoshida, R.; Hirai, T. Soft actuators of organized self-oscillating microgels. *Soft Matter* **2012**, *8*, 11447–11449.
63. Matsui, S.; Kureha, T.; Nagase, Y.; Okeyoshi, K.; Yoshida, R.; Sato, T.; Suzuki, D. Small-angle X-ray scattering study on internal microscopic structures of poly(*N*-isopropylacrylamide-*co*-tris(2,2'-bipyridyl))ruthenium(II) complex microgels. *Langmuir* **2015**, *31*, 7228−7237.
64. Matsui, S.; Inui, K.; Kumai, Y.; Yoshida, R.; Suzuki, D. Autonomously oscillating hydrogel microspheres with high-frequency swelling/deswelling and dispersing/flocculating oscillations. *ACS Biomater. Sci. Eng.* in press, DOI: 10.1021/acsbiomaterials.8b00850.
65. Mears, S. J.; Deng, Y.; Cosgrove, T.; Pelton, R. Structure of sodium dodecyl sulfate bound to a poly(NIPAM) microgel particle. *Langmuir* **1997**, *13*, 1901−1906.
66. Helen M. Crowther, H. M.; Saunders, B. R.; Sarah J. Mears, S. J.; Cosgrove, T.; Vincent, B.; King, S. M.; Yu, G. Poly(NIPAM) microgel particle de-swelling: a light scattering and small-angle neutron scattering study. *Colloid. Surf. A* **1999**, *152*, 327−333.

67. S. Seelenmeyer, S.; Deike, I.; Rosenfeldt, S.; Norhausen, Ch.; Dingenouts, N.; Ballauff, M.; Narayanan, T.; Lindner, P. Small-angle X-ray and neutron scattering studies of the volume phase transition in thermosensitive core–shell colloids. *J. Chem. Phys.* **2001**, *114*, 10471−10478.
68. Kratz, K.; Hellweg, T.; Eimer, W. Structural changes in PNIPAM microgel particles as seen by SANS, DLS, and EM techniques. *Polymer* **2001**, *42*, 6631−6639.
69. Fernández-Barbero, A.; Fernández-Nieves, A.; Grillo, I.; Lóez-Cabarcos, E. Structural modifications in the swelling of inhomogeneous microgels by light and neutron scattering. *Phys. Rev. E* **2002**, *66*, 051803.
70. Mason, T. G.; Lin, M. Y. Density profiles of temperature-sensitive microgel particles. *Phys. Rev. E* **2005**, *71*, 040801.
71. Keerl, M.; Pedersen, J. S.; Richtering, W. Temperature sensitive copolymer microgels with nanophase separated structure. *J. Am. Chem. Soc.* **2009**, *131*, 3093–3097.
72. Wellert, S.; Hertle, Y.; Richter, M.; Medebach, M.; Magerl, D.; Wang, W.; Demé, B.; Radulescu, A.; Müller-Buschbaum, P.; Hellweg, T.; Klitzing, R. Inner structure of adsorbed ionic microgel particles. *Langmuir* **2014**, *30*, 7168−7176.
73. Dingenouts, N.; Norhausen, C.; Ballauff, M. Observation of the volume transition in thermosensitive core-shell latex particles by small-angle X-ray scattering. *Macromolecules* **1998**, *31,* 8912−8917.
74. Seelenmeyer, S.; Deike, I.; Rosenfeldt, S.; Norhausen, Ch.; Dingenouts, N.; Ballauff, M.; Narayanan, T.; Linder, P. Small-angle X-ray and neutron scattering studies of the volume phase transition in thermosensitive core−shell colloids. *J. Chem. Phys.* **2001**, *114*, 10471−10478.
75. Saunders, B. R. On the structure of poly(*N*-isopropylacrylamide) microgel particles. *Langmuir* **2004**, *20*, 3925–3932.
76. Stieger, M.; Richtering, W.; Pedersen, J. S.; Lindner, P. Small-angle neutron scattering study of structural changes in temperature sensitive microgel colloids. *J. Chem. Phys.* **2004**, *120*, 6197−6206.
77. Suzuki, D.; Nagase, Y.; Kureha, T.; Sato, T. Internal structures of thermosensitive hybrid microgels investigated by means of small-angle X-ray scattering. *J. Phys. Chem. B* **2014**, *118*, 2194−2204.

78. Kureha, T.; Sato, T.; Suzuki, D. Relationship between temperature-induced changes in internal microscopic structures of poly(*N*-isopropylacrylamide) microgels and organic dye uptake behavior. *Langmuir* **2014**, *30*, 8717–8725.
79. Keidel, R.; Ghavami, A.; Lugo, D. M.; Lotze, G.; Virtanen, O.; Beumers, P.; Pedersen, J. S.; Bardow, A.; Winkler, R. G.; Richtering, W. Time-resolved structural evolution during the collapse of responsive hydrogels: The microgel-to-particle transition. *Sci. Adv.* **2018**, *4*, eaao7086.
80. Wu, C. A comparison between the 'coil-to-globule' transition of linear chains and the ''volume phase transition'' of spherical microgels. *Polymer* **1998**, *39*, 4609–4619.
81. Fernández-Nieves, A.; De las Nieves, F. J.; Fernández-Barbero. A. Static light scattering from microgel particles: Model of variable dielectric permittivity. *J. Chem. Phys.* **2004**, *120*, 374-378.
82. Ogawa, K. Effects of salt on intermolecular polyelectrolyte complexes formation between cationic microgel and polyanion. *Adv. Colloid Interface Sci.* **2015**, *226*, 115–121.
83. Pelton, R. H.; Pelton, H. M.; Morphesis, A.; Rowell, R. L. Particle sizes and electrophoretic mobilities of poly(*N*-isopropylacrylamide) latex. *Langmuir* **1989**, *5*, 816–818.
84. Ohshima, H.; Makino, K.; Kato, T.; Fujimoto, K.; Kondo, T.; Kawaguchi, H. Electrophoretic mobility of latex particles covered with temperature-sensitive hydrogel layers. *J. Colloid Interface Sci.* **1993**, *159*, 512–514.
85. Nabzar, L.; Duracher, D.; ElaÏssari, A.;* Chauveteau, G.; Pichot, C. Electrokinetic properties and colloidal stability of cationic amino-containing *N*-isopropylacrylamide-styrene copolymer particles bearing different shell structures. *Langmuir* **1998**, *14*, 5062–5069.
86. Daly, E.; Saunders, B. R. Temperature-dependent electrophoretic mobility and hydrodynamic radius measurements of poly(*N*-isopropylacrylamide) microgel particles : structural insights. *Phys. Chem. Chem. Phys.* **2000**, *2*, 3187−3193.
87. Utashiro, Y.; Takiguchi, M.; Satoh, M. Zeta potential of PNIPAM microgel particles dispersed in water—effects of charged radical initiators vs. OH^- ion adsorption. *Colloid Polym. Sci.* **2017**, *295*, 45–52.
88. Duracher, D.; Elaïssari, A.; Pichot, C. Preparation of poly(*N*-isopropylmethacrylamide) latexes kinetic studies and characterization. *J. Polym. Sci., Part A Polym. Chem.* **1999**, *27*, 1823−1837.

89. Wang, J.; Gan, D.; Lyon, L. A.; El-Sayed, M. A. Temperature-jump investigations of the kinetics of hydrogel nanoparticle volume phase transitions. *J. Am. Chem. Soc.* **2001**, *123*, 11284−11289.
90. Lin, C. L.; Chiu, W. Y.; Lee, C. F. Preparation, morphology, and thermoresponsive properties of poly(*N*-isopropylacrylamide)-based copolymer microgels. *J. Polym. Sci.: Part A Polym. Chem.* **2006**, *44*, 356–370.
91. Dupin, D.; Rosselgong, J.; Armes, S. P. Swelling kinetics for a pH-induced latex-to-microgel transition. *Langmuir* **2007**, *23*, 4035–4041.
92. Wang, Q.; Zhao, Y.; Xu, H.; Yang, X.; Yang, Y. Thermosensitive phase transition kinetics of poly(*N*-isopropylacrylamide-*co*-acrylamide) microgel aqueous dispersions. *J. Appl. Polym. Sci.* **2009**, *113*, 321–326.
93. Morse, A. J.; Armes, S. P.; Mills, P.; Swart, R. Stopped-flow kinetics of pH-responsive polyamine latexes: How fast is the latex-to-microgel transition? *Langmuir* **2013**, *29*, 15209−15216.
94. Fujimoto, K.; Nakajima, Y.; Kashiwabara, M.; Kawaguchi, H. Fluorescence analysis for thermosensitive hydrogel microspheres. *Polym. Int.* **1993**, *30*, 237−241.
95. Wong, J. E.; Mu1ller, C. B.; Laschewsky, A.; Richtering, W. Direct evidence of layer-by-layer assembly of polyelectrolyte multilayers on soft and porous temperature-sensitive PNiPAM microgel using fluorescence correlation spectroscopy. *J. Phys. Chem. B* **2007**, *111*, 8527–8531.
96. Welsch, N.; Dzubiella, J.; Graebert, A.; Ballauff, M. Protein binding to soft polymeric layers: a quantitative study by fluorescence spectroscopy. *Soft Matter* **2012**, *8*, 12043−12052.
97. Lehmann, S.; Seiffert, S.; Richtering, W. Diffusion of guest molecules within sensitive core–shell microgel carriers. *J. Colloid Interface Sci.* **2014**, *431*, 204–208.
98. Walta, S.; Pergushov, D. V.; Oppermann, A.; Steinschulte, A. A.; Geisel, K.; Sigolaeva, L. V.; Plamper, F. A.; W€oll, D.; Richtering, W. Microgels enable capacious uptake and controlled release of architecturally complex macromolecular species. *Polymer* **2017**, *119*, 50−58.
99. Hofmann, C. H.; Plamper, F. A.; Scherzinger, C.; Hietala, S.; Richtering, W. Cononsolvency revisited: solvent entrapment by *N*-isopropylacrylamide and *N*,*N*-diethylacrylamide microgels in different water/methanol mixtures. *Macromolecules* **2013**, *46*, 523−532.

100. Sierra-Martin, B.; Retama, J. R.; Laurenti, M.; Barbero, A. F.; Cabarcos, E. L. Structure and polymer dynamics within PNIPAM-based microgel particles. *Adv. Colloid Interface Sci.* **2014**, *205*, 113–123.

101. Kozhunova, E. Y.; Ji, Q.; Labuta, J.; Nasimova, I. R.; Makhaeva, E. E.; Ariga, K. ^{1}H NMR study of thermo-induced collapse of polyelectrolyte microgels. *Express Polym. Lett.* **2018**, *12*, 1005–1013.

102. Shu, T.; Shen, Q.; Wan, Y.; Zhang, W.; Su, L.; Zhang, X.; Serpe, M. J. Silver nanoparticle-loaded microgel-based etalons for H_2O_2 sensing. *RSC Adv.* **2018**, *8*, 15567–15574.

103. Hou, L.; Ma, K.; An, Z.; Wu, P. Exploring the volume phase transition behavior of POEGA- and PNIPAM-based core−shell nanogels from infrared-spectral insights. *Macromolecules* **2014**, *47*, 1144−1154.

104. Li, W.; Hu, L.; Zhu, J.; Li, D.; Luan, Y.; Xu, W.; Serpe, M. J. Comparison of the responsivity of solution-suspended and surface-bound poly(*N*-isopropylacrylamide)-based microgels for sensing applications. *ACS Appl. Mater. Interfaces* **2017**, *9*, 26539−26548.

105. Majcen, N.; Mohsen, R.; Snowden, M. J.; Mitchell, J. C.; Voncina, B. The development of a novel smart material based on colloidal microgels and cotton. *Adv. Colloid Interface Sci.* **2018**, *256*, 193–202.

106. Ye, L.; Miao, C.; Brook, M. A.; Pelton, R. Photoflocculation of TiO_2 microgel mixed suspensions. *Langmuir* **2008**, *24*, 9341−9343.

107. Suzuki, D.; Yamagata, T.; Murai, M. Multilayered composite microgels synthesized by surfactant-free seeded polymerization. *Langmuir* **2013**, *29*, 10579−10585.

108. Yang, J.; Hu, D.; Xue, M.; Yang, X. Synthesis of p(AM-*co*-MAA)/AEM composite microspheres with lichi–like surface structure using porous microgel as template. *J. Colloid Interface Sci.* **2014**, *418*, 350–359.

109. Suzuki, D.; Kobayashi, C. Raspberry-shaped composite microgel synthesis by seeded emulsion polymerization with hydrogel particles. *Langmuir* **2014**, *30*, 7085−7092.

110. Zhou, J.; Wei, J.; Ngai, T.; Wang, L.; Zhu, D.; Shen, J. Correlation between dielectric/electric properties and cross-linking/charge density distributions of thermally sensitive spherical PNIPAM microgels. *Macromolecules* **2012**, *45*, 6158−6167.

111. Füllbrandt, M.; Klitzing, R.; Schönhals, A. The dielectric signature of poly(*N*-isopropylacrylamide) microgels at the volume phase transition: dependence on the crosslinking density. *Soft Matter* **2013**, *9*, 4464–4471.
112. Su, W.; Zhao, K.; Wei, J.; Ngai, T. Dielectric relaxations of poly(*N*-isopropylacrylamide) microgels near the volume phase transition temperature: impact of crosslinking density distribution on the volume phase transition. *Soft Matter* **2014**, *10*, 8711−8723.
113. Yang, M.; Liu, C.; Lian, Y.; Zhao, K.; Zhu, D.; Zhou, J. Relaxations and phase transitions during the collapse of a dense PNIPAM microgel suspension—thorough insight using dielectric spectroscopy. *Soft Matter* **2017**, *13*, 2663−2676.
114. Snowden, M. J.; Chowdhry, B.Z.; Vincent B,; Morris, G.E. Colloidal copolymer microgels of *N*-isopropylacrylamide and acrylic acid: pH, ionic strength and temperature effects. *J. Chem. Soc, Faraday Trans.* **1996**, *92*, 5013–5016.
115. Gan, D.; Lyon, L. A. Tunable swelling kinetics in core-shell hydrogel nanoparticles. *J. Am. Chem. Soc.* **2001**, *123,* 7511–7517.
116. Woodward, N. C.; Chowdhry, B. Z.; Snowden, M. J.; Leharne, S. A.; Griffiths, P. C.; Winnington, A. L. Calorimetric investigation of the influence of cross-linker concentration on the volume phase transition of poly(*N*-isopropylacrylamide) colloidal microgels. *Langmuir* **2003**, *19*, 3202–3211.
117. Schneider, F.; Balaceanu, A.; Feoktystov, A.; Pipich, V.; Wu, Y.; Allgaier, J.; Pyckhout-Hintzen, W.; Pich, A.; Schneider, G. J. Monitoring the internal structure of poly(*N*-vinylcaprolactam) microgels with variable cross-link concentration. *Langmuir* **2014**, *30*, 15317−15326.
118. Henzler, K.; Haupt, B.; Lauterbach, K.; Wittemann, A.; Borisov, O.; Ballauff, M. Adsorption of *β*-lactoglobulin on spherical polyelectrolyte brushes: direct proof of counterion release by isothermal titration calorimetry. *J. Am. Chem. Soc.* **2010**, *132*, 3159–3163.
119. Welsch, N.; Becker, A. L.; Dzubiella, J.; Ballauff, M. Core–shell microgels as ‘‘smart’’ carriers for enzymes. *Soft Matter* **2012**, *8*, 1428–1436.
120. Singh, S.; Datta, A.; Borro, B. C.; Davoudi, M.; Schmidtchen, A.; Bhunia, A.; Malmsten, M. Conformational aspects of high content packing of antimicrobial peptides in polymer microgels. *ACS Appl. Mater. Interfaces* **2017**, *9*, 40094−40106.

121. Serpe, M. J.; Lyon, L. A. Optical and acoustic studies of pH-dependent swelling in microgel thin films. *Chem. Mater.* **2004**, *16*, 4373–4380.
122. Jeenanong, A.; Kawaguchi, H. SPR response of stimuli-sensitive microgel on sensor chip. *Colloids Surf. A* **2007**, *302*, 403–410.
123. Sorrell, C. D.; Lyon, L. A. Bimodal swelling responses in microgel thin films. *J. Phys. Chem. B* **2007**, *111*, 4060-4066.
124. Wei, J. ; Cai, J.; Li, Y.; Wu, B.; Gong, X.; Ngai, T. Investigation of cell behaviors on thermo-responsive PNIPAM microgel films. *Colloids Surf. B* **2015**, *132*, 202–207.
125. Howard, S. C.; Craig, V. S. J.; FitzGerald, P. A.; Wanless, E. J. Swelling and collapse of an adsorbed pH-responsive film-forming microgel measured by optical reflectometry and QCM. *Langmuir* **2010**, *26*, 14615–14623.
126. Feiler, A. A.; Davies, P. T.; Vincent, B. Adsorption of anionic gold nanoparticles by a layer of cationic microgel particles deposited on a gold-coated, quartz surface: studied by quartz crystal microbalance and atomic force microscopy. *Soft Matter* **2011**, *7*, 6660–6670.
127. Hoshino, Y.; Nakamoto, M.; Miura, Y. Control of protein-binding kinetics on synthetic polymer nanoparticles by tuning flexibility and inducing conformation changes of polymer chains. *J. Am. Chem. Soc.* **2012**, *134*, 15209−15212.
128. Wen, Q.; Vincelli, A. M.; Pelton, R. Cationic polyvinylamine binding to anionic microgels yields kinetically controlled structures. *J. Colloid Interface Sci.* **2012**, *369* 223–230.
129. Sigolaeva, L. V.; Gladyr, S. Y.; Gelissen, A. P. H.; Mergel, O.; Pergushov, D. V.; Kurochkin, I. N.; Plamper, F. A.; Richtering, W. Dual-stimuli-sensitive microgels as a tool for stimulated spongelike adsorption of biomaterials for biosensor applications. *Biomacromolecules* **2014**, *15*, 3735−3745.
130. Li, W.; Hu, L.; Zhu, J.; Li, D.; Luan, Y.; Xu, W.; Serpe, M. J. Comparison of the responsivity of solution-suspended and surface-bound poly(*N*-isopropylacrylamide)-based microgels for sensing applications. *ACS Appl. Mater. Interfaces* **2017**, *9*, 26539−26548.
131. Horigome, K.; Suzuki, D. Drying mechanism of poly(*N*-isopropylacrylamide) microgel dispersions. *Langmuir* **2012**, *28*, 12962−12970.
132. Cohin, Y.; Fisson, M.; Jourde, K.; Fuller, G. G.; Sanson, N.; Talini, L.; Monteux, C. Tracking the interfacial dynamics of PNiPAM soft microgels particles adsorbed at the air–water interface and in thin liquid films. *Rheol. Acta.* **2013**, *52*, 445−454.

133. Suzuki, D.; Horigome, K. Assembly of oppositely charged microgels at the air/water interface. *J. Phys. Chem. B* **2013**, *117*, 9073−9082.
134. Takizawa, M.; Sazuka, Y.; Horigome, K.; Sakurai, Y.; Matsui, S.; Minato, H.; Kureha, T.; Suzuki, D. Self-organization of soft hydrogel microspheres during the evaporation of aqueous droplets. *Langmuir* **2018**, *34*, 4515−4525.
135. Morse, A. J.; Madsen, J.; Growney, D. J.; Armes, S. P.; Mills, P.; Swart, R. Microgel colloidosomes based on pH-responsive poly(*tert*-butylaminoethyl methacrylate) latexes. *Langmuir* **2014**, *30*, 12509−12519.
136. Minato, H.; Murai, M.; Watanabe, T.; Matsui, S.; Takizawa, M.; Kureha, T.; Suzuki, D. The deformation of hydrogel microspheres at the air/water interface. *Chem. Commun.* **2018**, *54*, 932−935.
137. Schürings, M.; Nevskyi, O.; Eliasch, K.; Michel, A.; Liu, B.; Pich, A.; Böker, A.; Plessen, G.; Wöll, D. Diffusive motion of linear microgel assemblies in solution. *Polymers* **2016**, *8*, 413.
138. Debord, S. B.; Lyon, L. A. Influence of particle volume fraction on packing in responsive hydrogel colloidal crystals. *J. Phys. Chem. B* **2003**, *107*, 2927–2932.
139. Kwok, M.; Ngai, T. A confocal microscopy study of micron-sized poly (*N*-isopropylacrylamide) microgel particles at the oil–water interface and anisotopic flattening of highly swollen microgel. *J. Colloid Interface Sci.* **2016**, *461*, 409–418.
140. Gau, E.; Mate, D. M.; Zou, Z.; Oppermann, A.; Töpel, A.; Jakob, F.; Wöll, D.; Schwaneberg, U.; Pich, A. Sortase-mediated surface functionalization of stimuli-responsive microgels. *Biomacromolecules* **2017**, *18*, 2789−2798.
141. Betzig, E.; Patterson, G. H.; Sougrat, R.; Lindwasser, O. W.; Olenych, S.; Bonifacino, J. S.; Davidson, M. W.; Lippincott-Schwartz, J.; Hess, H. F. Imaging intracellular fluorescent proteins at nanometer resolution. *Science* **2006**, *313*, 1642–1645.
142. Conley, G. M.; Nöjd, S.; Braibanti, M.; Schurtenberger, P.; Scheffold, F. Superresolution microscopy of the volume phase transition of pNIPAM microgels. *Colloids Surf. A* **2016**, *499*, 18–23.
143. Conley, G. M.; Aebischer, P.; Nöjd, S.; Schurtenberger, P.; Scheffold, F. Jamming and overpacking fuzzy microgels: deformation, interpenetration, and compression. *Sci. Adv.* **2017**, *3*, e1700969.

144. Crowther, H. M.; Vincent, B. Swelling behavior of poly-*N*-isopropylacrylamide microgel particles in alcoholic solutions. *Colloid Polym. Sci.* **1998**, *276*, 46–51.
145. Saunders, B. R.; Vincent, B. Microgel particles as model colloids: theory, properties and applications. *Adv. Colloid Interface Sci.* **1999**, *80*, 1–25.
146. Horigome, K.; Ueki, T.; Suzuki, D. Direct visualization of swollen microgels by scanning electron microscopy using ionic liquids. *Polym. J.* **2016**, *48*, 273–279.
147. Kobayashi, C.; Watanabe, T.; Murata, K. Kureha, T.; Suzuki, D. Localization of polystyrene particles on the surface of poly(*N*-isopropylacrylamide-*co*-methacrylic acid) microgels prepared by seeded emulsion polymerization of styrene. *Langmuir* **2016**, *32*, 1429−1439.
148. Watanabe, T.; Song, C.; Murata, K.; Kureha, T.; Suzuki, D. Seeded emulsion polymerization of styrene in the presence of water-swollen hydrogel microspheres. *Langmuir* **2018**, *34*, 8571−8580.
149. Gelissen, A. P. H.; Oppermann, A.; Caumanns, T.; Hebbeker, P.; Turnhoff, S. K.; Tiwari, R.; Eisold, S.; Simon, U.; Lu, Y.; Mayer, J.; Richtering, W.; Walther, A.; Wöll, D. 3D structures of responsive nanocompartmentalized microgels. *Nano Lett.* **2016**, *16*, 7295−7301.
150. Wiedemair, J.; Serpe, M. J.; Kim, J.; Masson, J. F. ; Lyon, L. A.; Mizaikoff, B.; Kranz, C. In-situ AFM studies of the phase-transition behavior of single thermoresponsive hydrogel particles. *Langmuir* **2007**, *23*, 130–137.
151. Höfl, S.; Zitzler, L.; Hellweg, T.; Herminghaus, S.; Mugele, F. Volume phase transition of ‘‘smart’’ microgels in bulk solution and adsorbed at an interface: A combined AFM, dynamic light, and small angle neutron scattering study. *Polymer* **2007**, *48*, 245–254.
152. Tagit, O.; Tomczak, N.; Vancso, G. J. Probing the morphology and nanoscale mechanics of single poly(*N*-isopropylacrylamide) microgels across the lower-critical-solution temperature by atomic force microscopy. *Small* **2008**, *4*, 119–126.
153. Schmidt, S.; Zeiser, M.; Hellweg, T.; Duschl, C.; Fery, A.; Möhwald, H. Adhesion and mechanical properties of PNIPAM microgel films and their potential use as switchable cell culture substrates. *Adv. Funct. Mater.* **2010**, *20*, 3235–3243.
154. South, A. B.; Lyon, L. A. Direct observation of microgel erosion via in-liquid atomic force microscopy. *Chem. Mater.* **2010**, *22*, 3300–3306.

155. Burmistrova, A.; Richter, M.; Uzum, C.; Klitzing, R. Effect of cross-linker density of p(NIPAM-*co*-AAc) microgels at solid surfaces on the swelling/shrinking behaviour and the Young's modulus. *Colloid. Polym. Sci.* **2011**, *289*, 613–624.
156. Mourran, A.; Wu, Y.; Gumerov, R. A.; Rudov, A. A.; Potemkin, I. I.; Pich, A.; Möller, M. When colloidal particles become polymer coils. *Langmuir* **2016**, *32*, 723–730.
157. Cors, M.; Wrede, O.; Genix, A.; Anselmetti, D.; Oberdisse, J.; Hellweg, T. Core−shell microgel-based surface coatings with linear thermoresponse. *Langmuir* **2017**, *33*, 6804−6811.
158. Aufderhorst-Roberts, A.; Baker, D.; Foster, R. J.; Cayre, O.; Mattsson, J.; Connell, S. D. Nanoscale mechanics of microgel particles. *Nanoscale* **2018**, *10*, 16050−16061.
159. Cho, K.; Fasoli, J. B.; Yoshimatsu, K.; Shea, K. J.; Corn, R. M. Measuring melittin uptake into hydrogel nanoparticles with near-infrared single nanoparticle surface plasmon resonance microscopy. *Anal. Chem.* **2015**, *87*, 4973−4979.
160. Maley, A. M.; Terada, Y.; Onogi, S.; Shea, K. J.; Miura, Y.; Corn, R. M. Measuring protein binding to individual hydrogel nanoparticles with single-nanoparticle surface plasmon resonance imaging microscopy. *J. Phys. Chem. C* **2016**, *120*, 16843−16849.
161. Ando, T.; Kodera, N.; Takai, E.; Maruyama, D.; Saito, K.; Toda, A. A high-speed atomic force microscope for studying biological macromolecules. *Proc. Natl. Acad. Sci. USA* **2001**, *98*, 12468–12472.
162. Ando, T.; Uchihashi, T.; Fukuma, T. High-speed atomic force microscopy for nano-visualization of dynamic biomolecular processes. *Prog. Surf. Sci.* **2008**, *83*, 337–437.
163. Ando, T.; Uchihashi, T.; Scheuring, S. Filming biomolecular processes by high-speed atomic force microscopy. *Chem. Rev.* **2014**, *114*, 3120–3188.
164. Uchihashi, T.; Scheuring, S. Applications of high-speed atomic force microscopy to real-time visualization of dynamic biomolecular processes. *BBA - General Subjects* **2018**, *1862*, 229–240.
165. Shinohara, K.; Kodera, N.; Ando, T. Single-molecule imaging of a micro-Brownian motion of a chiral helical π-conjugated polymer as a molecular spring driven by thermal fluctuations. *Chem. Lett.* **2009**, *38*, 690–691.
166. Itani, T.; Santillan, J. J. Dissolution behavior of photoresists: an in-situ analysis. *J. Photopolym. Sci. Technol.* **2010**, 23, 639–642.

167. Inoue, S.; Uchihashi, T.; Yamamoto, D.; Ando, T. Direct observation of surfactant aggregate behavior on a mica surface using high-speed atomic force microscopy. *Chem. Commun.* **2011**, *47*, 4974–4976.

2. Chapter I

" Adsorption dynamics of microgels at solid–liquid interfaces"

*Part of this work was published in "Shusuke Matsui, Takuma Kureha, Seina Hiroshige, Mikihiro Shibata, Takayuki Uchihashi, and Daisuke Suzuki *Angewandte Chemie International Edition*, **2017**, *56*, 12146-12149."
(https://onlinelibrary.wiley.com/doi/full/10.1002/anie.201705808)

2.1. Introduction

In order to observe the dynamic stimulus-responsive behaviors of individual microgels by using HS-AFM, it is necessary to adsorb microgels on a solid substrate in aqueous solution. In the first place, understanding dynamic contact and adsorption phenomena of colloidal microspheres onto solid surfaces in aqueous solution are highly important in an industrial or biological context, for e.g. the coating of solid surfaces with colloidal microspheres, and the adsorption of blood platelets onto injured regions in blood vessels, which stops bleeding. In terms of pharmaceutical applications, drug delivery vehicles consisting of artificial polymeric microspheres have to effectively adsorb onto diseased sites for an effective transportation of drugs. Theoretically, the adsorption of rigid colloidal microspheres onto solid surfaces is dominated by electrostatic and van der Waals interactions.[1] However, the process that occurs between the microspheres and the surface at the moment of physical contact is poorly understood.[2] Especially as colloidal microspheres usually exhibit at least some degree of elasticity (deformability), the microspheres can be subject to deformation upon contact with solid surfaces. The deformability plays an important role for their biological functionality, e.g. their biodistribution and circulation times.[3] Such adsorption or deformation of the microspheres on solid surfaces have so far been investigated by AFM and so forth.[4] However, to the best of our knowledge, how this deformability affects the dynamic contact and adsorption behavior of the microspheres onto the surface has not yet been addressed, due to the difficulties associated with the direct visualization of the dynamic adsorption and deformation behavior of individual microspheres at the nanoscale in real time.

Against this background, the author first visualized individual microspheres during their adsorption and subsequent deformation by using HS-AFM, and discovered that the deformability

of individual microspheres strongly impacts the adsorption kinetics. In this chapter, HS-AFM techniques have been applied to artificial polymeric microspheres, especially microgels, with different softness as model colloids under liquid conditions, and the relationship between the adsorption kinetics and the elasticity of the microspheres that adsorb onto solid substrates were investigated.

2.2. Experimental Section

Materials

N-isopropylacrylamide (NIPAm, 98%), *N*,*N*′-methylenebis(acrylamide) (BIS, 97%), acrylic acid (AAc, 99%), ethyl acrylate (EA, 97%), methyl methacrylate (MMA, 98%), styrene (St, 99%), sodium dodecyl sulfate (SDS, 95%), potassium persulfate (KPS, 95%), and 2,2′-azobis(2-methylpropinamidine)dihydrochloride (V-50, 95%) were purchased from Wako Pure Chemical Industries (Japan) and used as received. 3-Aminopropyltriethoxysilane (APTES) was purchased from Shin-Etsu Silicones (Japan). For the synthesis of (4-vinyl-4′-methyl-2,2′-bipyridine)bis(2,2′-bipyridine)bis(hexafluorophosphate) [$Ru(bpy)_3$ cationic monomer], a previously reported method was used.[23] Water for all reactions, including the preparation of solutions and the purification of polymers, was distilled and subsequently subjected to ion exchange (EYELA, SA-2100E1).

Microgel synthesis

Poly(NIPAm-*co*-AAc) (**pNA**) microgels were synthesized by radical precipitation polymerization in aqueous solution. For that purpose, a mixture of NIPAm (1.511 g/89 mol.%, 1.477 g/87 mol.%, or 1.443 g/85 mol.%), BIS (0.024 g/1 mol.%, 0.070 g/3 mol.%, or 0.115 g/5 mol.%), AAc (0.109 g/10 mol.%, 0.108 g/10 mol.%, or 0.108 g/10 mol.%) in water (90 mL) was poured into a three-necked round-bottomed flask (200 mL) equipped with a mechanical stirrer, condenser, and a nitrogen gas inlet. The initial total monomer concentration (150 mM) was maintained. To remove any oxygen, the monomer solution was heated to 70 °C in an oil bath under nitrogen sparging (30 min) and constant stirring (250 rpm). After stabilizing the solution for 30 min, SDS (0.115 g/4 mM, 0.115 g/4 mM, or 0.115 g/4 mM) was dissolved in water (5 mL) and added to the flask. Then, KPS (0.054 g/2 mM, 0.054 g/2 mM, or 0.054 g/2 mM) dissolved in water (5 mL) was added to the flask in order to initiate the polymerization. After stirring for 4 h, the dispersion was cooled to room temperature. The obtained microgels were purified twice by the following procedure:

centrifugation (415 000 *g* / 15 °C), decantation of the supernatant, and redispersion of the precipitate in water. The dispersion was then dialyzed for 5 days, whereby the water was changed daily. The microgels were denoted as **pNA(1)**, **pNA(3)**, or **pNA(5)**, whereby the numbers in parentheses refer to the mole percentage of BIS in the polymerization feed.

PolyNIPAm (**pN**) microgels were synthesized by radical precipitation polymerization in aqueous solution. A mixture of NIPAm (1.681 g, 99 mol.%) and BIS (0.023 g, 1 mol.%) in water (90 mL) was poured into a three-necked round-bottomed flask (200 mL) equipped with a mechanical stirrer, condenser, and a nitrogen gas inlet. The solution was purged as described above. After stabilization for 30 min, SDS (0.058 g, 2 mM) dissolved in water (5 mL) was added to the flask, and polymerization was initiated by adding KPS (0.054 g, 2 mM) in water (5 mL). The dispersion was stirred for 4 h and cooled to room temperature. The thus obtained microgels were purified as described above. The dispersion was then dialyzed for 4 days, whereby the water was changed daily.

Cationic poly(NIPAm-*co*-Ru(bpy)$_3$) (**pNRu**) microgels were synthesized by radical precipitation polymerization in aqueous solution. A mixture of NIPAm (0.224 g, 88 mol.%), BIS (0.035 g, 10 mol.%), and Ru(bpy)$_3$ (0.041 g, 2 mol.%) in water (28 mL) was poured into a three-necked round-bottomed flask (50 mL) equipped with a mechanical stirrer, condenser, and a nitrogen gas inlet. The initial total monomer concentration (75 mM) was maintained. After purging the solution as described above and stabilization (30 min), the polymerization was initiated by addition of V-50 (0.016 g, 2 mM) in water (2 mL). The dispersion was stirred for 4 h, and then cooled to room temperature. The thus obtained microgels were purified as described above. The dispersion was then dialyzed for 2 days, whereby the water was changed daily.

Synthesis of elastomeric microspheres

Poly(ethyl acrylate) (**pEA**) microspheres were synthesized by surfactant-free emulsion polymerization. EA (3.008 g, 100 mol.%) in water (95 mL) was poured into a three-necked round-bottomed flask (200 mL) equipped with a mechanical stirrer, condenser, and a nitrogen gas inlet. The initial total monomer concentration (300 mM) was maintained. To remove any oxygen from the solution, it was heated to 70 °C in an oil bath under nitrogen sparging (30 min) and constant stirring (300 rpm). After stabilization for 30 min, KPS (0.054 g, 2 mM) in water (5 mL) was added to initiate the polymerization. The dispersion was stirred for 24 h, cooled to room temperature, and

then dialyzed for 7 days, whereby the water was changed daily.

Synthesis of rigid microspheres

Poly(methyl methacrylate) (**pMMA**) and polystyrene (**pSt**) microspheres were synthesized by surfactant-free emulsion polymerization. MMA (10.012 g, 100 mol.%) or St (5.2075 g, 100 mol.%) in water (95 mL) was poured into a three-necked round-bottomed flask (200 mL) equipped with a mechanical stirrer, condenser, and a nitrogen gas inlet. The initial total monomer concentration (MMA: 1000 mM; St: 500 mM) was maintained. After removing oxygen from the solutions as described for **pEA** and stabilization for 30 min, KPS (0.054 g, 2 mM) in water (5 mL) was added to initiate the polymerizations. The dispersions were stirred for 24 h, cooled to room temperature, and dialyzed for 7 days, whereby the water was changed daily.

Dynamic light scattering (DLS) measurements

The hydrodynamic diameters of the microspheres in aqueous solution were estimated by dynamic light scattering (DLS; Malvern Instruments Ltd.; ZetasizerNanoS). The DLS data represent averages of three individual measurements of 15 consecutive runs of the intensity autocorrelation (acquisition time: 30 s). The concentration of the microspheres in the DLS experiments was approximately 0.001 wt%. Before the measurements, the samples were allowed to thermally equilibrate at 25 °C for 5 min. The time-dependent scattering intensity was detected at a total scattering angle of 173° (refractive index n = 1.33). The hydrodynamic diameters of the microspheres were calculated from the measured diffusion coefficients using the Stokes–Einstein equation (Zetasizer software v6.12).

Electrophoretic mobility (EPM)

The electrophoretic mobilities (EPMs) of the microspheres were determined by a Zetasizer NanoZS system (Malvern, Zetasizer software Ver. 4.20). The EPM data represent averages of three individual measurements of 20 consecutive runs. Before the measurements, the samples were allowed to thermally equilibrate at 25 °C for 5 min. The microgel concentration in the measurements was approximately 0.01 wt%, and the concentration of the elastomeric or rigid microspheres was approximately 0.001 wt% in pure water.

HS-AFM observations

A laboratory-built HS-AFM was used in this study, and the instrument has previously been described elsewhere.[10] All images and movies shown in this paper were acquired in the tapping mode, in which a cantilever (length: 6–7 μm; width: 2 μm; thickness: 90 nm) oscillates near a mechanical resonance. The cantilever oscillation was detected by an optical-beam-deflection detector with a red laser (650 nm). Typical values for the spring constant, resonant frequency, and quality factor in aqueous solution of this cantilever are ~0.1 N/m, ~600 kHz, and ~2, respectively. An amorphous carbon tip was grown on the original bird-beak tip by electron beam deposition, and the carbon tip was subsequently sharpened (radius: ~4 nm) by plasma etching under an argon atmosphere. For the HS-AFM imaging of polymeric microspheres, the cantilever free-oscillation amplitude was set to 5~30 nm, and the set-point amplitude was set to 70-90% of the free-oscillation amplitude depending on the microsphere size.

In order to modify the electric properties of the mica surfaces, these were chemically modified with 3-aminopropyltriethoxysilane (APTES), which leads to the formation of positively charged surfaces.[18] For that purpose, an APTES-diluted aqueous solution (1 wt%; 3 μL) was dropped on a freshly cleaved mica surface, and the substrate was incubated for 3 min at room temperature. After the incubation, the mica surface was rinsed with pure water to remove any excess APTES. The adsorption behavior of the microspheres on the APTES-treated mica substrates (AP mica) was observed by removing 8 μL of water from the observation solution (80 μL pure water) and replacing it with the same volume of a microsphere dispersion (0.1 wt%) during the recording of the images. All HS-AFM imaging was performed at room temperature (~25 °C) under the following conditions: scanning area = 1500 × 1500 nm^2; 120 ×120 $pixels^2$; frame rate = 1 fps.

2.3. Results and discussion

2.3.1. Synthesis of microgels, elastomers, and rigid microspheres

The softness of polymeric microspheres varies from highly soft hydrogels (elastic modulus: ~ several tens of kPa),[6] to elastomers (elastic modulus: ~ several hundreds of kPa),[7] and rigid polymers (elastic modulus: ~ several GPa).[8] Hydrogel microspheres, i.e., pNA(x) microgels (x = molar ratio of cross-linker in the polymerization feed) were synthesized from *N*-isopropyl acrylamide (NIPAm), acrylic acid (AAc, 10 mol.%), and the cross-linker *N*,*N*'-

methylenebis(acrylamide) (BIS; 1, 3, or 5 mol.%) by aqueous free-radical precipitation polymerization[9] (**Table 2.1**). Elastomeric poly(ethyl acrylate) (pEA; $T_g \sim -8$ °C),[10] as well as rigid poly(methyl methacrylate) (pMMA; $T_g \sim 105$ °C)[10] and polystyrene (pSt; $T_g \sim 107$ °C)[10] microspheres with different glass-transition temperatures (T_g) were synthesized by soap-free emulsion polymerization (**Table 2.2**).

Table 2.1. Chemical composition, hydrodynamic diameters (D_h), and electrophoretic mobility (EPM) of the microgels measured in pure water, as well as the degree of deformation of the microgels in aqueous solution (D_h/h).

	NIPAm (mol.%)	BIS (mol.%)	AAc (mol.%)	D_h (nm)	EPM (10^{-8} $m^2V^{-1}s^{-1}$)	D_h/h
pNA(1)	89	1	10	378 ± 12	−2.50 ± 0.13	16.7 ± 4.9
pNA(3)	87	3	10	257 ± 5	−2.74 ± 0.18	2.9 ± 0.8
pNA(5)	85	5	10	242 ± 14	−2.88 ± 0.24	2.2 ± 0.7

Table 2.2. Chemical composition, hydrodynamic diameters (D_h), and electrophoretic mobility (EPM) of the elastomeric and rigid microspheres measured in pure water, as well as the degree of deformation of the microspheres in aqueous solution (D_h/h).

	EA (mol.%)	MMA (mol.%)	St (mol.%)	D_h (nm)	EPM (10^{-8} $m^2V^{-1}s^{-1}$)	D_h/h
pEA	100	0	0	198 ± 1	−2.49 ± 0.02	0.7 ± 0.1
pMMA	0	100	0	402 ± 2	−3.24 ± 0.12	N/A
pSt	0	0	100	250 ± 2	−1.76 ± 0.03	N/A

2.3.2. Effect of electrostatic interactions between the microgels and the substrate on the adsorption behavior

Initially, the author examined the effect of the electrostatic interactions on the adsorption behavior between the microspheres and negatively or positively charged substrates in aqueous solution (**Table 2.3**; **Figures 2.1-2.3**). For this purpose, freshly cleaved negatively charged mica substrates, or a mica substrates treated with 3-aminopropyltriethoxysilane (APTES), which are expected to exhibit positive net charges (AP mica),[11] were used in this study. The author found

that electrostatic attractions between the microspheres and the substrates are necessary to adsorb the microspheres on the substrates.

Table 2.3. Chemical composition, hydrodynamic diameters (D_h), and electrophoretic mobility (EPM) of weakly anionic and cationic microgels measured in pure water.

	NIPAm (mol.%)	BIS (mol.%)	$Ru(bpy)_3$ (mol.%)	D_h (nm)	EPM (10^{-8} $m^2V^{-1}s^{-1}$)
pN	99	1	0	226 ± 2	−0.64 ± 0.04
pNRu	88	10	2	166 ± 9	+1.90 ± 0.10

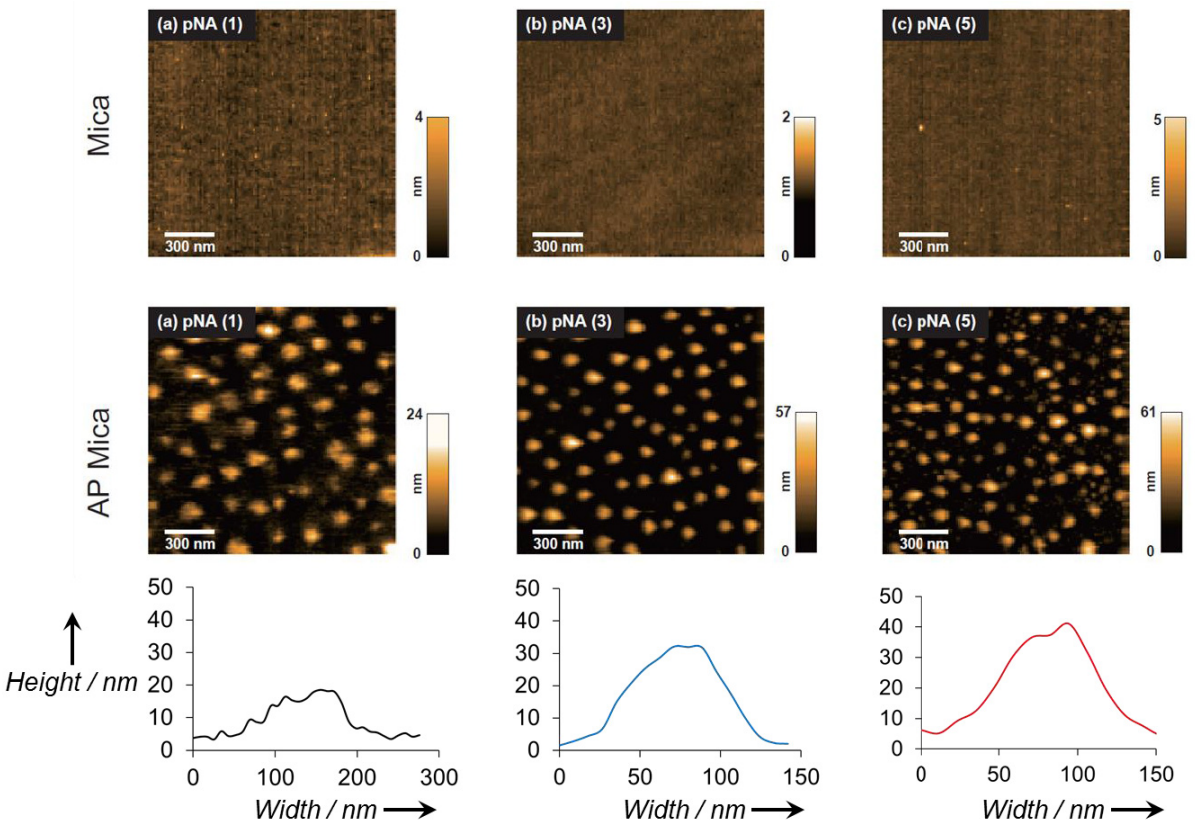

Figure 2.1. HS-AFM images of (a) pNA(1), (b) pNA(3), and (c) pNA(5) microgels adsorbed onto different substrates (mica or AP mica) in pure water, and typical height profiles of adsorbed microgels. A microgel dispersion (3 µL; 0.1 wt%) was dropped onto the surface of freshly cleaved

mica or AP mica substrates, and incubated for 5 min at room temperature. The substrate was then rinsed with pure water to remove any non-adsorbed microgel and placed in the sample folder (filled with 80 μL water). The HS-AFM measurement was performed at room temperature. Pixels: 120 × 120; scan range: 1500 × 1500 nm^2; frame rate: 1 fps. Anionic pNA microgels did not adsorb onto the negatively charged mica substrates, while they adsorbed onto the positively charged AP mica substrates.

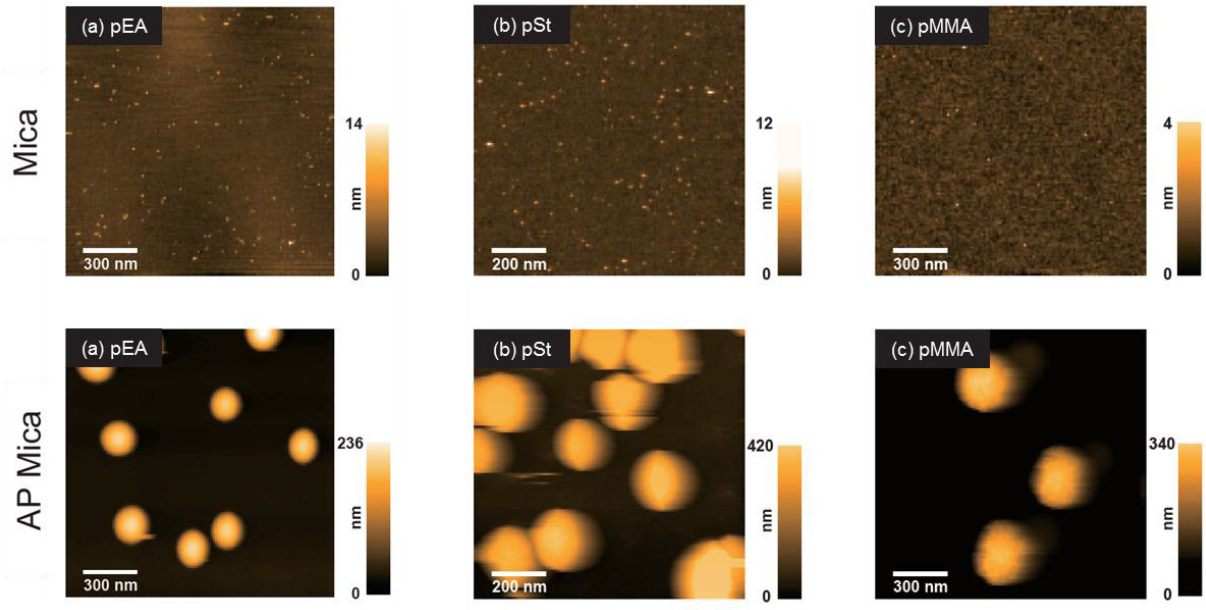

Figure 2.2. HS-AFM images of adsorbed (a) anionic pEA, (b) pSt, and (c) pMMA microspheres in pure water using different substrates (mica or AP mica). Anionic pEA, pSt, and pMMA microspheres did not adsorb onto the negatively charged mica substrates, while they adsorbed onto the positively charged AP mica substrates.

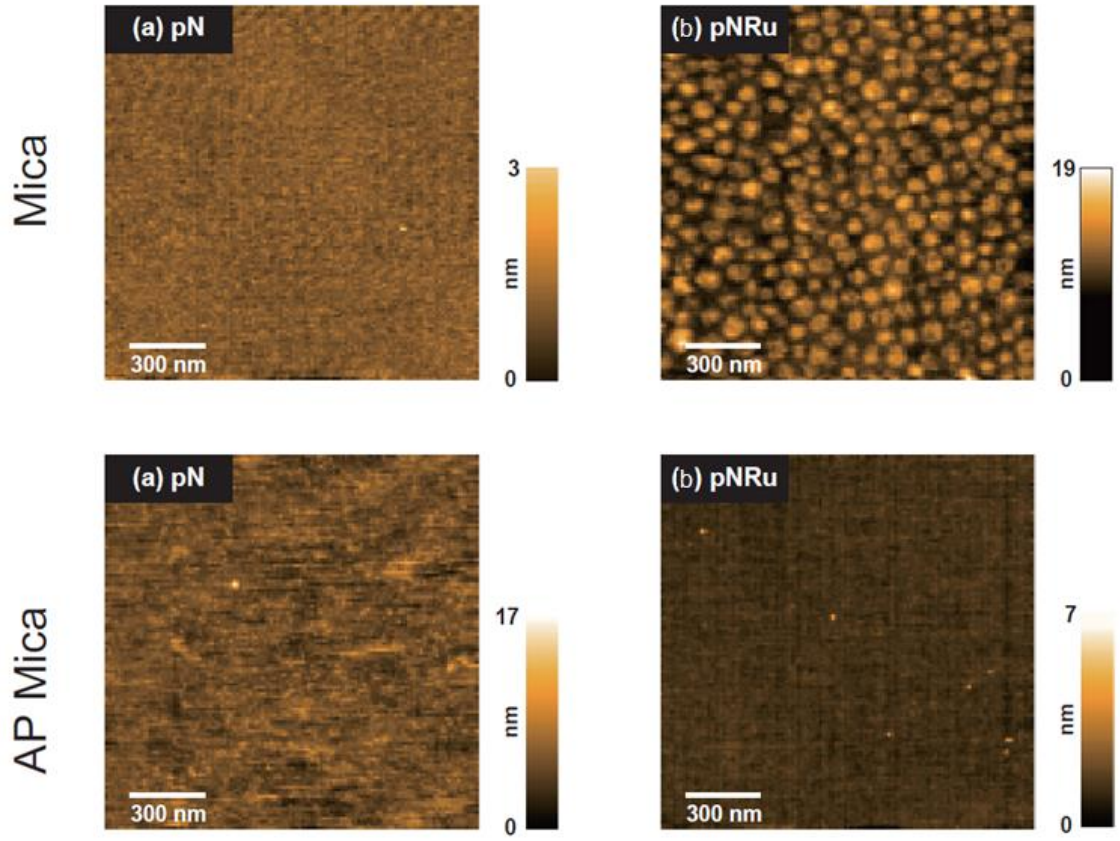

Figure 2.3. HS-AFM images of adsorbed (a) weakly anionic pN and (b) cationic pNRu microgels in pure water using different substrates (mica or AP mica). Weakly anionic pN microgels did not adsorb onto the negatively charged mica or positively charged AP mica substrates. Cationic pNRu microgels adsorbed onto the negatively charged mica substrates, while they did not adsorb onto the positively charged AP mica substrates.

2.3.3. Observation of the dynamic adsorption behavior of microgels at solid–liquid interfaces by HS-AFM

To observe the real-time adsorption behavior of negatively charged microspheres by HS-AFM, a positively charged AP mica was initially monitored by HS-AFM in water (80 μL). Then, part of the water (8 μL) was removed, and a dispersion of microspheres (0.1 wt%, 8 μL) was injected; the dispersion was thoroughly distributed in the water by repeated pipetting during the recording of the images (**Figure 2.4**).

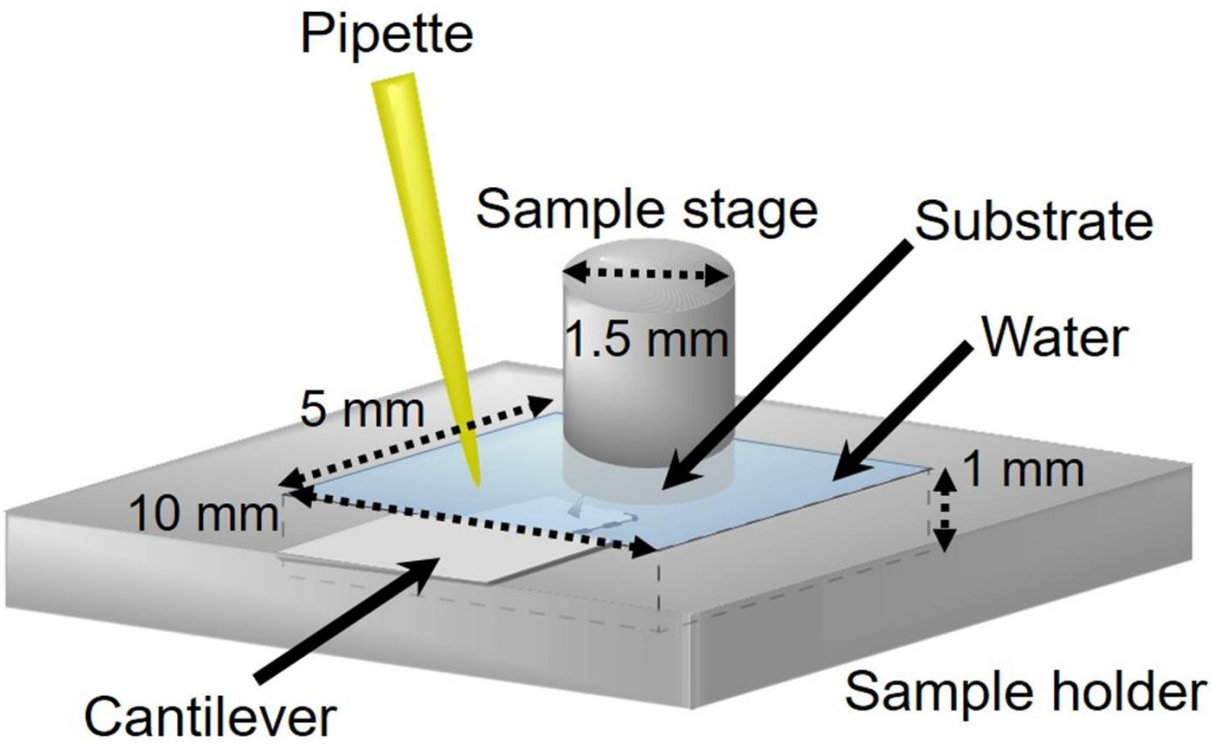

Figure 2.4. Schematic illustration of the HS-AFM sample folder.

After the injection of the microgel or elastomeric microsphere dispersions, microspheres appeared in the HS-AFM images, and the number of adsorbed microspheres increased with time up to saturation (**Figure 2.5**). On the other hand, after the injection of the rigid pMMA or pSt microsphere dispersions, the microspheres diffused on the surface but were not bound onto the surface.

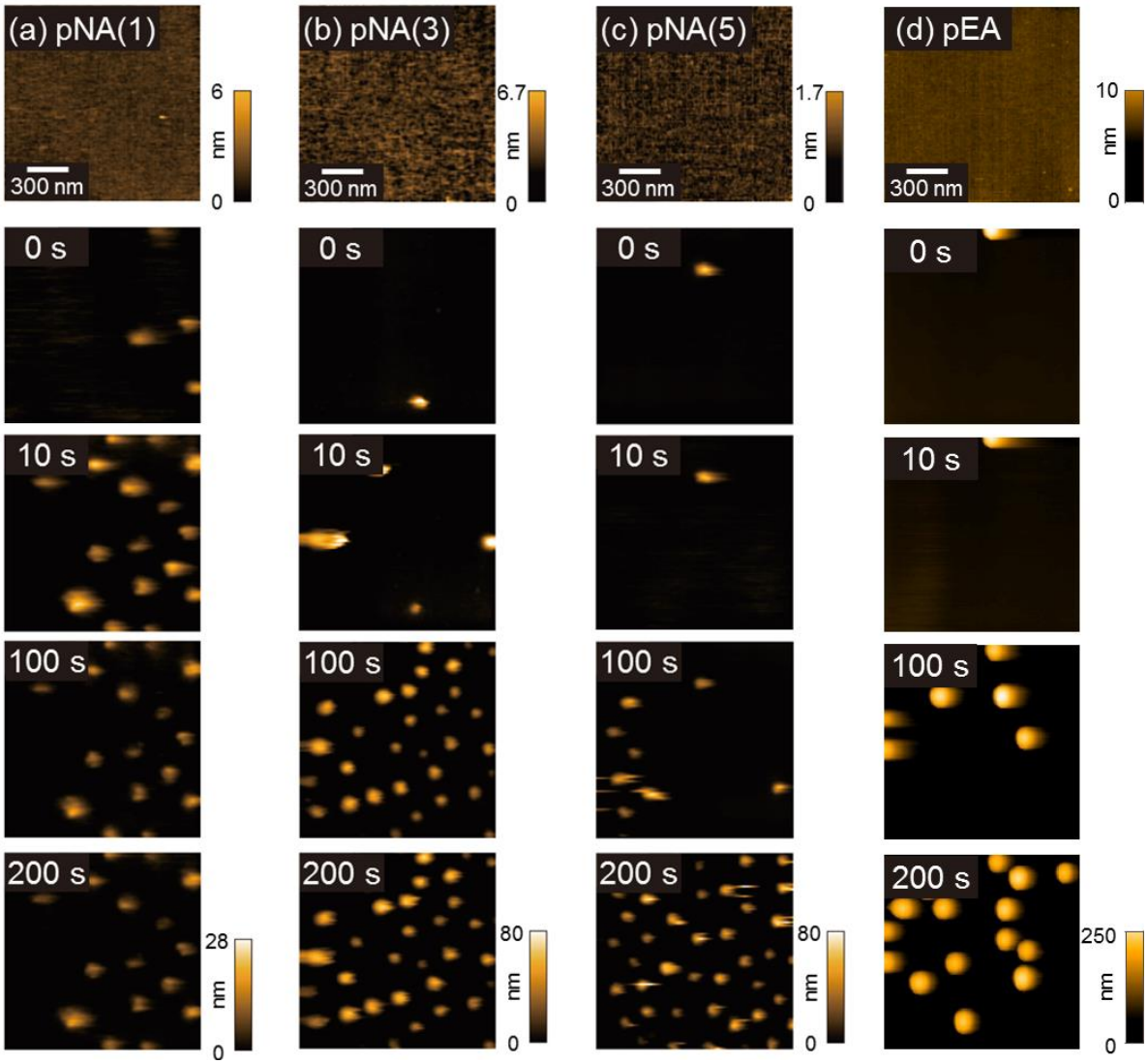

Figure 2.5. HS-AFM images of the time-dependent adsorption of microgels with different cross-linking densities and elastomeric pEA microspheres onto AP mica substrates: (a) pNA(1), (b) pNA(3), (c) pNA(5), and (d) pEA; [microspheres] = 0.01 wt%; pixel: 120 × 120; scan range: 1500 × 1500 nm^2; frame rate: 1 fps.

To quantitatively evaluate the observed adsorption behavior, the number of adsorbed microspheres within a 1500 × 1500 nm^2 area of the HS-AFM images was counted and plotted as a function of time. **Figure 2.6** shows the number of microspheres adsorbed on the substrates. Here, the number is normalized by the saturated number and the adsorption rate is simply estimated from dividing the saturated number of microspheres with the time required for the saturation. The adsorption rate of the pNA(5) microgels with higher cross-linking density (0.58 s^{-1}) was lower than

that of the pNA(3) (1.11 s^{-1}) and the pNA(1) (1.98 s^{-1}) microgels with lower cross-linking densities, or that of the elastomeric pEA microspheres (0.24 s^{-1}) (**Figure 2.6**), indicating that the adsorption rate of the microgels decreases with increasing cross-linking density. A significant effect of the size of the microgels on their adsorption behavior was not observed under the applied experimental conditions (**Figure 2.7**). These results suggest that the adsorption rate cannot be rationalized exclusively by electrostatic interactions, i.e., the adsorption behavior of the microspheres may be controlled by their deformability on the substrate rather than by their electrophoretic mobility (EPM). This indicates that the adsorption rate should be determined by the balance between the electrostatic interactions and the deformability of the microspheres.

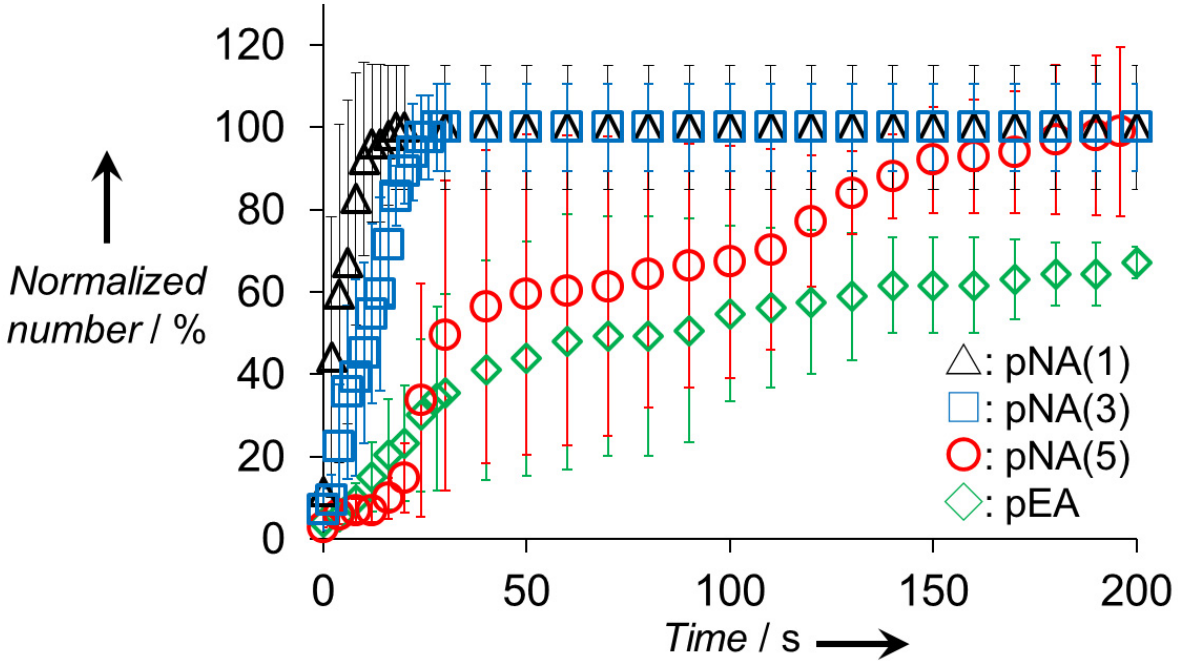

Figure 2.6. Normalized number of adsorbed microgels with different cross-linking densities and of elastomeric pEA microspheres as a function of time ($N = 3$).

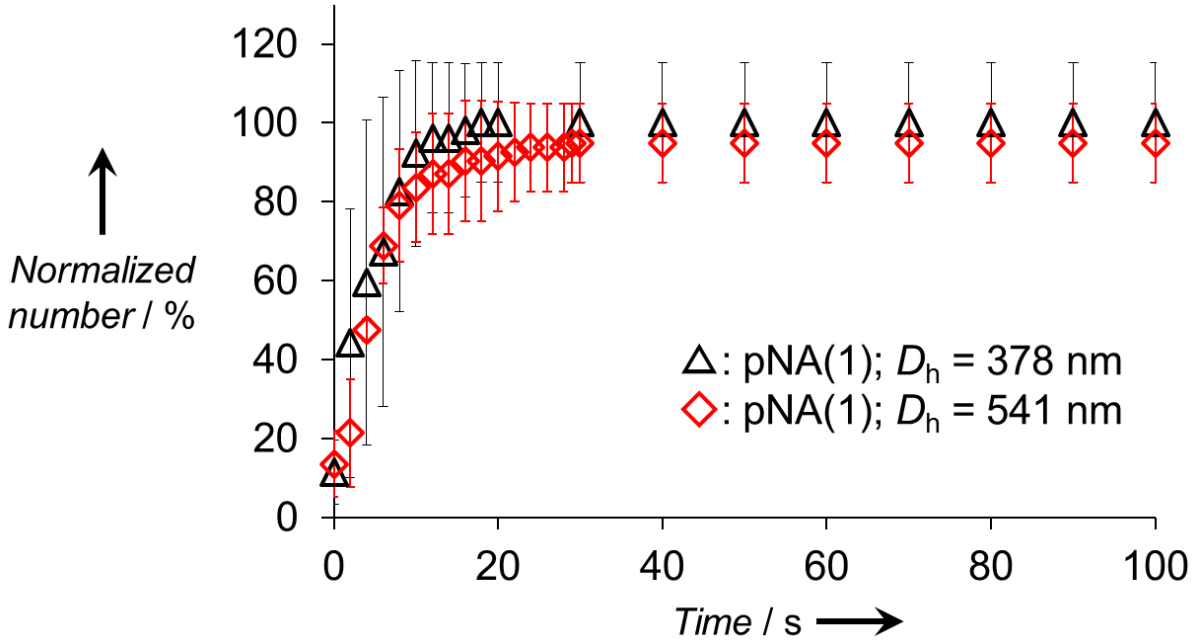

Figure 2.7. Normalized number of adsorbed microgels with different size (D_h = 378 nm and D_h = 541 nm; difference in volume by a factor of ~2.9) as a function of time (N = 3). The adsorption behavior of these microgels is comparable.

2.3.4. Relationship between the deformability and adsorption kinetics of microgels

To confirm the effect of the deformability of individual microspheres on the adsorption kinetics, the author evaluated the height (h) of the adsorbed microspheres from the HS-AFM images immediately after the adsorption on the substrate (**Figure 2.8**), while the hydrodynamic diameters (D_h) of the microspheres were estimated based on dynamic light scattering (DLS) measurements. The degree of deformation induced immediately after the adsorption on the substrate was then defined as D_h/h. **Figure 2.9** shows the plots of the correlation between the adsorption rate and D_h/h of the microspheres. For all microgels, the degrees of deformation were > 1 immediately after adsorption (**Figure 2.9** and **Table 2.1**), indicating that all microgels immediately deformed on the substrate. The degree of deformation of the pNA(5) microgels with a high cross-linking density (D_h/h = 2.2) was lower than those of the pNA(3) (D_h/h = 2.9) and the pNA(1) (D_h/h = 16.7) microgels with lower cross-linking densities. Furthermore, the degree of deformation immediately after adsorption affects the net adsorption rate of the microgels onto the substrate (**Figure 2.9**). On the other hand, the degrees of deformation of the elastomeric pEA

microspheres were ≈ 1 (**Figure 2.9** and **Table 2.2**), indicating that these microspheres should not be deformed on the substrate as much as the microgels.

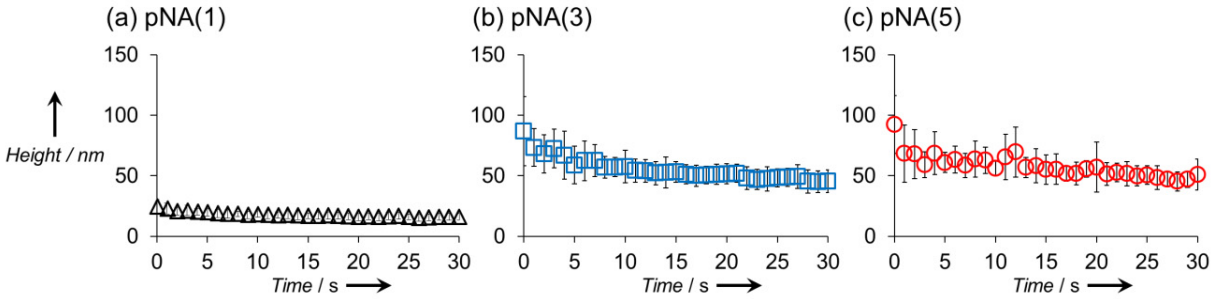

Figure 2.8. Time-dependence of the height profiles of the pNA microgels after the adsorption onto the substrates (0 -30 s). (a) pNA(1), (b) pNA(3), and (c) pNA(5) microgels. The height of all adsorbed pNA microgels immediately after the adsorption (just appeared on the image, 0 s) is much smaller than the hydrodynamic diameter in water, indicating high deformation on the substrate. After that, the height of the adsorbed microgels decreased and reached almost an equilibrium state.

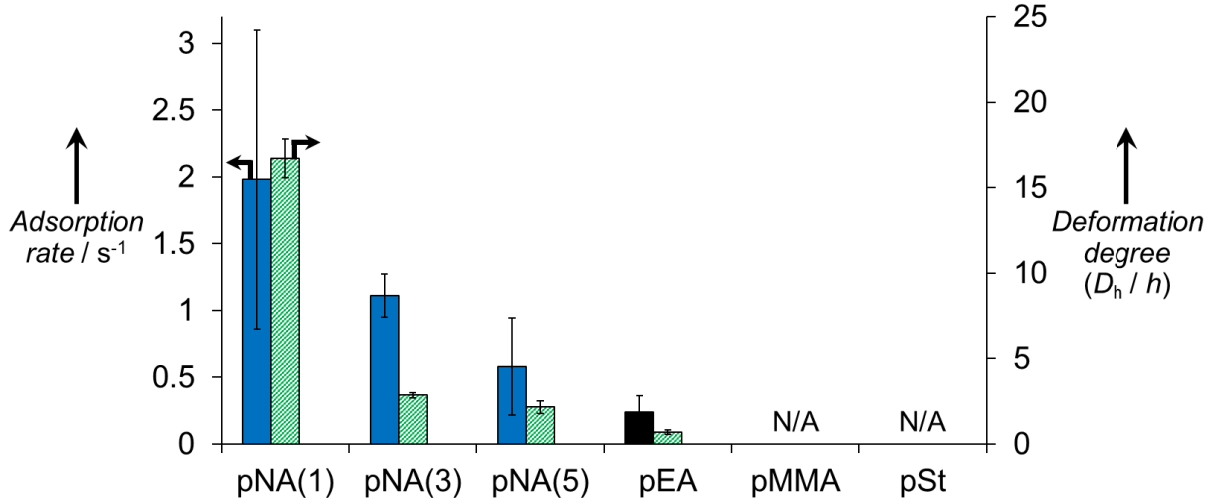

Figure 2.9. The adsorption rate of microspheres obtained from HS-AFM images ($N = 3$; left axis and left bar), and the degree of deformation (D_h/h) of the polymeric microspheres immediately after the adsorption onto the substrate in aqueous solution ($N = 15$; right axis and right bar).

According to the JKR theory,[12] the total adhesion energy (E_0) of two surfaces in equilibrium contact under zero load is given by $E_0 = -1.2\ \pi a_0^2 \gamma$, whereby $a_0 = (12\ \pi R^2 \gamma / K)^{1/3}$.[13]

Here, γ represents the interfacial energy, a_0 the contact radius between the spheres and the surface, while R and K are the radius and the elastic modulus of a sphere, respectively. In the case of rigid microspheres without obvious deformation, the adsorption energy of the microspheres on the solid surface should be very small, given by that the contact radius of the microspheres is small due to the large elastic modulus. Hence, rigid microspheres can desorb immediately after the adsorption onto the substrate. In contrast, soft and deformable microgels with a small elastic modulus deform rapidly and collapse on the surface after getting in contact with the surface. This rapid and drastic deformation provides a relatively large adsorption energy to the microspheres, as the contact radius of the adsorbed microgels increases rapidly. Thus, the adsorption rate should be dominated by the instantaneous deformability immediately after the adsorption onto the substrate.

2.4. Conclusions

In conclusion, the effect of the deformability of individual polymeric microspheres on the adsorption kinetics on solid surfaces was examined by monitoring the adsorption processes of microspheres onto solid surfaces in aqueous solution using HS-AFM. The adsorption rates in the presence of electrostatic attractions greatly depend on the deformability of the microspheres, and the adsorption rate decreases in the order pNA(1) > pNA(3) > pNA(5) > pEA, suggesting that highly deformable microgels with a low cross-linking density adsorb faster than elastomeric or rigid microspheres. This result should lead to the development of new design guidelines for polymeric microspheres with applications in biomaterials such as drug delivery vehicles that are focused on the "softness" of the microspheres, as it may allow effective adsorption on target sites under blood flow conditions.

2.5. References

1. Adamczyk, Z.; Warszyński, P. Role of electrostatic interactions in particle adsorption. *Adv. Colloid Interface Sci.* **1996**, *63*, 41-149.
2. Adamczyk, Z. Particle adsorption and deposition: role of electrostatic interactions. *Adv. Colloid Interface Sci.* **2003**, *100-102*, 267-347.
3. Adamczyk, Z.; Nattich-Rak, M.; Sadowska, M.; Michna, A.; Szczepaniak, K. Mechanisms of nanoparticle and bioparticle deposition – Kinetic aspects. *Colloids Surf., A* **2013**, *439*, 3-22.

4. Merkel, T. J.; Jones, S. W.; Herlihy, K. P.; Kersey, F. R.; Shields, A. R.; Napier, M.; Luft, J. C.; Wu, H.; Zamboni, W. C.; Wang, A. Z.; Bear, J. E.; DeSimone, J. M. Using mechanobiological mimicry of red blood cells to extend circulation times of hydrogel microparticles. *Proc. Natl. Acad. Sci. USA* **2011**, *108*, 586-591.
5. Johnson, C. A.; Lenhoff, A. M. Adsorption of charged latex particles on mica studied by atomic force microscopy. *J. Colloid Interface Sci.* **1996**, *179*, 587-599.
6. Wiedemair, J.; Serpe, M. J.; Kim, J.; Masson, J.; Lyon, L. A.; Mizaikoff, B.; Kranz, C. In-situ AFM studies of the phase-transition behavior of single thermoresponsive hydrogel particles. *Langmuir* **2007**, *23*, 130-137.
7. Höfl, S.; Zitzler, L.; Hellweg, T.; Herminghaus, S.; Mugele, F. Volume phase transition of ‘‘smart’’ microgels in bulk solution and adsorbed at an interface: A combined AFM, dynamic light, and small angle neutron scattering study. *Polymer* **2007**, *48*, 245-254.
8. Burmistrova, A.; Richter, M.; Eisele, M.; Üzüm, C.; Klitzing, R. The effect of co-monomer content on the swelling/shrinking and mechanical behaviour of individually adsorbed PNIPAM microgel particles. *Polymers* **2011**, *3*, 1575-1590.
9. Mourran, A.; Wu, Y.; Gumerov, R. A.; Rudov, A. A.; Potemkin, I. I.; Pich, A.; Möller, M. M. When colloidal particles become polymer coils. *Langmuir* **2016**, *32*, 723-730.
10. Ando, T.; Uchihashi, T.; Fukuma, T. High-speed atomic force microscopy for nano-visualization of dynamic biomolecular processes. *Prog. Surf. Sci.* **2008**, *83*, 337-437.
11. Ando, T.; Uchihashi, T.; Scheuring, S. Filming biomolecular processes by high-speed atomic force microscopy. *Chem. Rev.* **2014**, *114*, 3120-3188.
12. Imran, A. B.; Esaki, K.; Gotoh, H.; Seki, T.; Ito, K.; Sakai, Y.; Takeoka, Y. Extremely stretchable thermosensitive hydrogels by introducing slide-ring polyrotaxane cross-linkers and ionic groups into the polymer network. *Nat. Commun.* **2014**, *5*, 5124.
13. Sawada, J.; Aoki, D.; Uchida, S.; Otsuka, H.; Takata, T. Synthesis of vinylic macromolecular rotaxane cross-linkers endowing network polymers with toughness. *ACS Macro Lett.* **2015**, *4*, 598-601.
14. Ishiyama, C.; Higo, Y. Effects of humidity on Young’s modulus in poly(methyl methacrylate). *J. Polym. Sci. Part B: Polym. Phys.* **2002**, *40*, 460-465.
15. Pelton, R. H.; Chibante, P. Preparation of aqueous latices with *N*-isopropylacrylamide. *Colloids Surf.* **1986**, *20*, 247-256.

16. Pelton, R. Temperature-sensitive aqueous microgels. *Adv. Colloid Interface Sci.* **2000**, *85*, 1-33.
17. Penzel, E.; Rieger, J.; Schneider, H. A. The glass transition temperature of random copolymers: 1. Experimental data and the Gordon-Taylor equation. *Polymer* **1997**, *38*, 325-337.
18. Lyubchenko, Y.; Shlyakhtenko, L. S.; Ando, T. Imaging of nucleic acids with atomic force microscopy. *Methods* **2011**, *54*, 274-283.
19. Johnson, K. L.; Kendall, K.; Roberts, A. D. Surface energy and the contact of elastic solids. *Proc. R. Soc. London A* **1971**, *324*, 301-313.
20. Carrilla, J. M. Y.; Raphael, E.; Dobrynin, A. V. Adhesion of nanoparticles. *Langmuir* **2010**, *26*, 12973-12979.
21. Butt, H. J.; Pham, J. T.; Kappl, M. Forces between a stiff and a soft surface. *Curr. Opin. Colloid Interface Sci.* **2017**, *27*, 82-90.
22. Israelachvili, J. *Intermolecular and Surface Forces*; Academic Press: London, **1992**.
23. Ghosh, P. K.; Spiro, T. G. *J. Am. Chem. Soc.* **1980**, *102*, 5543–5549.

3. Chapter II

"Monitoring the thermoresponsive behavior of individual microgels"

*Part of this work was published in " Shusuke Matsui, Yuichiro Nishizawa, Takayuki Uchihashi, and Daisuke Suzuki, *ACS Omega* **2018**, *3*, 10836–10842."
(https://pubs.acs.org/doi/abs/10.1021/acsomega.8b01770)

3.1. Introduction

In **Chapter I**, it was found that the softness of microgels plays crucial role for their dynamic adsorption onto solid surfaces in aqueous solution, i.e., the softer microgels the faster adsorption. In the present chapter, the author has demonstrated direct visualization of stimulus-responsive morphological changes in individual microgels with high-spatiotemporal resolution using HS-AFM and light scattering technique. Especially, how highly water-swollen microgels respond to "temperature changes" by combining light scattering technique and temperature-controlled HS-AFM have been investigated (**Figure 3.1**).

3.2. Experimental Section

Materials

N-Isopropyl acrylamide (NIPAm, 98%), *N*,*N*′-methylenebis(acrylamide) (BIS, 97%), sodium dodecyl sulfate (SDS, 95%), and potassium persulfate (KPS, 95 %) were purchased from Wako Pure Chemical Industries (Japan) and used as received. The water used in all reactions, the preparation of solutions, and the purification of polymers was distilled and ion-exchanged (EYELA, SA-2100E1).

Microgel synthesis

PolyNIPAm microgels were synthesized by aqueous free-radical precipitation polymerization. A mixture of NIPAm (8.402 g/99 mol% or 8.063 g/95 mol%), BIS (0.116 g, 1 mol% or 0.578 g/5 mol%), and SDS (0.072 g/0.5 mM for N1) in water (495 mL) was placed in a three-necked round-bottom flask (1000 mL) equipped with a mechanical stirrer, condenser, and nitrogen gas inlet. The

monomer solution was heated in an oil bath to 70 °C under nitrogen sparging (30 min) and constant stirring (250 rpm). After stabilization for 30 min, the KPS initiator (0.270 g/2 mM) dissolved in water (5 mL) was added to the flask to initiate the polymerization reaction. Thereafter, stirring was continued for 4 h before the dispersion was cooled to room temperature. The obtained microgels were purified by two cycles of centrifugation (70,000 *g* or 415,000 *g*; 15 °C), decantation of the supernatant, and redispersion of the precipitate in water. The dispersion was then dialyzed for a week with daily water changes.

Dynamic light scattering (DLS) measurements

The hydrodynamic diameter (D_h) of the microgels was determined by DLS (Malvern Instruments Ltd., ZetasizerNanoS) measurements in aqueous solution. The DLS data represent averages of three individual measurements of 15 consecutive runs (30 s acquisition time of the intensity autocorrelation). The microgel concentration was fixed at 0.001 wt%. The samples were allowed to thermally equilibrate at each temperature for 10 min before the measurements. The time-dependent scattering intensity was detected at a total scattering angle of 173°. The D_h of the microgels was calculated from the measured diffusion coefficients using the Stokes–Einstein equation (Zetasizer software v6.12).

High-speed atomic force microscopy (HS-AFM)

We used the laboratory-built HS-AFM in this study, the details of which are described elsewhere.[1-2] For the HS-AFM imaging, small cantilevers (length: 6–7 μm; width: 2 μm; thickness: 90 nm) developed by Olympus were employed. Typical spring constant, resonant frequency, and quality factor values for the aqueous solution of the cantilever are ~0.1 N/m, ~600 kHz, and ~2, respectively. Because the small cantilever has only a blunt bird-beak structure at the end, a sharp amorphous carbon tip was grown on the original tip by electron beam deposition. Then the carbon tip was etched to ~4 nm in radius by a RF plasma etcher under an argon atmosphere. For the HS-AFM imaging of the microgels, the cantilever free-oscillation amplitude was set to 5–30 nm and the set-point amplitude to 70–90% of the free-oscillation amplitude (depending on the size of the microgels).

Droplets (3 μL) including the microgel dispersion ([microgel] = 0.001 wt%) were loaded on highly oriented pyrolytic graphite (HOPG) substrates. After incubation (5 min), the substrate was

thoroughly rinsed with pure water to remove residual microgels, and HS-AFM imaging was performed at room temperature ($T \approx 25$ °C; scanning area: 1000 × 1000 nm^2; 120 × 120 pixels^2; frame rate = 1 fps).

To monitor the real-time thermo-responsive morphological changes in the microgels, a temperature control device was equipped in the HS-AFM. Heating the solution was carried out by flowing a DC current through indium-tin-oxide (ITO) glass at the bottom of the cantilever holder. The thermocouple was attached to the cantilever holder and immersed in the solution. The solution temperature can be controlled by a feedback control on the software of the HS-AFM. Using this system, the temperature of the aqueous solution within the HS-AFM fluid cell was increased at a rate of ~1.5 °C / min. The temperature was measured every 10 s at different values of input voltage (1.7 to +0.2 V every 30 s) and plotted as a function of time (**Figure 3.1(b)**).

3.3. Results and discussion

3.3.1. Synthesis and characterization of thermoresponsive microgels

Thermo-responsive microgels were obtained from the aqueous free-radical precipitation polymerization of *N*-isopropyl acrylamide (NIPAm) and the cross-linker *N*,*N*'-methylenebis(acrylamide) (BIS; 1 or 5 mol%; hereafter denoted N1 and N5, respectively) (**Table 3.1**). **Figure 3.2** shows the hydrodynamic diameter (D_h) of the polyNIPAm microgels in water as a function of the temperature determined by dynamic light scattering (DLS). The D_h of the microgels decreases with increasing temperature, reaching an equilibrium at ~40 °C. The volume phase transition temperature (VPTT) for N1 and N5 was estimated to be ~33 °C and ~35 °C, respectively, based on the maximum change ratio of the volume of the microgels.

Table 3.1. Chemical composition and DLS-derived D_h values for the microgels in aqueous solution.

Code	NIPAm [mol%]	BIS [mol%]	D_h at 25 °C [nm]	D_h at 40 °C [nm]
N1	99	1	396 ± 15	157 ± 1
N5	95	5	450 ± 28	242 ± 1

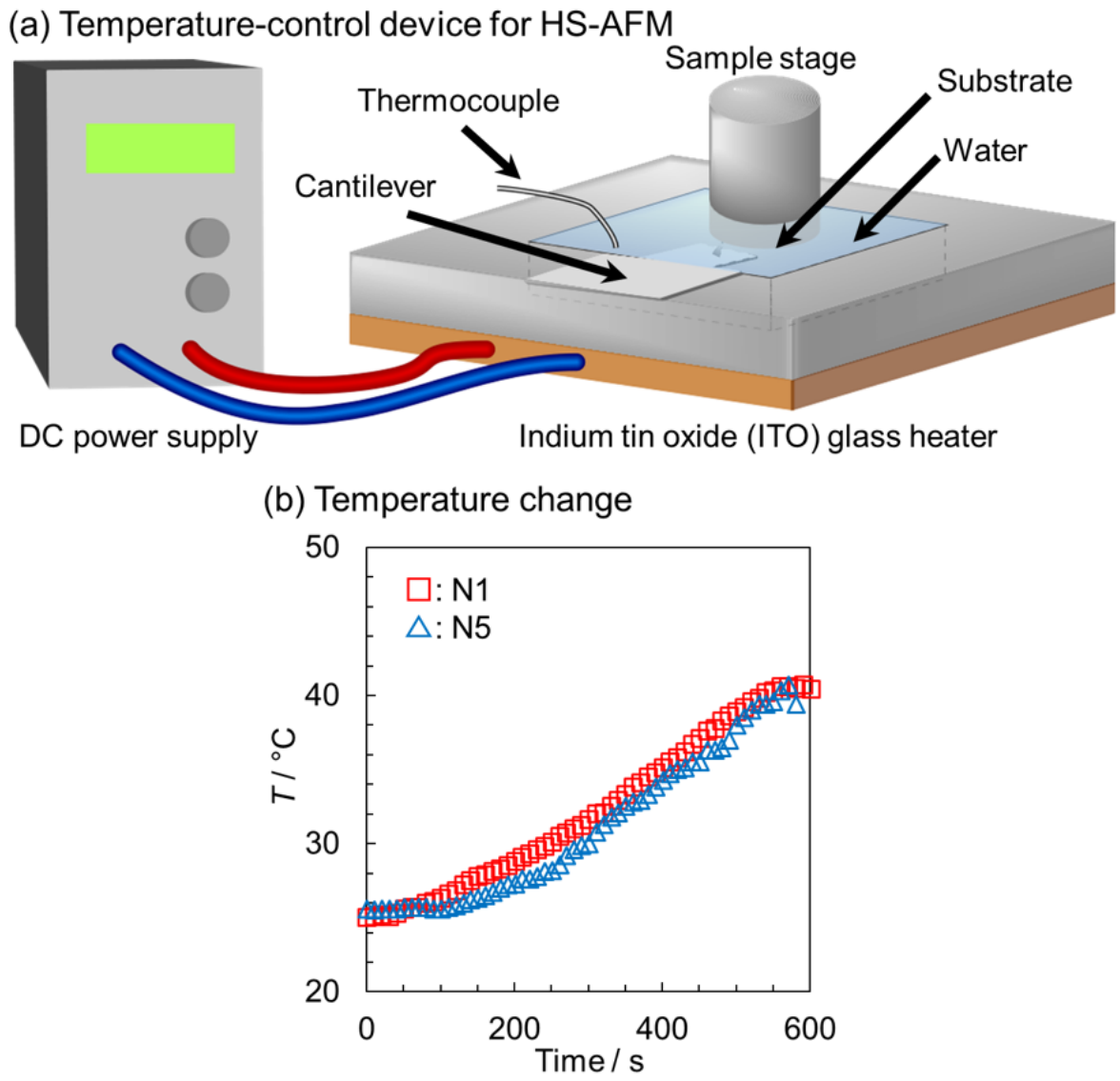

Figure 3.1. (a) Schematic illustration of the HS-AFM apparatus equipped with the temperature-control device. **(b)** Time dependence of the temperature change in the sample holder during the HS-AFM measurements.

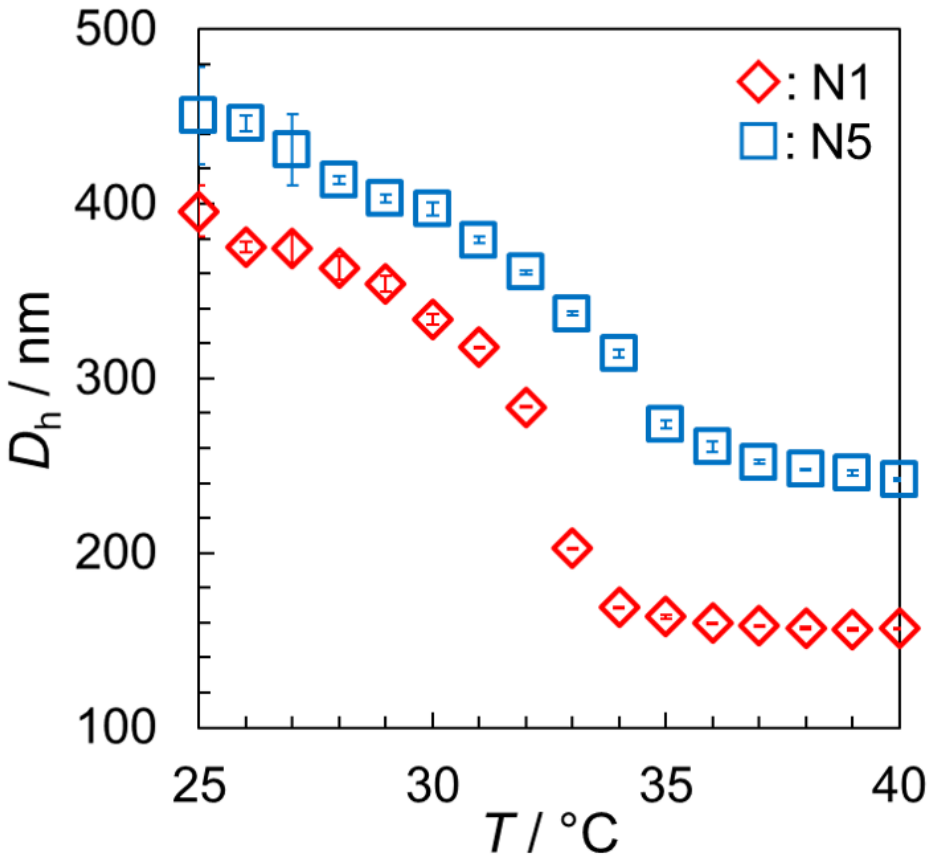

Figure 3.2. Temperature dependence of the DLS-derived D_h values of N1 and N5 microgels in aqueous solution.

3.3.2. Observation of the thermoresponsive behavior of microgels using HS-AFM

In order to visualize the microgels deposited on a substrate by HS-AFM, 3 μL of a microgel dispersion (0.001 wt%) were placed on a highly oriented pyrolytic graphite (HOPG) substrate. Subsequently, the substrate was thoroughly rinsed with pure water to remove any excess microgels. The adsorbed microgels on the HOPG substrate were imaged by HS-AFM in pure water at room temperature (~25 °C) and then, the temperature-control device was employed to heat the solution (~1.5 °C/min) during the imaging (**Figure 3.1(b)**). **Figure 3.3(a)** shows clipped HS-AFM images of the N1 microgels during the heating. The N1 microgels exhibited an inhomogeneously collapsed morphology surrounded by a flattened corona of a loosely cross-linked polymer shell at 25 °C (**Figure 3.3(a)**), which is probably due to their highly soft nature. Here, a maximum height of the adsorbed microgels was approximately 50 nm ((**Figure 3.3(b)** at 25.0 °C and **Figure 3.3(e)**),

which was ~8 times smaller than D_h of the N1 microgels at 25 °C (396 nm), indicating highly deformed N1 microgels on the substrate due to their high softness. Upon heating the solution, the height of the N1 microgels gradually decreased (**Figure 3.3(e)**). During the whole process, the N1 microgels exhibited an inhomogeneous and non-hemispherical morphology (**Figures 3.3(a)** and **3.3(b)**). In contrast, the N5 microgels with a higher cross-linking density exhibited a relatively hemispherical morphology at 25 °C compared to that of the N1 microgels on the same substrate. Here, a maximum height of the adsorbed N5 microgel was 146 nm (**Figure 3.3(d)** at 25.6 °C and **Figure 3.3(f)**), which was ~3 times smaller than the D_h of the N5 microgels at 25 °C (450 nm). Upon heating the solution, the N5 microgels gradually contracted, and then, polymer-rich domains clearly appeared on the surface (**Figure 3.3(c)**).

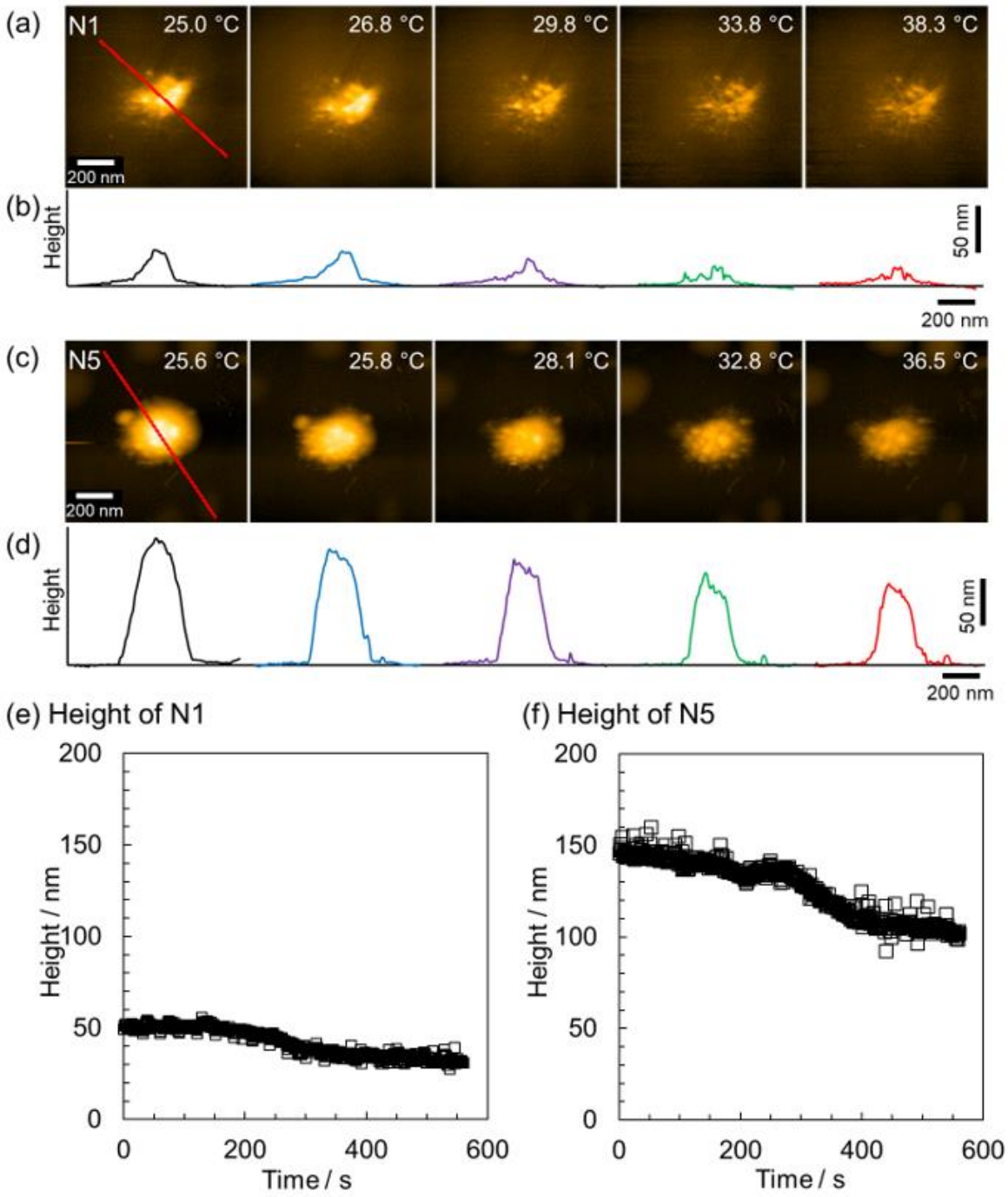

Figure 3.3. HS-AFM images of **(a)** N1 and **(c)** N5 microgels as a function of the temperature. Temperature dependence for the cross-section profiles of **(b)** N1 and **(d)** N5. **(e, f)** Time dependence of the maximum height of **(e)** N1 and **(f)** N5 measured from the HS-AFM images.

3.3.3. Relationship between the height of the microgels on the substrate and D_h

Figure 3.4 shows the temperature dependences of the normalized height of the microgels determined by the HS-AFM images and the normalized D_h of the microgels determined by DLS. Here, the heights and D_h of the microgels correspond to non-equilibrium and equilibrium state of the microgels at each temperature, respectively. Both the height and D_h of the N1 microgels gradually decreased up to ~31 °C and then rapidly decreased up to the VPTT (~33 °C), above which both the height and D_h approached the equilibrium state (**Figure 3.4(a)** and **(b)**). In the case of the N5 microgels with a higher cross-linking density, both the height and D_h gradually decreased up to the VPTT (~35 °C), above which both the height and D_h reached a near-equilibrium state (**Figure 3.4(c)** and **(d)**). Since the tendencies of the temperature dependence for the normalized height and D_h of these microgels are similar, it can be concluded that the size change of the microgels detected by HS-AFM must follow the temperature change on the individual microgel level. This behavior seems to be reflected in the rapid stimulus-responsiveness of microgels.

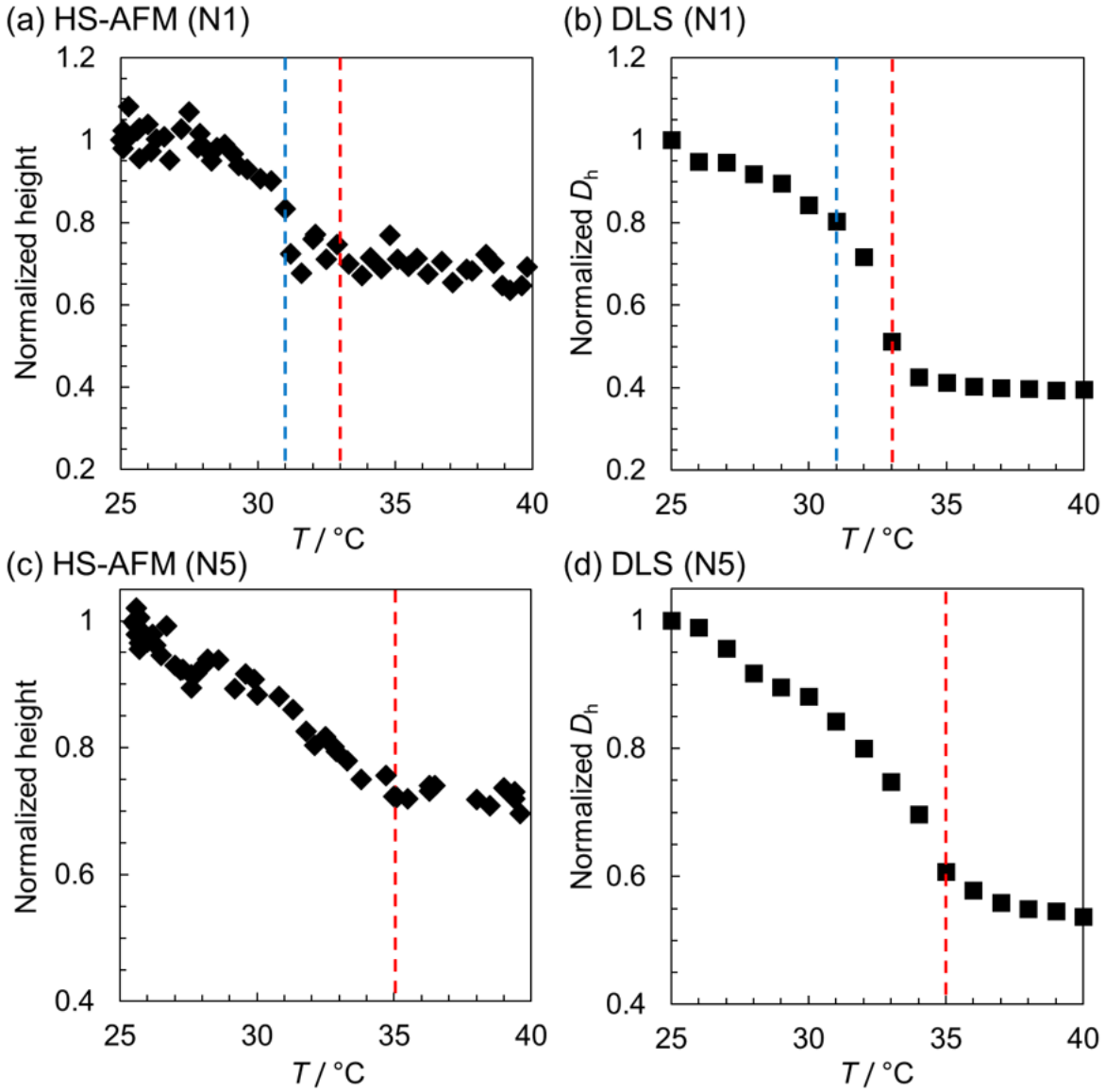

Figure 3.4. Normalized height of **(a)** N1 and **(c)** N5 microgels measured by HS-AFM imaging, and normalized D_h (**b**: N1 and **d**: N5) determined by DLS as a function of the temperature.

3.3.4. Magnified time-lapse HS-AFM images of an individual N5 microgel

Figure 3.5 shows the magnified HS-AFM images for the N5 microgels upon heating the solution. While the microgels gradually contracted, domains (several tens of nanometer in size) continuously and simultaneously formed on the microgels even at ~27.0 °C, i.e., well below the VPTT of the microgels (~35 °C). These domains persisted near the VPTT and did not disappear, not even at near 40 °C, where the microgels had almost entirely collapsed. According to a previous

study using small-angle neutron scattering (SANS), swollen pNIPAm-based microgels prepared by precipitation polymerization in aqueous solution present a core–shell structure with uniform segment distribution within the core and thin shell (~20 nm), where the shell thickness is not affected by the temperature.[3] Considering the present study, the surface and/or shell of the microgels may not always exhibit a uniform structure, that may transform into a inhomogeneous raspberry structure upon heating. On the other hand, Höfl et al. have observed the appearance of a surface pattern on pNIPAm-based microgels adsorbed on a substrate above the VPTT by conventional AFM.[4] They speculated that such surface patterns are probably due to the presence of collapsed dangling polymer chains that lead to rigid globules on the microgel surface.[4] Additionally, Ikkai et al. have observed a microphase separation (size scale: 20–30 nm) in a weakly charged microgel near the VPTT by SANS[5] that is comparable to the domain size found in the present study. Based on these reports, the formation of domains observed in the present study upon increasing the temperature should presumably be attributed to polymer collapsing and/or polymer–polymer association. The author has clarified that the domain formation occurs gradually at temperatures below the VPTT, and that the domain formation as well as the contraction of the microgels occurs simultaneously upon increasing the temperature.

It should be noted that the density fluctuation near the volume phase transition is largely influenced by the adsorption of the microgels on the solid substrate.[6] This means that the thermo-responsive behavior of microgels in the dispersed state or adsorbed on a solid substrate might be different, although reports describing such differences in detail remain elusive. Nevertheless, the author believe that the findings in the present study are significant and help clarify the relationship between the morphology/structure and physical properties of microgels adsorbed on solid substrates, which may lead to the development of advanced functional materials, such as switchable cell culture substrates for tissue engineering,[7] where the surface roughness as well as hydrophilicity/hydrophobicity are important parameters.

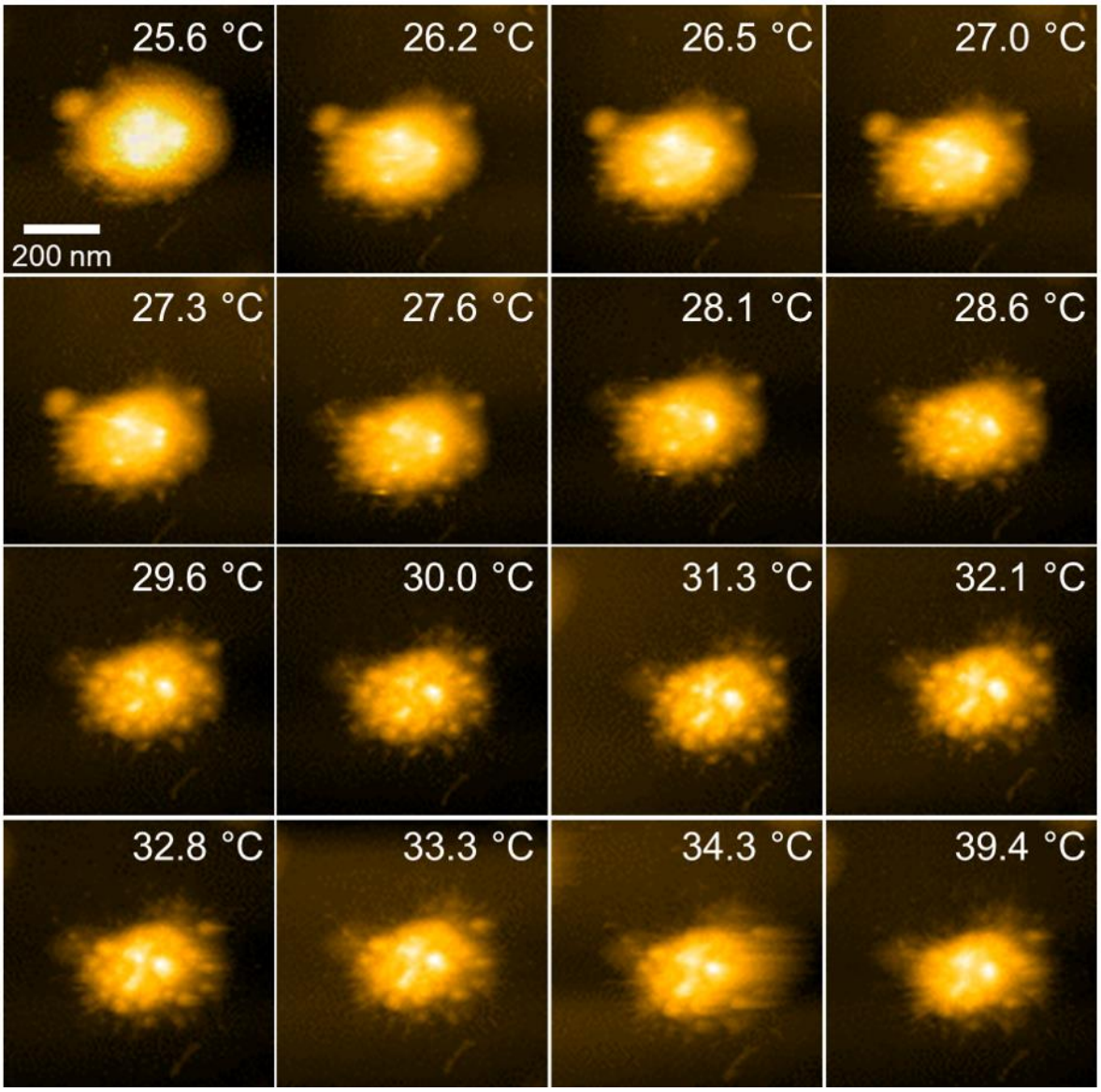

Figure 3.5. Detailed time-lapse HS-AFM images of an individual N5 microgel as a function of the temperature.

3.4. Conclusions

The author has successfully observed temperature-induced morphological changes on individual microgels at the nanoscale in real time by temperature-controlled HS-AFM. The morphology of substrate-adsorbed microgels varies with cross-linking density. The change of shape of the microgels follows the change in temperature, whereby the normalized height and D_h of the microgels showed similar behavior due to the rapid stimulus-responsiveness of the microgels. Furthermore, the formation of domains was observed during the collapse of the microgel structures,

even below the VPTT; these domains persist, even in the collapsed state, which indicates that the contracted microgel state may not always be a homogeneous sphere, but often an inhomogeneous raspberry shape. The direct visualization of the behavior of individual microgels on the nanoscale is important to gain further insight into thermo-responsive materials. In the near future, it should be possible to apply temperature-controlled HS-AFM to a wider range of temperatures and stimulus-responsive materials, which may further accelerate the development of novel smart materials.

3.5. References

1. Ando, T.; Uchihashi, T.; Scheuring, S. Filming biomolecular processes by high-speed atomic force microscopy. *Chem. Rev.* **2014**, *114*, 3120–3188.
2. Matsui, S.; Kureha, T.; Hiroshige, S.; Shibata, M.; Uchihashi, T.; Suzuki, D. Fast adsorption of soft hydrogel microspheres on solid surfaces in aqueous solution. *Angew. Chem., Int. Ed.* **2017**, *56*, 12146–12149.
3. Saunders, B. R. On the structure of poly(*N*-isopropylacrylamide) microgel particles. *Langmuir* **2004**, *20*, 3925–3932.
4. Höfl, S.; Zitzler, L.; Hellweg, T.; Herminghaus, S.; Mugele, F. Volume phase transition of ‘‘smart’’ microgels in bulk solution and adsorbed at an interface: A combined AFM, dynamic light, and small angle neutron scattering study. *Polymer* **2007**, *48*, 245-254.
5. Ikkai, F.; Shibayama, M. Gel-size dependence of temperature-induced microphase separation in weakly-charged polymer gels. *Polymer* **2007**, *48*, 2387−2394.
6. Wellert, S.; Hertle, Y.; Richter, M.; Medebach, M.; Magerl, D.; Wang, W.; Demé, B.; Radulescu, A.; Müller-Buschbaum, P.; Hellweg, T.; Klitzing, R. Inner structure of adsorbed ionic microgel particles. *Langmuir* **2014**, *30*, 7168−7176.
7. Schmidt, S.; Zeiser, M.; Hellweg, T.; Duschl, C.; Fery, A.; Möhwald, H. Adhesion and mechanical properties of PNIPAM microgel films and their potential use as switchable cell culture substrates. *Adv. Funct. Mater.* **2010**, *20*, 3235–3243.

4. Chapter III

"Development of fast-driven autonomously oscillating microgels"

*Part of this work was published in " Shusuke Matsui, Kohei Inui, Yuki Kumai, Ryo Yoshida, and Daisuke Suzuki, *ACS Biomaterials Science & Engineering*, in press,
DOI: 10.1021/acsbiomaterials.8b00850"
(https://pubs.acs.org/doi/10.1021/acsbiomaterials.8b00850)

4.1. Introduction

Through **Chapter I** to **II**, the typical dynamic behaviors of conventional stimulus-responsive microgels, such as adsorption onto solid/liquid interface, and temperature-responsiveness, were evaluated using HS-AFM visualization and other ensemble measurements. Consequently, the insight into dynamic behaviors of stimulus-responsive microgels deepened and new design guidelines for microgels were found. As mentioned in **Introductory remarks**, the next challenge is development of autonomously oscillating microgels, which stand advancement of conventional stimulus-responsive microgels.

One of the characteristics of the oscillating microgels that need to be controlled for future applications is their oscillation period, i.e., driving-speed. In this context, it is especially important to shorten the oscillation from a materials science perspective. If the potential for the rapid stimuli-responsiveness of microgels can be fully used, applications such as new types of fast-driven actuators similar to the human heart beat are conceivable. However, the difficulty associated with shortening the oscillation period of the microgels is due to the fact that microgels aggregate irreversibly at higher temperatures, i.e. around the VPTT. The microgels become increasingly hydrophobic due to the shrinking of the polymer chain, and interparticle electrostatic repulsion is screened under high ionic strength conditions, where the BZ reaction occurs at high frequency. So far, one study has reported a “macrogel” based on a non-thermo-responsive polymer that increases the reaction substrate concentration and temperature condition for oscillation. The shortest hitherto reported oscillation period (2 s) has been observed for a non-thermo-responsive poly(vinylpyrrolidone-*co*-Ru(bpy)$_3$) macrogel by increasing the reaction temperature to 46 °C.[1]

However, more recently, another group has reported that such a non-thermo-responsive poly(*N,N'*-dimethylacrylamide-*co*-Ru(bpy)$_3$) macrogels do not exhibit swelling/deswelling oscillations.[2] Therefore, microgels with higher VPTTs are required not only to suppress microgel aggregation and to conduct the oscillation reaction at higher temperature, but also to enable swelling/deswelling and dispersing/flocculating oscillation.

In this chapter, the author designed a new type of oscillating microgel that is able to withstand high temperatures in order to achieve fast swelling/deswelling and dispersing/flocculating oscillation. For that purpose, a neutral and hydrophilic acrylamide (AAm) monomer was introduced as a comonomer in a conventional pNIPAm-based oscillating microgel with the expectation to increase the VPTT of these microgels. Since the BZ reaction must be conducted under high ionic conditions (>300 mM),[3] charged monomers are not suitable to increase the VPTT due to the charge screening effect. In addition, the chemical structure of AAm is similar to that of NIPAm, and thus, it seems feasible to expect a successful copolymerization.[4] After generating such fast-oscillating microgels, the author attempted to prepare a microgel-organized macrogel that exhibits fast swelling/deswelling oscillation.

4.2. Experimental Section

Materials

N-isopropyl acrylamide (NIPAm, 98%), acrylamide (AAm, 95%), *N*-(3-aminopropyl)methacrylamide hydrochloride (APMA), *N*,*N*′-methylenebis(acrylamide) (BIS, 97%), 2,2'-azobis(2-methylpropinamidine)dihydrochloride (V-50, 95%), sodium chloride (NaCl, 99.5%), malonic acid (MA, 98%), sodium bromate ($NaBrO_3$, 99.5%), nitric acid (HNO_3, 16 M), cerium(III) sulfate *n*-hydrate ($Ce(SO_4)\cdot nH_2O$, 78–88%), cerium(IV) sulfate tetrahydrate ($Ce(SO_4)_2\cdot 4H_2O$), heptane (97%), and ethanol (99.5%) were purchased from Wako Pure Chemical Industries and used as received. A glutaraldehyde solution (50 wt% in H_2O) was purchased from Sigma-Aldrich and used as received. The Ru(bpy)$_3$ monomer, [Ru(II)(4-vinylinyl-4'-methyl-2,2'-bipyridine)bis(2,2'-bipyridine)][PF_6]$_2$, was synthesized according to a previously reported method.[5] Distilled and ion-exchanged water (EYELA, SA-2100E1) was used for all reactions, solutions, purification procedures, and measurements.

Microgel synthesis

Poly(NIPAm-*co*-AAm-*co*-Ru(bpy)$_3$) microgels were synthesized by a surfactant-free aqueous radical precipitation polymerization.[6] For that purpose, a mixture of NIPAm, AAm, Ru(bpy)$_3$, BIS, and water (25 mL) was placed in a three-necked round-bottom flask (50 mL) equipped with a stirrer, a condenser, and a nitrogen gas inlet. The comonomer ratio (NIPAm : AAm : Ru(bpy)$_3$: BIS) was varied according to the desired AAm and Ru(bpy)$_3$ content, while the cross-linker (BIS) concentration remained constant. Under nitrogen sparging and constant stirring, the solution was heated in an oil bath to 70 °C or 90 °C. After stabilization of the solution for 30 min, the initiator (V-50, 2 mM) was dissolved in water (5 mL) and added to the flask to start the polymerization, which was allowed to proceed for 4 h, before the resulting dispersion was cooled to room temperature. The obtained microgels were purified twice by repeated centrifugation (415,000 × *g* at 25 °C), decantation of the supernatant, and re-dispersion of the precipitate in water. The dispersion was then dialyzed for several days with daily water replacements. The obtained microgels are denoted as NA*X*Ru*Y*(*Z*), wherein N, A, and Ru refer to NIPAm, AAm, and Ru(bpy)$_3$, respectively, while *X* and *Y* represent the mole percentage of AAm and Ru(bpy)$_3$ added to the polymerization reaction, respectively, while *Z* denotes the polymerization temperature.

In order to obtain a macrogel assembled from autonomously oscillating microgels, a poly(NIPAm-*co*-AAm-*co*-APMA-*co*-Ru(bpy)$_3$) microgel was synthesized by a surfactant-free aqueous radical precipitation polymerization in the same way. A mixture of NIPAm (57 mol%), AAm (20 mol%), BIS (20 mol%), Ru(bpy)$_3$ monomer (2 mol%), and APMA (1 mol%) in water (75 mL) was poured in a three-necked round-bottom flask (200 mL) equipped with a mechanical stirrer, condenser, and nitrogen gas inlet. The initial total monomer concentration was maintained at 75 mM. The monomer solution was heated in an oil bath to 90 °C under nitrogen sparging for 30 min and constant stirring (250 rpm). After stabilization for 30 min, the initiator (V-50, 2 mM) dissolved in water (5 mL) was added to the flask to initiate the polymerization. This mixture was stirred for 4 h, after which the dispersion was cooled to room temperature. The thus obtained microgels were purified two times by repeated centrifugation (415,000 × *g* at 25 °C), decantation of the supernatant, and re-dispersion of the precipitate in water. The dispersion was then dialyzed for several days with daily water replacements. APMA was selected to provide the microgels with amino groups and allow the covalent cross-linking of the microgels. Here, glutaric dialdehyde was used to induce a chemical reaction between the amino groups located on the exterior of the microgels, as described in a previous report.[7]

Quantification of the amount of $Ru(bpy)_3$ incorporated in the microgels

The amount of $Ru(bpy)_3$ contained within the microgels was determined based on the amount of $Ru(bpy)_3$ remaining in the supernatant after the centrifugation of the dispersion. The amount of $Ru(bpy)_3$ in the supernatant was determined by UV-vis spectroscopy (JASCO, V-630iRM). The measurement wavelength was 458 nm, corresponding to the maximum absorbance of $[Ru(bpy)_3]^{2+}$. The measurements were performed at 25 °C. Before the measurements, the samples were allowed to thermally equilibrate at 25 °C for 10 min.

Hydrodynamic diameter of the microgels

The D_h of the microgels in water was measured by dynamic light scattering (DLS, Malvern Instruments Ltd., ZetasizerNanoS). In the microgels the $Ru(bpy)_3$ concentration of all samples was adjusted to 100 µM. The samples of the reduced $[Ru(bpy)_3]^{2+}$ state contained 1 mM Ce^{3+} and 300 mM HNO_3, while the oxidized $[Ru(bpy)_3]^{3+}$ samples included 1 mM Ce^{4+} and 300 mM HNO_3. The $Ru(bpy)_3$ moieties in the microgels were oxidized or reduced by the Ce^{4+} or Ce^{3+} ions, respectively. Before the DLS measurements, all samples were allowed to equilibrate thermally at the desired temperature for 10 min. The averaged value of 3 sets of 15 measurements with a 30 s acquisition time for intensity autocorrelation was taken. The scattering intensity was measured at 173°. The D_h value of the microgels was calculated from the measured diffusion coefficients using the Stokes-Einstein equation (Zetasizer software v7.12).

Measurement of the critical flocculation temperature of the microgels

The temperature dependence of the optical transmittance of the microgel dispersions was monitored by UV-vis spectroscopy (JASCO, V-630iRM). The measurements were conducted at 25 °C to 70 °C (heating rate: 0.5 °C/min) under constant stirring (800 rpm). The microgels were dispersed in a solution containing 1 mM Ce^{3+} and 300 mM HNO_3 (reduced $[Ru(bpy)_3]^{2+}$ state) or in a solution containing 1 mM Ce^{4+} and 300 mM HNO_3 (oxidized $[Ru(bpy)_3]^{3+}$ state). The $Ru(bpy)_3$ concentration in the microgels in all systems was adjusted to 100 µM. Here, the measurement wavelength was 570 nm, corresponding to the isosbestic point of $[Ru(bpy)_3]^{2+}$ and $[Ru(bpy)_3]^{3+}$ in order to eliminate any effects of the absorption of the Ru complex on the transmittance.

Oscillation behavior of the microgel dispersions

The oscillatory behavior of the microgels was detected by UV-vis spectroscopy (JASCO, V-630iRM) as changes in the optical transmittance as a function of time. A mixture of HNO_3, $NaBrO_3$, and a microgel dispersion was poured in the sample holder and, after 10 min of thermal equilibration, the oscillation reaction was initiated by adding MA (the final volume was adjusted to 2.5 mL). Measurements were performed at 570 nm, which is the isosbestic point of $[Ru(bpy)_3]^{2+}$ and $[Ru(bpy)_3]^{3+}$, under constant stirring at 800 rpm at the desired temperature. In a bulk solution without microgels (used as the control), the BZ reaction was performed and data were obtained at 458 nm, which is the wavelength of the maximum absorbance of $[Ru(bpy)_3]^{2+}$. The $Ru(bpy)_3$ concentration in all oscillation reaction systems was adjusted to 100 μM. The oscillation periods and amplitudes of transmittance in this study were averaged between the second and sixth oscillations.

Preparation of a macrogel composed of oscillating microgels

Concentrated microgel dispersions (pastes; final concentration: 8 wt%) containing 10 mM $NaBrO_3$ were prepared at 28 °C by centrifugation. For that purpose, the paste (1.2 g) and 500 μL of heptane were placed in a sample tube, and the mixture was stirred using a magnetic stirrer at 25 °C and 800 rpm to prepare an oil in water emulsion, which is defined by oil droplets that are dispersed in the microgel dispersion and stabilized by adsorption of microgels, which act as surfactants on the water-oil interface,[8, 9] in order to create spaces or voids within the macrogel. These spaces were created to increase the amplitude of the swelling/deswelling oscillation. An aqueous glutaraldehyde solution (30 μL, 50 wt%) was added to the emulsion in order to induce a chemical reaction between the amino groups located on the microgel exterior. The reaction was continued at 4 °C overnight, before the heptane was removed using a mixture of ethanol and water. In this study, the macrogel was cut into pieces of approximately 1 mm × 1 mm × 1 mm in size.

Oscillatory behavior of the macrogel

The oscillation behavior of the macrogel was examined with an optical microscope (LZ-LED-T, Kenis) equipped with a digital camera (ImageX Earth Type S-2.0M, Kikuchi-Optical Co., Ltd). The cubic-shaped macrogel was immersed in 750 μL of an aqueous solution containing $NaBrO_3$

and HNO_3. After 30 min for equilibration, 150 μL of an MA solution was injected to the solution to start the BZ reaction (final volume: 1 mL; MA: 300 mM, $NaBrO_3$: 300 mM, and HNO_3: 500 mM, at 35 °C). Images of the macrogel were collected every 2 s using the ImageX Earth Type S-2.0M Version 3.0.5 software and are presented as a spatiotemporal series.

4.3 Results and Discussion

4.3.1. Synthesis of poly(NIPAm-*co*-AAm-*co*-Ru(bpy)$_3$) microgels

Poly(NIPAm-*co*-AAm-*co*-Ru(bpy)$_3$) microgels were synthesized by a surfactant-free aqueous radical precipitation polymerization (**Figure 4.1** and **Table 4.1**). Initially, the polymerization was conducted at 70 °C using a conventional method.[6] At values over 20 mol% of added AAm, microgels were not obtained (**Table 4.1, entries 1–3, "N.A."**). It was considered that nucleation did not occur since the polymer chains were not in globular state at 70 °C due to the increased lower critical solution temperature (LCST) upon copolymerization of NIPAm with the more hydrophilic AAm. During the precipitation polymerization, all monomers are soluble in water, whereas the polymer chains undergo phase separation into globules and precipitate above the LCST of the polymer. Then, homogeneous nucleation occurs and colloidal stable microgel particles are formed via a growing process.[10, 11] Consequently, the polymerization was conducted at higher temperature, 90 °C. As a result, the microgels could be obtained and the amount of AAm fed into the polymerization reaction could be increased up to a maximum of 20 mol% (**Table 4.1, entries 4–7**). However, with increasing amount of AAm, the amount of Ru(bpy)$_3$ incorporated in the microgels decreased (**Table 4.1, entries 4–7**). To increase the amount of Ru(bpy)$_3$ incorporated in the microgels, the amount of added Ru(bpy)$_3$ was increased (**Table 4.1, entry 8-9**), since the VPTT increases with the number of charged groups fixed in the gel matrix.[12]

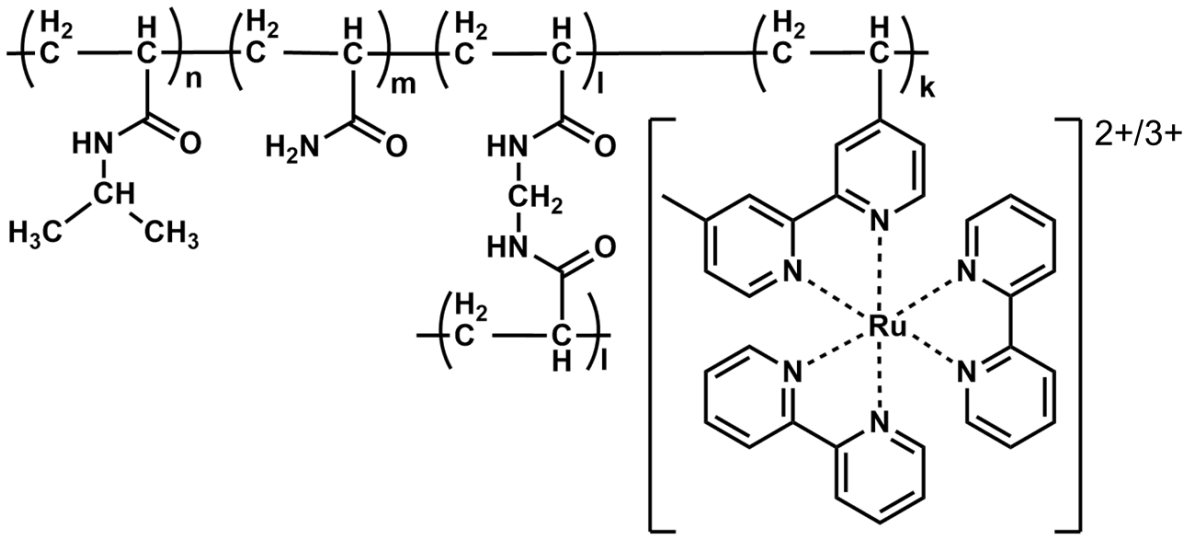

Figure 4.1. Chemical structure of poly(NIPAm-*co*-AAm-*co*-Ru(bpy)$_3$) microgels.

Table 4.1. Synthetic conditions, hydrodynamic diameter, amount of Ru(bpy)$_3$ incorporated in the oscillating microgels, and CFT of the microgels in the reduced and oxidized Ru(bpy)$_3$ state. 'NA': microgels could not be obtained.

entry	code	NIPAm [mol%]	AAm [mol%]	Ru(bpy)$_3$ [mol%]	BIS [mol%]	temp. [°C]	D_h at 25 °C [nm]	Ru(bpy)$_3$ introduced [mol%]	CFT [°C]	
									reduced Ru^{2+}	oxidized Ru^{3+}
1	NRu2(70)	93	0	2	5	70	184±6	0.81	33	46
2	NA10Ru2(70)	83	10	2	5	70	154±2	0.56	37	45
3	NA20Ru2(70)	73	20	2	5	70	NA	NA	NA	NA
4	NRu2(90)	93	0	2	5	90	152±2	1.06	31	51
5	NA10Ru2(90)	83	10	2	5	90	132±1	0.71	35	65
6	NA20Ru2(90)	73	20	2	5	90	135±2	0.56	41	68
7	NA30Ru2(90)	63	30	2	5	90	NA	NA	NA	NA
8	NA20Ru3(90)	72	20	3	5	90	161±1	0.98	42	>70
9	NA20Ru4(90)	71	20	4	5	90	126±5	0.66	39	58

4.3.2. Evaluation of the critical flocculation temperature of microgels

In order to confirm the increase in VPTT due to the introduction of AAm in the microgels, the temperature dependence of optical transmittance for microgel dispersions in the reduced $[Ru(bpy)_3]^{2+}$ and oxidized $[Ru(bpy)_3]^{3+}$ states under $[HNO_3]$ = 300 mM aqueous solution, which is close to the reaction conditions of the BZ reaction, were investigated (**Figure 4.2 and 4.3**). The

transmittance decreased with shrinking microgels upon increasing the temperature and it increased after reaching a minimum point. As we confirmed in our previous study, the increased transmittance above the minimum point is due to the flocculation of the microgels.[29] Thus, the inflection point of the transmittance is defined as the critical flocculation temperature (CFT). The CFT values for the microgels are shown in **Table 4.1**. All microgels in the oxidized $[Ru(bpy)_3]^{3+}$ state have a higher CFT than those in the reduced $[Ru(bpy)_3]^{2+}$ state, which is due to the increased hydrophilicity of the $[Ru(bpy)_3]^{3+}$ moieties in the copolymer chain relative to that of the $[Ru(bpy)_3]^{2+}$ moieties.[13] The CFT of the microgels in both reduced and oxidized $Ru(bpy)_3$ states increases with increasing amount of AAm in the polymerization. Compared with conventional NRu2(90) microgels that do not contain AAm, the oxidized $[Ru(bpy)_3]^{3+}$ states of NA20Ru2(90) microgels exhibit a greater CFT increase than that for the reduced states, i.e., the CFT of the reduced states increased by 10 °C (NRu2(90): 31 °C → NA20Ru2(90): 41 °C), while that of the oxidized states increased by 18 °C (NRu2(90): 51 °C → NA20Ru2(90): 68 °C). It seems that the increase in hydrophilicity may arise from a synergistic effect of the oxidized state of $Ru(bpy)_3$ and the copolymerization with AAm leads, which to a larger increase in the CFT. In order to further increase the CFT of the microgels, the amount of $Ru(bpy)_3$ in the polymerization was increased (**Table 4.1, entry 8)**. As a result, the CFT in the reduced $[Ru(bpy)_3]^{2+}$ state barely changed, but the CFT of the oxidized $Ru(bpy)_3^{3+}$ species increased further (reduced state; NA20Ru2(90): 41 °C → NA20Ru3(90): 42 °C; oxidized state; NA20Ru2(90): 68 °C → NA20Ru3(90): > 70 °C). In order to confirm the volume change of the microgels that accompanies the redox reaction, the temperature dependence of the hydrodynamic diameter of the NRu2(90) and NA20Ru3(90) microgels in the reduced and oxidized $Ru(bpy)_3$ states was monitored by DLS (**Figure 4.4**). The differences in colloidal stability of the microgels between the reduced $[Ru(bpy)_3]^{2+}$ and oxidized $[Ru(bpy)_3]^{3+}$ states is due to the aforementioned hydrophilicity of the $[Ru(bpy)_3]^{2+/3+}$ moieties in the copolymer chain.[13] The difference in the diameter of the microgels for the reduced and oxidized $Ru(bpy)_3$ states below the temperature at which the microgels aggregate was considered the predicted volume change during oscillation.[6] In the NA20Ru3(90) microgel, the volume change (maximum diameter change ratio: ~15 % at 20 °C) derived from pNIPAm was confirmed even after copolymerization with AAm. Based on these results, the author envisioned that the NA20Ru3(90) microgel should be able to withstand the BZ reaction conditions that are required

for short oscillation periods (e.g. high ionic concentration and high temperature) without losing volume change.

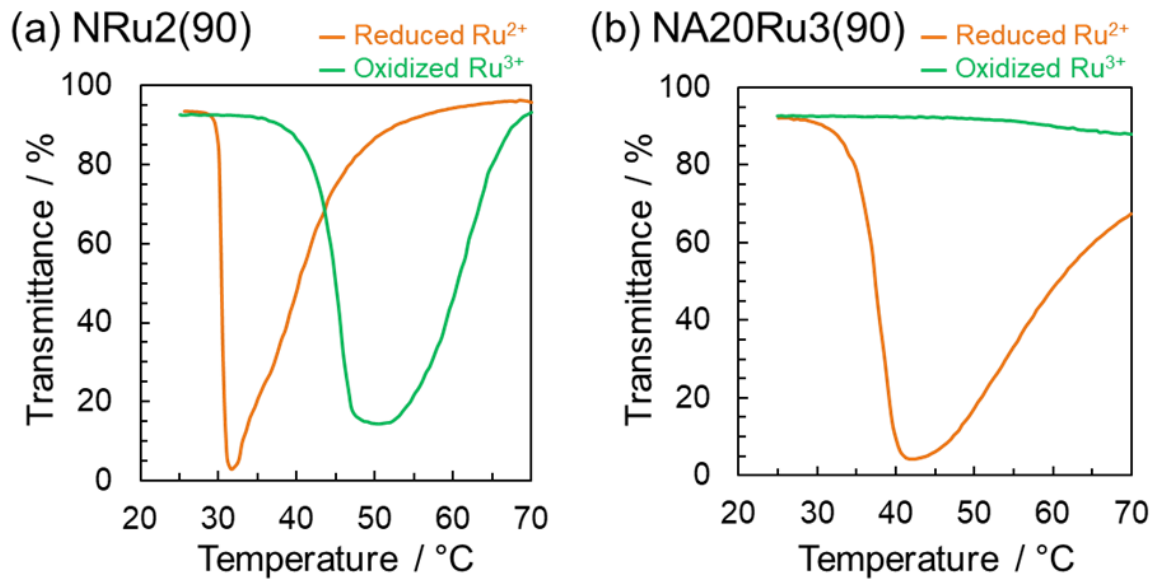

Figure 4.2. Temperature dependence of the optical transmittance of **(a)** NRu2(90) and **(b)** NA20Ru3(90) microgels ([$Ru(bpy)_3$] = 100 μM) in the reduced (1 mM Ce^{3+} and 300 mM HNO_3; orange line) and oxidized (1 mM Ce^{4+} and 300 mM HNO_3; green line) $Ru(bpy)_3$ states.

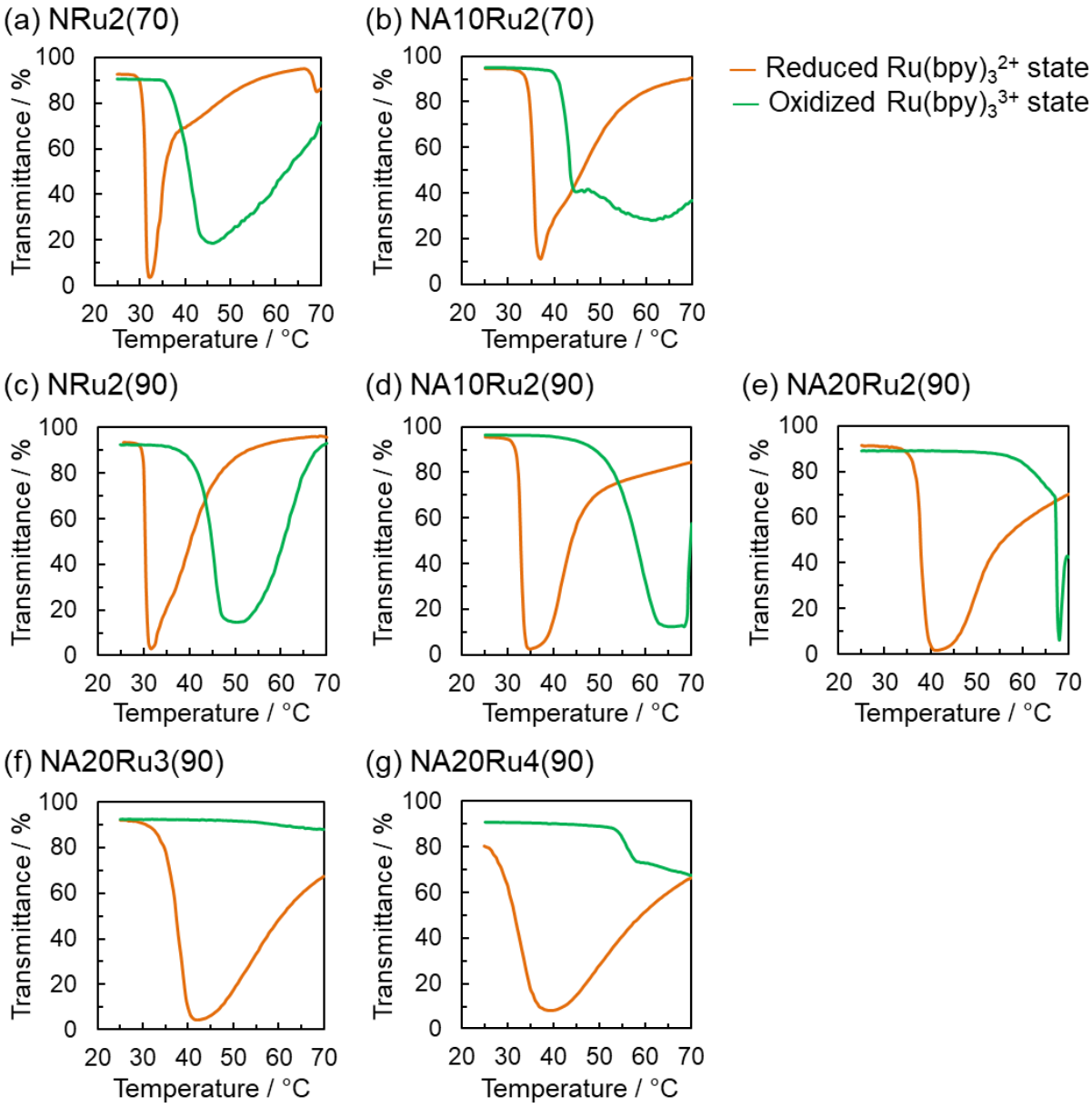

Figure 4.3. Temperature dependence of the optical transmittance of **(a)** NRu2(70), **(b)** NA10Ru2(70), **(c)** NRu2(90), **(d)** NA10Ru2(90), **(e)** NA20Ru2(90), **(f)** NA20Ru3(90), and **(g)** NA20Ru4(90) microgel dispersions ($[Ru(bpy)_3]$ = 100 μM) in the reduced $[Ru(bpy)_3]^{2+}$ (1 mM Ce^{3+} and 300 mM HNO_3, orange line) and oxidized $[Ru(bpy)_3]^{3+}$ (1 mM Ce^{4+}, 300 mM HNO_3, green line) states.

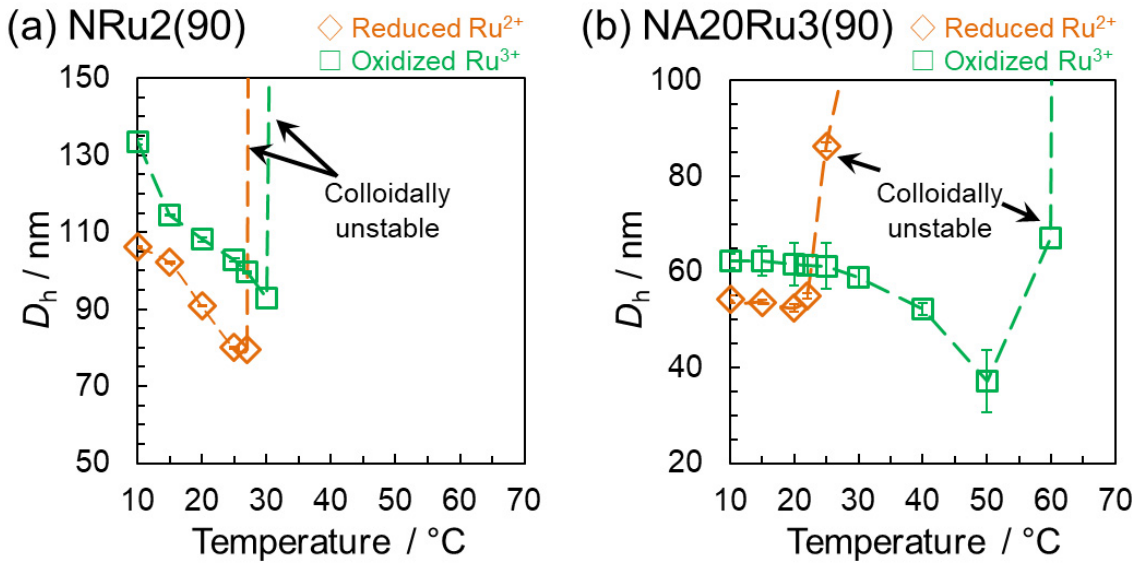

Figure 4.4. Temperature dependence of the hydrodynamic diameter of **(a)** NRu2(90) and **(b)** NA20Ru3(90) microgels ([$Ru(bpy)_3$] = 100 μM) in the reduced $[Ru(bpy)_3]^{2+}$ (1 mM Ce^{3+} and 300 mM HNO_3; orange line) and oxidized $[Ru(bpy)_3]^{3+}$ (1 mM Ce^{4+} and 300 mM HNO_3; green line) states.

4.3.3. Optimization of the BZ reaction conditions

The author attempted to shorten the oscillation period for conventional NRu2(90) microgels without AAm by optimizing the substrate concentration in the BZ reaction, because attempts to shorten the oscillation period of the microgels remain elusive to the best of our knowledge. The oscillations were detected by time-dependent changes in the optical transmittance of the microgel dispersions by UV-vis spectroscopy. Firstly, the HNO_3 concentration was fixed at 300 mM, which is an appropriate concentration for the BZ reaction to proceed[3] and to keep the ionic strength of the system as low as possible. Secondly, the MA and $NaBrO_3$ concentrations were changed (**Figure 4.5**), as these concentrations generally exert a strong influence on the oscillation period, and especially for the general BZ reaction in microgel systems.[14] The oscillation period decreases with increasing initial MA and $NaBrO_3$ concentrations, but oscillation was not observed, or oscillation period was relatively long at the conditions above a certain concentrations where the microgels aggregated irreversibly (**Figure 4.5**; "No oscillation"). As a result, the shortest period achieved was 25 s at 25 °C ([HNO_3] = 300 mM, [$NaBrO_3$] = 300 mM, and [MA] = 100 mM).

Next, the author compared the temperature dependence of the oscillation period for conventional NRu2(90) and NA20Ru3(90) microgels with a highest CFT. It is well known that

the oscillation period decreases with increasing temperature of the BZ reaction.[15] Thus, the concentrations were fixed to the condition where the NRu2(90) microgel showed the shortest oscillation period ([HNO_3] = 300 mM, [$NaBO_3$] = 300 mM, and [MA] = 100 mM), and the temperature dependence of the oscillation period for the NRu2(90) and NA20Ru3(90) microgels and an aqueous solution of $Ru(bpy)_3$, i.e. a control for the microgel systems, were examined. As shown in **Figure 4.6**, the oscillation period for all samples decreased with increasing temperature. Although oscillation did not occur above 28 °C in the conventional NRu2(90) microgels without AAm due to aggregation, it occurred in the case of the NA20Ru3(90) microgels above 50 °C. Specifically, NA20Ru3(90) microgels exhibit similar behavior to the bulk solution and short oscillation periods (~7 s at 50 °C; **Figure 4.6**). It should be noted that this oscillation period is more than four times shorter than that of conventional NRu2(90) microgels without AAm.

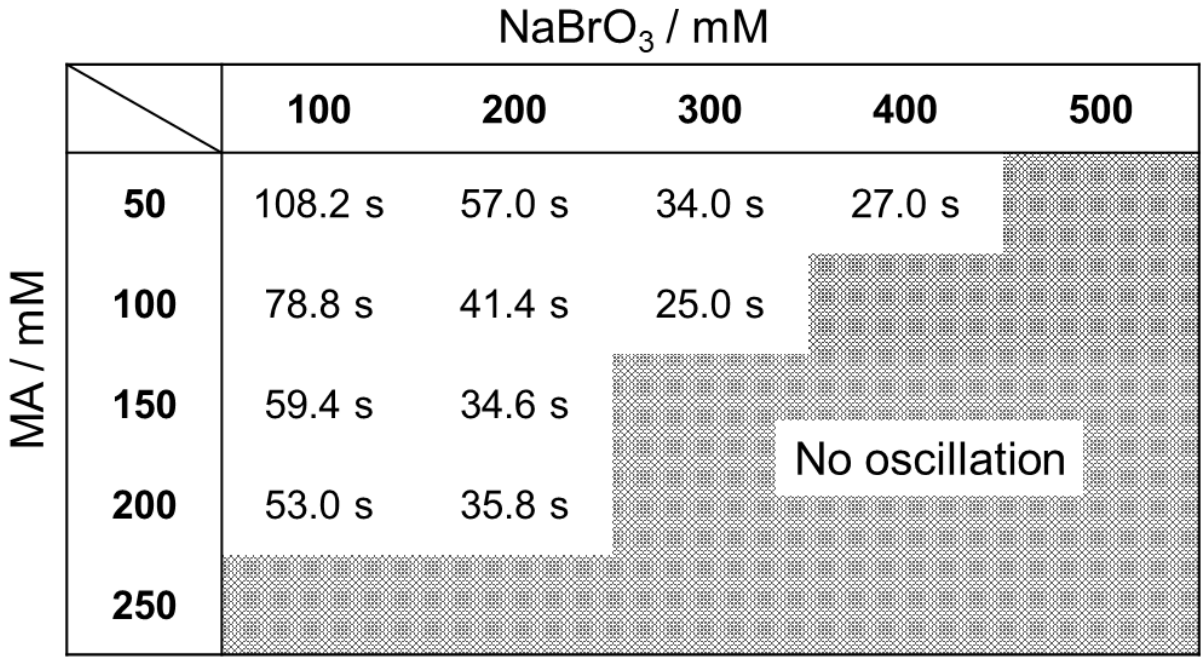

Figure 4.5. The influence on the oscillation period of the initial $NaBrO_3$ and MA concentrations at 25 °C ([$Ru(bpy)_3$] = 100 μM, [HNO_3] = 300 mM).

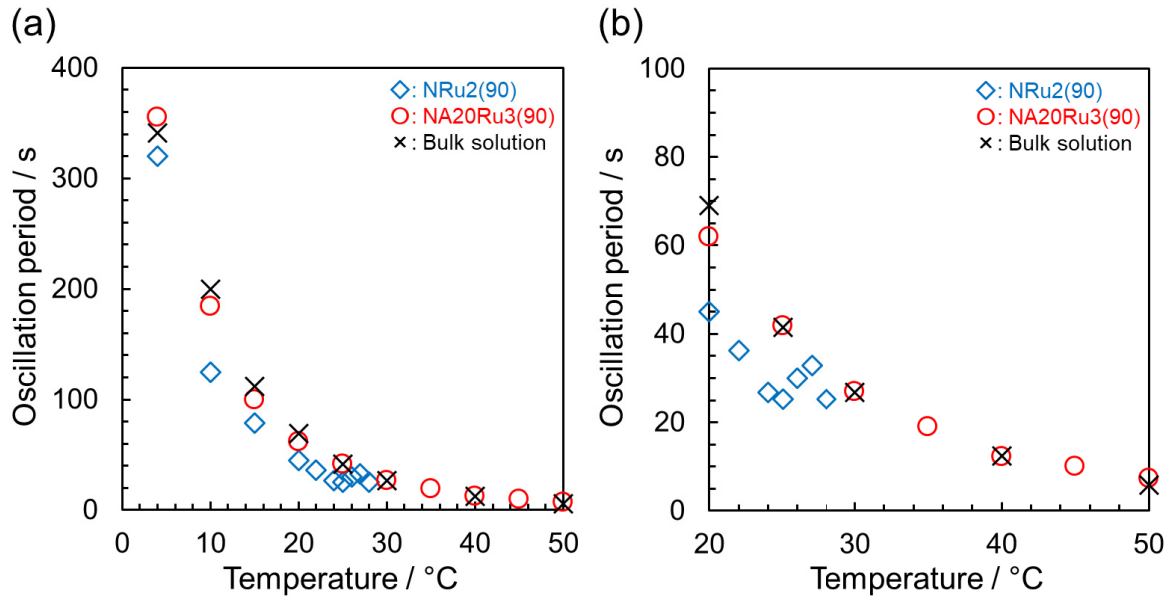

Figure 4.6. Temperature dependence of the oscillation period for the NRu2(90) and NA20Ru3(90) microgels, as well as the bulk solution ([$Ru(bpy)_3$] = 100 μM, [HNO_3] = 300 mM, [$NaBrO_3$] = 300 mM, and [MA] = 100 mM). Temperature range: **(a)** 0-50 °C, **(b)** 20-50 °C.

4.3.4. Characterization of oscillation waveforms

Some typical waveforms at specific temperatures obtained in this study are shown in **Figure 4.7** and **Figure 4.8**. The amplitude of transmittance oscillation for the NRu2(90) and NA20Ru3(90) microgels at low temperature (10 °C) was relatively small ~1 %, but the amplitude of the NRu2(90) without AAm increased dramatically to ~70% transmittance at 25 °C due to the dispersing/flocculating oscillation, whereas the amplitude of NA20Ru3(90) slightly rose to ~4 % (**Figure 4.7**). Dispersing/flocculating oscillation is induced by flocculation of the microgels in the reduced $[Ru(bpy)_3]^{2+}$ state and the oscillation amplitude is larger according to the decreased transmittance.[6] Above 30 °C, the NRu2(90) microgels without AAm do not oscillate anymore due to irreversible aggregation, and the amplitude of the NA20Ru3(90) dramatically increased to ~40 %, commensurate with dispersing/flocculating oscillation. On the other hand, the life time of the oscillation of the microgels decreased with increasing temperature (**Figure 4.9**). The temperature region where dispersing/flocculating oscillation occurs is relatively broad for the NA20Ru3(90) microgels compared to conventional NRu2(90) microgels without AAm (**Figure 4.10**; NRu2(90): ~25 °C; NA20Ru3(90): 25 °C-70 °C). The increased temperature region should be attributed to the large difference between the CFT of the reduced and oxidized $Ru(bpy)_3$ states.

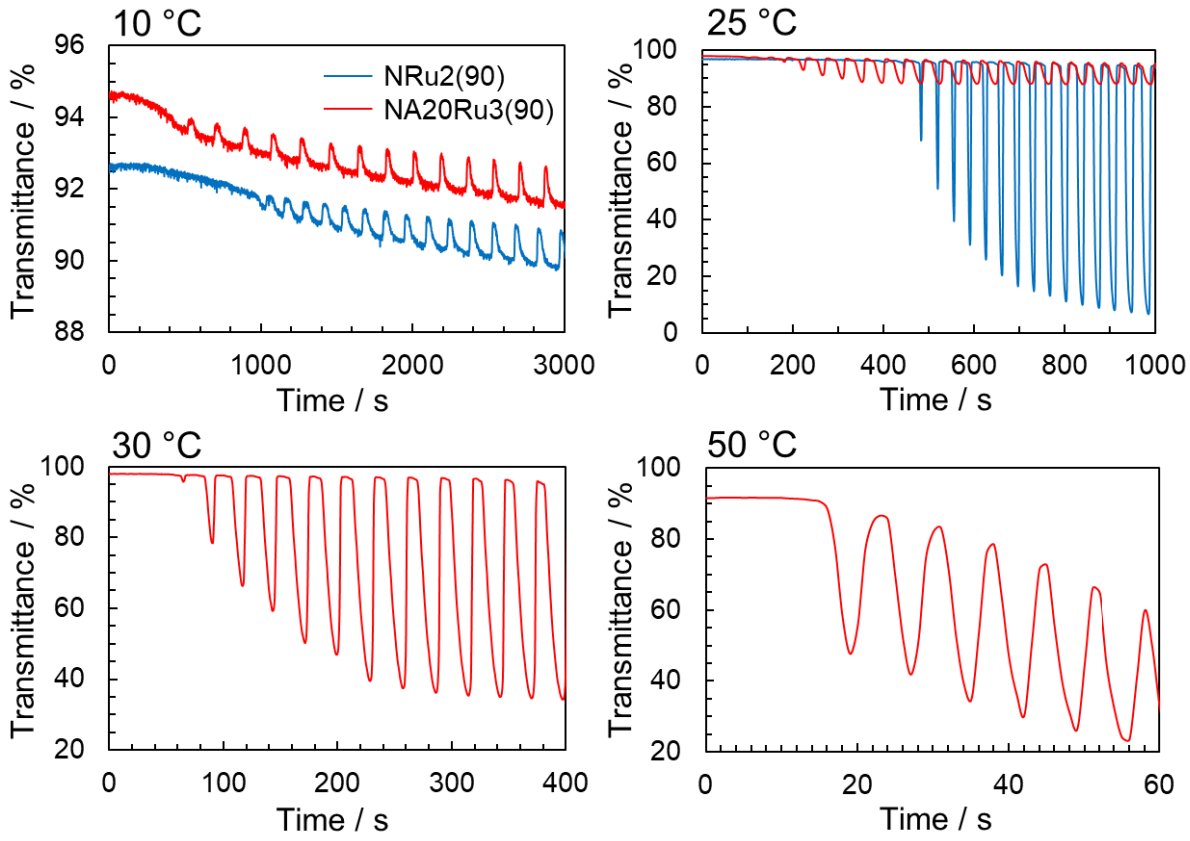

Figure 4.7. Typical oscillation wave forms for theNRu2(90) and NA20Ru3(90) microgels at 10, 25, 30, and 50 °C ([$Ru(bpy)_3$] = 100 μM, [HNO_3] = 300 mM, [$NaBrO_3$] = 300 mM, and [MA] = 100 mM).

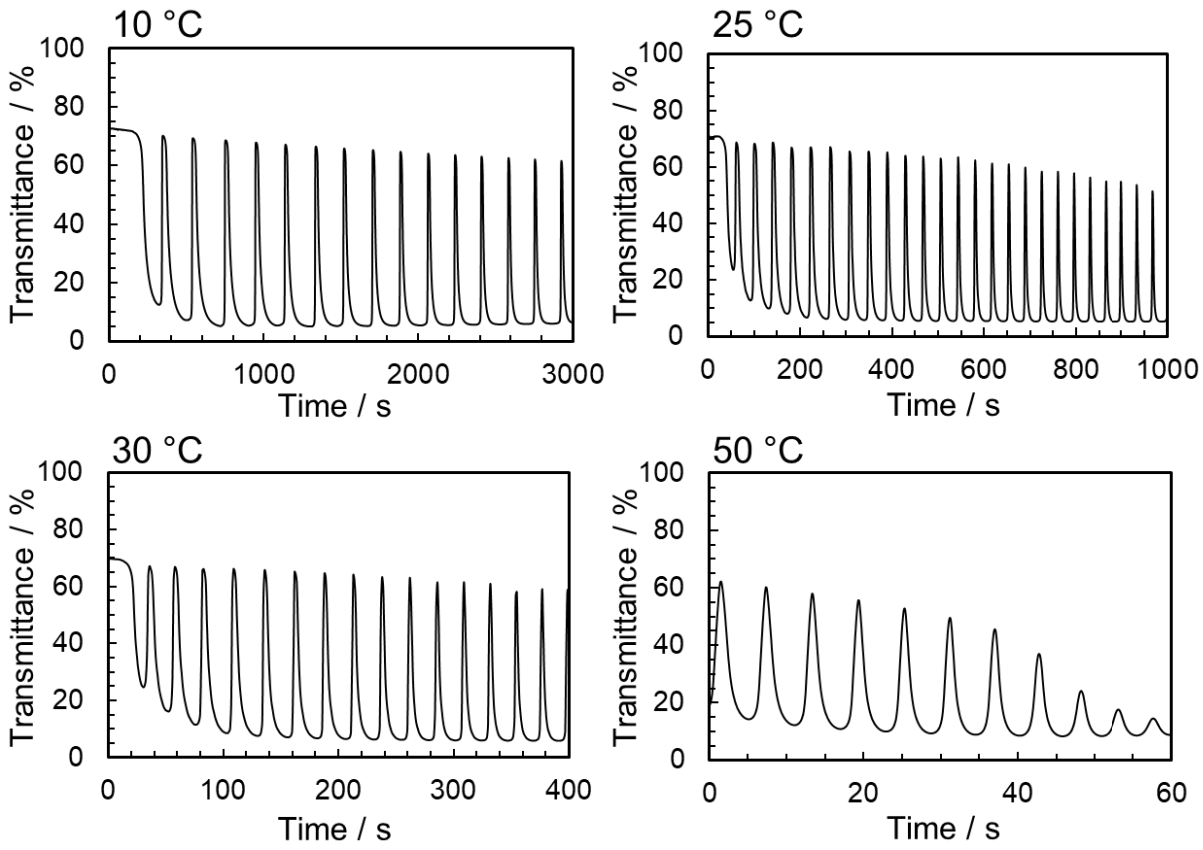

Figure 4.8. Typical oscillation waveforms for the bulk solution at 10, 25, 30, and 50 °C ([$Ru(bpy)_3$] = 100 μM, [HNO_3] = 300 mM, [$NaBrO_3$] = 300 mM, and [MA] = 100 mM).

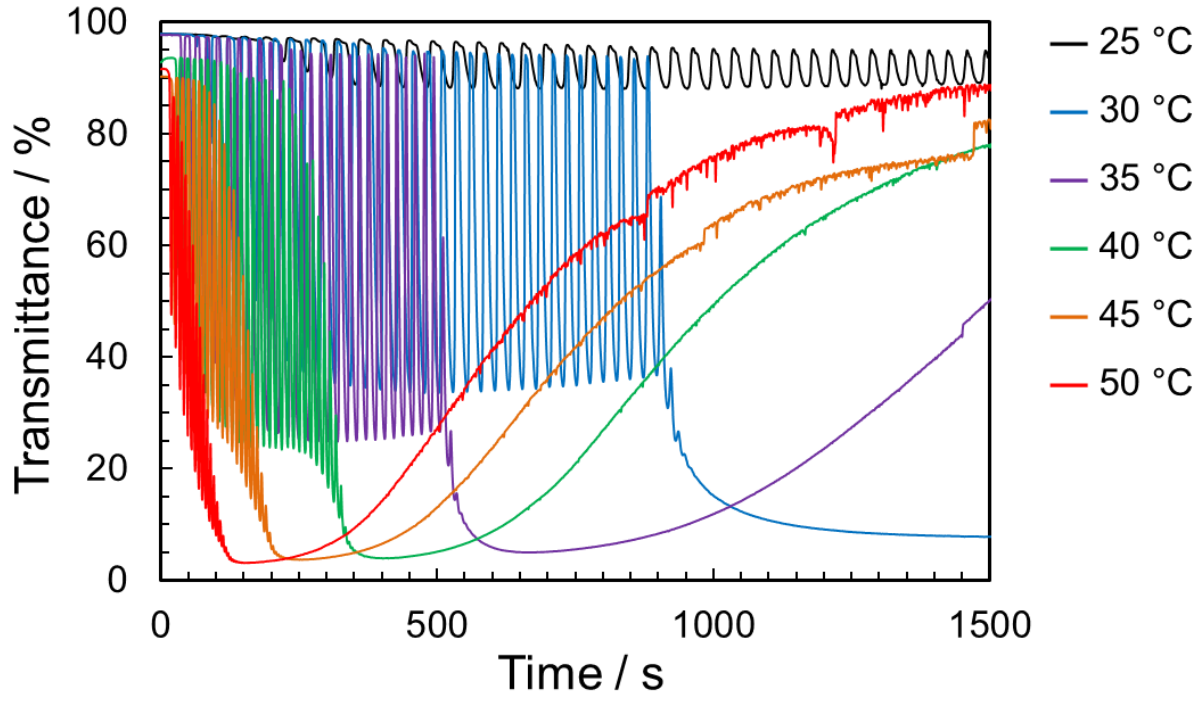

Figure 4.9. Typical oscillation waveforms for the NA20Ru3(90) microgels with different temperatures at 25, 30, 35, 40, 45 and 50 °C ([Ru(bpy)$_3$] = 100 μM, [HNO_3] = 300 mM, [$NaBrO_3$] = 300 mM, and [MA] = 100 mM).

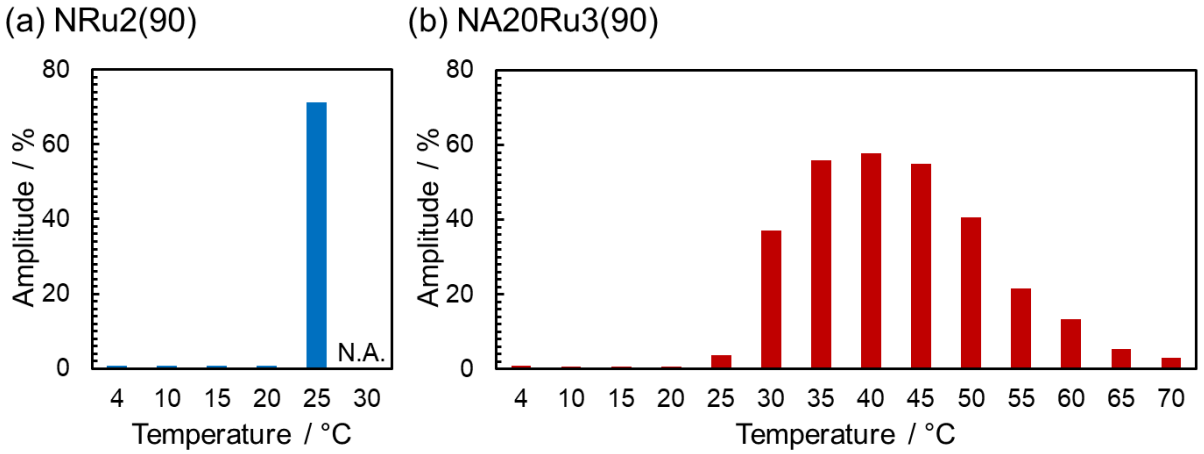

Figure 4.10. Oscillation amplitude of the optical transmittance for **(a)** NRu2(90) and **(b)** NA20Ru3(90) microgel dispersions ([Ru(bpy)$_3$] = 100 μM, [HNO_3] = 300 mM, [$NaBO_3$] = 300 mM, and [MA] = 100 mM).

Real time observations was carried out with the naked eye under such conditions that short period oscillation (~ 7s) could be observed. **Figure 4.11** shows video camera images for the time-dependent dispersing/flocculating oscillation for NA20Ru3(90) microgel dispersions. The letter "microgel" behind could be seen when the microgel was in the dispersed state (transparent), but it was obscured by turbidity in the flocculated state. It should be noted that the entire turbidity in the cell and the color of the dispersion (redox states of $Ru(bpy)_3$) changed at the same time every ~7 s, indicating that the BZ reaction and dispersing/flocculating oscillation are synchronized, even under such short-period conditions. The changes in dispersion and flocculation states of the microgels rapidly (single-order seconds) follow the redox change, and thus aptly reflect the rapid stimuli-responsiveness of the microgels.

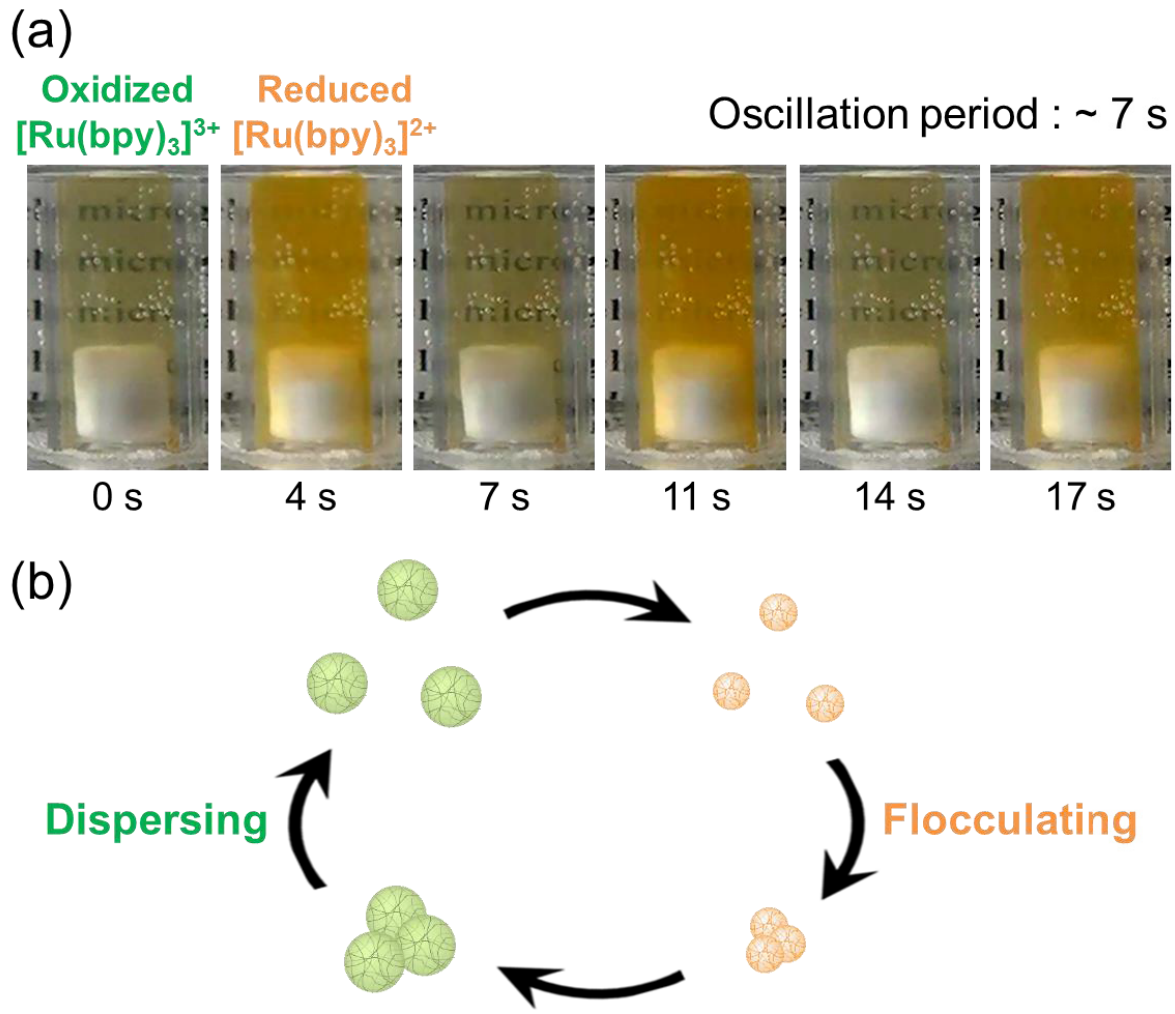

Figure 4.11. (a) Time-lapse video camera images of the NA20Ru3(90) microgel dispersion in the cell during dispersing/flocculating oscillation (0 s; the time when stable dispersing/flocculating oscillation began to be observed). The sample preparation procedure is the same as that used for the oscillation study using UV-vis spectroscopy, which is described in the experimental section ($[Ru(bpy)_3]$ = 100 μM, $[HNO_3]$ = 300 mM, $[NaBrO_3]$ = 300 mM, and [MA] = 100 mM at 50 °C under constant stirring at 800 rpm). **(b)** Schematic illustration of dispersing/flocculating oscillation of the microgels.

4.3.5. Arrhenius dependence of the oscillation frequency

The reasons for such short oscillation periods are discussed below. In our previous study, the Arrhenius equation [1], which describes a linear relationship between the oscillation frequency and temperature, could be fitted below the VPTT of the microgels:[6, 12]

$$\ln F_{osc} = \ln A_{osc} - E_{osc}/RT \quad [1]$$

where F_{osc} is the frequency of the oscillation, A_{osc} the collision factor, E_{osc} the apparent activation energy, R the gas constant (R = 8.314 J K^{-1} mol^{-1}), and T the temperature in Kelvin. The oscillation frequency of the NRu2(90) microgels decreased around and above the VPTT due to dispersing/flocculating oscillation, and the corresponding plots deviated from the Arrhenius equation due to reducing diffusibility of the BZ reaction substrates and intermediates in the deswollen microgels (**Figure 4.12**).[6, 12] The oscillation frequency of the NA20Ru3(90) microgels were plotted as a function of the temperature in accordance with the Arrhenius equation (**Figure 4.13(a)**). The oscillations are possible at temperatures >25 °C, where the dispersing/flocculating oscillation starts, although the corresponding plot deviates from the Arrhenius equation >25 °C (**Figure 4.13(a)**). In this regard, the activation energy of the Arrhenius equation was considered.[16, 17] It should be noted that the activation energies were calculated between 4 °C and 20 °C, where both the NRu2(90) and NA20Ru3(90) microgels did not show dispersing/flocculating oscillation (**Figure 4.13(b)**) in order to avoid the effect of flocculation of the microgels. The activation energy of the NA20Ru3(90) microgels is closer to that of the bulk solution than that of the conventional NRu2(90) microgels without AAm ($E_{osc, NRu2}$ = 81.7 kJ mol^{-1}; $E_{osc, NA20Ru3}$ = 74.5 kJ mol^{-1}; $E_{osc, bulk\ solution}$ = 68.2 kJ mol^{-1}), which suggests that the reaction efficiency required per period oscillation for the NA20Ru3(90) microgels might be better than that of the NRu2(90) microgels without AAm. Based on these results, the author concluded that copolymerization of the neutral and hydrophilic monomer AAm into the oscillating microgels might not only suppress the aggregation of deswollen microgels at high temperature but also might not inhibit the BZ reaction in the microgels.

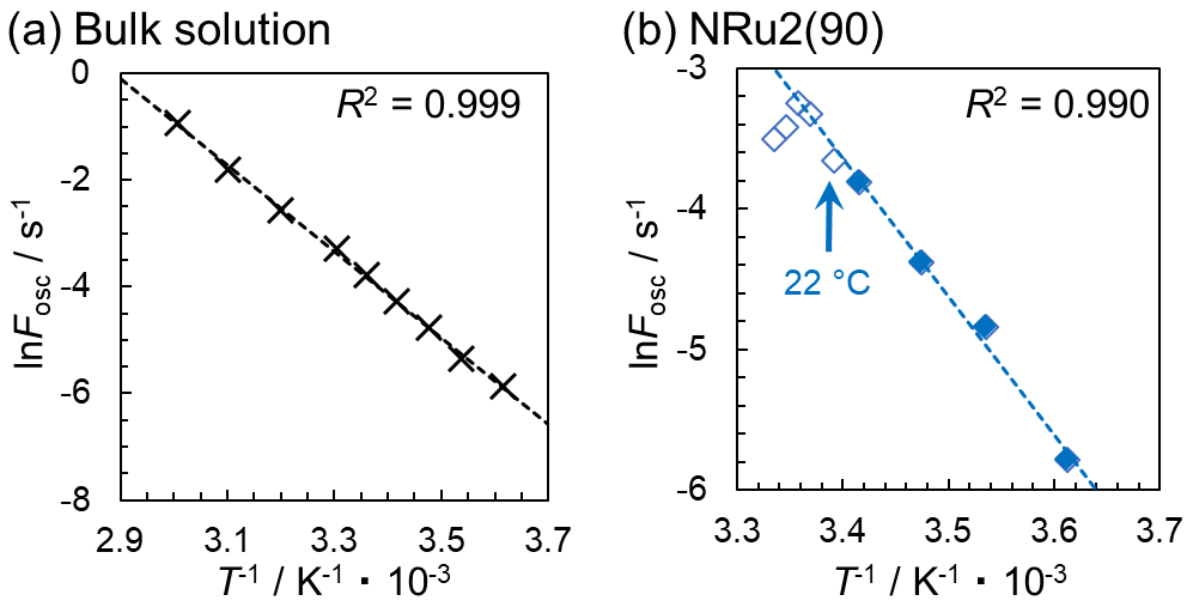

Figure 4.12. Arrhenius dependence of the oscillation frequency of **(a)** bulk solution and **(b)** NRu2(90) microgel dispersions ([Ru(bpy)$_3$] = 100 μM, [HNO_3] = 300 mM, [$NaBO_3$] = 300 mM, and [MA] = 100 mM).

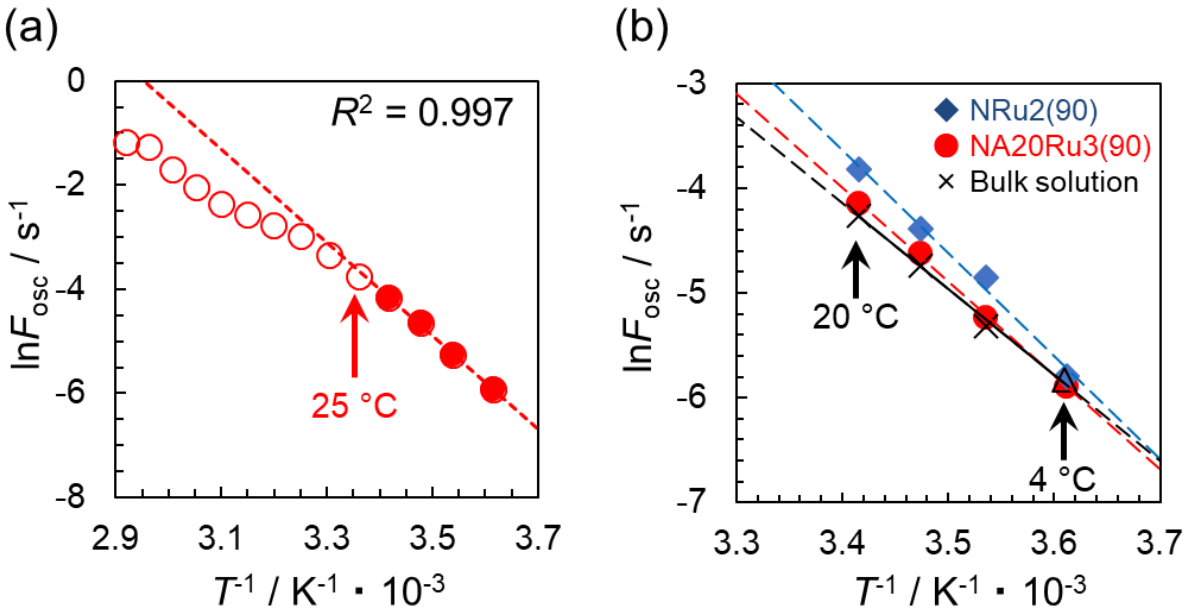

Figure 4.13. (a) Arrhenius dependence of the oscillation frequency of NA20Ru3(90) microgel dispersions ([Ru(bpy)$_3$] = 100 μM, [HNO_3] = 300 mM, [$NaBO_3$] = 300 mM, and [MA] = 100 mM). **(b)** Comparison of the Arrhenius plot for the estimation of the activation energy (temperature range: 4-20 °C).

4.3.6. Preparation of fast-oscillating macrogels

As an application for such fast oscillations, the author designed a macrogel assembled from oscillating microgels according to a previously reported method.[7] So far, the increase in the amplitude of the macrogel length due to dispersing/flocculating oscillation of the microgels has been demonstrated, but the oscillation period has not yet been discussed. Compared to microgel dispersion systems, macrogels may easily present irreversible aggregation as the microgels are adjacent to each other and as the macrogels are not stirred; the control of short oscillation periods in such macrogels should accordingly be particularly difficult. Currently, the shortest reported oscillation period for macrogels is >190 s.[7] In this work, a macrogel that exhibits the individual functions of the oscillating microgels copolymerized with AAm was prepared aiming for a faster oscillation. Following a previous report,[7] amino groups were introduced in the composition of the oscillating microgels copolymerized with AAm, which were then chemically cross-linked to obtain the macrogel (an optical microscopy image of the prepared macrogel is shown in **Figure 4.14(a)**). Upon inducing the BZ reaction, volume oscillation was observed (**Figure 4.14(b)** and **(c)**). A short oscillation period of ~23 s at 35 °C was determined, which is approximately nine times shorter than that previously reported.[7] Therefore, the macrogel displays the properties of its microgel components and represents a short-oscillation-period material. Based on these results, it is feasible to expect promising applications for the oscillating microgels copolymerized with AAm as autonomous actuators operating at short times (**Figure 4.14**).

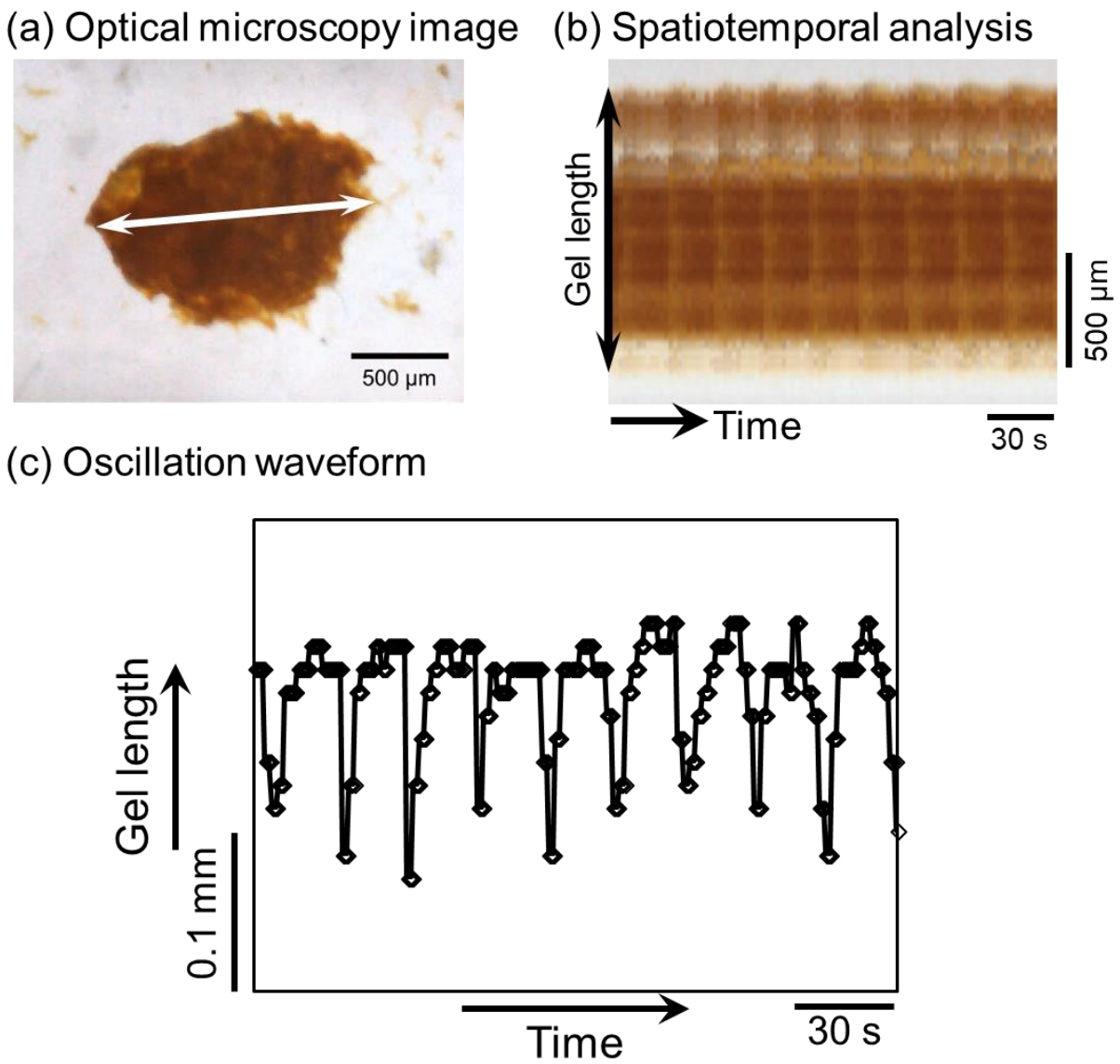

Figure 4.14. (a) Optical microscopy image of the macrogel (the gel length was measured along the white line). **(b)** Spatiotemporal analysis of the gel length. **(c)** Oscillation waveform of the macrogel length ([HNO_3] = 500 mM, [$NaBrO_3$] = 300 mM, and [MA] = 300 mM at 35 °C).

4.4 Conclusions

The author has designed oscillating microgels based on poly(NIPAm-*co*-AAm-*co*-Ru(bpy)$_3$), which contain neutral and hydrophilic AAm monomers in order to suppress the irreversible aggregation of the microgels during oscillation under high ionic strength and temperature conditions, where the BZ reaction occurs at high frequency. The dispersing/flocculating oscillation of the microgels is synchronized with the redox oscillation of the BZ reaction at an order of single seconds (oscillation period: ~7 s) under optimized reaction conditions, resulting in a real-time dispersing/flocculating oscillation. Moreover, a macrogel that exhibits the properties of the constituent microgels was prepared, for which swelling/deswelling oscillation with a remarkable short period (~23 s) was observed. It should be possible to use these microgels as advanced bioinspired or biomimetic materials in e.g. autonomously oscillating micropumps that work at short periods that are similar to that of the human heartbeat. In the future, it would be possible to observe the volume oscillation behavior of individual oscillating microgels by using HS-AFM.

4.5 References

1. Nakamaru, S.; Maeda, S.; Hara, Y.; Hashimoto, S. Control of autonomous swelling-deswelling behavior for a polymer gel. *J. Phys. Chem. B* **2009**, *113*, 4609−4613.
2. Hidaka, M.; Yoshida, R. Self-oscillating gel composed of thermosensitive polymer exhibiting higher LCST. *J. Controlled Release* **2011**, *150*, 171−176.
3. Yoshida, R.; Onodera, S.; Yamaguchi, T.; Kokufuta, E. Aspects of the Belousov−Zhabotinsky reaction in polymer gels. *J. Phys. Chem. A* **1999**, *103*, 8573−8578.
4. Zhang, J.; Pelton, R. The surface tension of aqueous poly (*N*-isopropylacrylamide-*co*-acrylamide). *J. Polym. Sci., Part A: Polym. Chem.* **1999**, *37*, 2137−2143.
5. Ghosh, P. K.; Spiro, T. G. Photoelectrochemistry of tris(bipyridyl)ruthenium(II) covalently attached to n-type SnO_2. *J. Am. Chem. Soc.* **1980**, *102*, 5543−5549.
6. Suzuki, D.; Sakai, T.; Yoshida, R. Self-flocculating/selfdispersing oscillation of microgels. *Angew. Chem., Int. Ed.* **2008**, *47*, 917−920.
7. Suzuki, D.; Kobayashi, T.; Yoshida, R.; Hirai, T. Soft actuators of organized self-oscillating microgels. *Soft Matter* **2012**, *8*, 11447−11449.

8. Ngai, T.; Behrens, S. H.; Auweter, H. Novel emulsions stabilized by pH and temperature sensitive microgels. *Chem. Commun.* **2005**, *0*, 331−333.
9. Suzuki, D.; Tsuji, S.; Kawaguchi, H. Janus microgels prepared by surfactant-free pickering emulsion-based modification and their self-assembly. *J. Am. Chem. Soc.* **2007**, *129*, 8088−8089.
10. Pelton, R. H.; Chibante, P. Preparation of aqueous latices with *N*-isopropylacrylamide. *Colloids Surf.* **1986**, *20*, 247−256.
11. Pelton, R. Temperature-sensitive aqueous microgels. *Adv. Colloid Interface Sci.* **2000**, *85*, 1−33.
12. Suzuki, D.; Yoshida, R. Temporal control of self-oscillation for microgels by cross-linking network structure. *Macromolecules* **2008**, *41*, 5830−5838.
13. Yoshida, R.; Takahashi, T.; Yamaguchi, T.; Ichijo, H. Selfoscillating gel. *J. Am. Chem. Soc.* **1996**, *118*, 5134−5135.
14. Suzuki, D.; Yoshida, R. Effect of initial substrate concentration of the Belousov−Zhabotinsky reaction on self-oscillation for microgel system. *J. Phys. Chem. B* **2008**, *112*, 12618−12624.
15. Ruoff, P. Antagonistic balance in the Oregonator: about the possibility of temperature-compensation in the Belousov-Zhabotinsky reaction. *Phys. D* **1995**, *84*, 204−211.
16. Pullela, S. R.; Shen, J.; Marquez, M.; Cheng, Z. A comparative study of temperature dependence of induction time and oscillatory frequency in polymer-immobilized and free catalyst Belousov-Zhabotinsky reactions. *J. Polym. Sci., Part B: Polym. Phys.* **2009**, *47*, 847−854.
17. Hara, Y.; Jahan, R. A. Activation energy of aggregation-disaggregation self-oscillation of polymer chain. *Int. J. Mol. Sci.* **2012**, *13*, 16281−16290.

5. Summary

In this thesis, the dynamic behavior of stimulus-responsive microgels was revealed through nanoscale visualization using HS-AFM and other ensemble measurements such as scattering and spectroscopy techniques. First, the adsorption dynamics that engage in every colloidal microspheres could be monitored, and it was found that the importance not only interaction between the microspheres and interfaces but also more deepen insight that deformability of microspheres dramatically affects the adsorption dynamics. This design concept for microspheres that focuses on “softness“ will be important not only for many industrial e.g. coatings and cosmetics, but also for biological applications e.g. drug delivery systems and artificial blood.

In addition, temperature-induced nanoscopic morphological changes in single microgels were directly visualized at nanoscale using HS-AFM. The author believes that the results will help to clarify the relationship between the morphology/structure and the physical properties of microgels adsorbed on solid substrates, which may lead to the development of advanced functional materials such as switchable cell culture substrates for tissue engineering.

Moreover, based on rapid stimulus-responsive property of microgels, the author developed new type of autonomously oscillating microgels that show fast swelling/deswelling and dispersing/flocculating oscillations at periods of single-order seconds, by suppressing irreversible aggregation of the microgels through optimization of the chemical structure. The microgels will be evaluated by HS-AFM observation, and applied as advanced active materials in such as autonomously oscillating micropumps that work at short periods similar to that of the human heartbeat.

The present study demonstrates not only the significance that combination of real-time nanoscopic visualization and ensemble measurements for clarifying realistic behavior of synthetic stimulus-responsive nanomaterials, but also future potential toward development of autonomously driving materials such as active matter.

List of Publications

1. Shusuke Matsui, Takuma Kureha, Seina Hiroshige, Mikihiro Shibata, Takayuki Uchihashi* and Daisuke Suzuki*:
"Fast Adsorption of Soft Hydrogel Microspheres on Solid Surfaces in Aqueous Solution"
Angewandte Chemie International Edition, 56, pp12146-12149 (2017).
DOI: 10.1002/anie.201705808

2. Shusuke Matsui, Yuichiro Nishizawa, Takayuki Uchihashi*, Daisuke Suzuki*:
"Monitoring Thermo-responsive Morphological Changes in Individual Hydrogel Microspheres"
ACS Omega, 3, pp10836-10842 (2018).
DOI: 10.1021/acsomega.8b01770

3. Shusuke Matsui, Kohei Inui, Yuki Kumai, Ryo Yoshida, and Daisuke Suzuki*
"Autonomously Oscillating Hydrogel Microspheres with High-Frequency Swelling/deswelling and Dispersing/flocculating Oscillations"
ACS Biomaterials Science & Engineering, in press.
DOI: 10.1021/acsbiomaterials.8b00850

Other Publications

1. Takuma Kureha, Seina Hiroshige, Shusuke Matsui, and Daisuke Suzuki*:
"Water-immiscible bioinert coatings and film formation from aqueous dispersions of poly(2-methoxyethyl acrylate) microspheres"
Colloids and Surfaces B: Biointerfaces, 155, pp166-172 (2017).
DOI: http://doi.org/10.1016/j.colsurfb.2017.04.001

2. Haruka Minato, Masaki Murai, Takumi Watanabe, Shusuke Matsui, Masaya Takizawa, Takuma Kureha* and Daisuke Suzuki*:
"The Deformation of Hydrogel Microspheres at the Air/Water Interface"
Chemical Communications, 54, pp932-935 (2018).
DOI: 10.1039/C7CC09603H.

3. Masaya Takizawa, Yuka Sazuka, Koji Horigome, Yuki Sakurai, Shusuke Matsui, Haruka Minato, Takuma Kureha and Daisuke Suzuki*:
"Self-organization of Soft Hydrogel Microspheres during the Evaporation of Aqueous Droplets"
Langmuir, 34, pp4515-4525 (2018).
DOI: 10.1021/acs.langmuir.8b00230

Reviews

1. 鈴木大介*、松井秀介:
「時間周期的に体積と集合状態を変化させる自律駆動ゲル微粒子の微細構造変化と機能の相関」
新学術領域『動的秩序と機能』ニュースレター　2015 年 8 月号　Vol.24、p5 (2015)

2. 乾滉平、松井秀介、鈴木大介*:
「ソフトゲル微粒子の自己組織化」
日本油化学会「オレオサイエンス」、第 17 巻、第 2 号、pp55-62 (2017)

3. Daisuke Suzuki*, Koji Horigome, Takuma Kureha, Shusuke Matsui, Takumi Watanabe:
"Polymeric Hydrogel Microspheres: Design, Synthesis, Characterization, Assembly and Applications"
Polymer Journal, 49, pp695-702 (2017).
*Focus Review.

4. 広重聖奈、松井秀介、鈴木大介*:
「進化するコーティング技術 ―コーティング材料の「今まで」と「これから」」
化学、第 73 巻、第 2 号、pp64-65 (2018).

5. Daisuke Suzuki, Koji Horigome, Takuma Kureha, Shusuke Matsui, Takumi Watanabe.
"Polymeric hydrogel microspheres: design, synthesis, characterization, assembly and applications"
高分子 Hot Topics, 5 月号 (2018).

Oral Presentation (International conference)

1. ○Shusuke Matsui, Takayuki Uchihashi, Daisuke Suzuki
"High-Speed AFM Reveals Detail Understanding in Adsorption of Soft Hydrogel Microspheres onto Solid Substrate in Aqueous Solution"
255th ACS National Meeting (New Orleans, America) March 21th (2018) Oral (COLL 660)

Oral Presentation (National conference)

1. ○Shusuke Matsui, Yuki Sakurai, Yuki Kumai, Ryo Yoshida, Takuma Kureha, Daisuke Suzuki
「Autonomously Oscillating Microgels and Microgel Assemblies with Higher frequency」
第 65 回高分子年次大会、神戸国際会議場・展示場、兵庫、5 月 25 日(2016)、口頭英語
(1L31) Polymer Preprints, Japan Vol. 65, No. 1 (2016)

2. ○松井秀介、呉羽拓真、広重聖奈、柴田幹大、内橋貴之、鈴木大介
「高速 AFM による高分子微粒子の固液界面上における動的挙動のリアルタイム可視化」
新学術領域研究「動的秩序と機能」第 3 回若手研究会、片山津温泉加賀観光ホテル、石川、10 月 12 日(2016)、口頭(1)

3. ○松井秀介、蓬生健介、柴田幹大、内橋貴之、鈴木大介
「高速原子間力顕微鏡によるヒドロゲル微粒子の環境応答挙動とタンパク質吸脱着挙動のリアルタイム可視化」
第 19 回高分子ミクロスフェア討論会、千葉大学、千葉、11 月 9 日(2016)、口頭(3-08A)
※高分子ミクロスフェア討論会学生優秀発表賞

4. ○松井秀介、呉羽拓真、蓬生健介、柴田幹大、内橋貴之、鈴木大介
「高速原子間力顕微鏡による高分子ゲル微粒子の刺激応答挙動とタンパク質複合挙動のリアルタイム観察」
第 28 回高分子ゲル研究討論会、東京大学、東京、1 月 17 日(2017)、口頭(21)

5. ○松井秀介、呉羽拓真、広重聖奈、柴田幹大、内橋貴之、鈴木大介
「高速原子間力顕微鏡による高分子微粒子の固体表面への吸着挙動のリアルタイム評価」
第 68 回コロイドおよび界面化学討論会、神戸大学、兵庫、9 月 6 日(2017)、口頭(1F47)

6. ○松井秀介、蓬生健介、内橋貴之、鈴木大介:
「高速 AFM によるハイドロゲル微粒子のタンパク質吸着挙動の動的可視化」
第 28 回日本 MRS 年次大会、北九州国際会議場、福岡、12 月 18 日(2018)、
口頭(F3-O18-015)

7. ○松井秀介、西澤佑一朗、内橋貴之、鈴木大介:
「高速 AFM によるハイドロゲル微粒子の刺激応答挙動の評価」
第 28 回日本 MRS 年次大会、北九州国際会議場、福岡、12 月 19 日(2018)、
口頭(F6-O19-013)
※奨励賞

8. ○松井秀介、内橋貴之、鈴木大介:
「ハイドロゲル微粒子の水中基板上における動的挙動の可視化」
第 30 回高分子ゲル研究討論会、東京工業大学、東京、1 月 17 日(2019)、口頭(34)

6. Acknowledgements

First of all, I would like to express the deepest appreciation to my supervisor Prof. Dr. Daisuke Suzuki (Shinshu University) for a lot of fruitful help and support and for introducing me to the world of science as a researcher. My appreciation can't be expressed in words.

I am very grateful to Prof. Dr. Takayuki Uchihashi (Nagoya Univ.) and Prof. Dr. Mikihiro Shibata (Kanazawa Univ.) and Prof. Dr. Hiroki Watanabe (Nagoya Univ.) for useful discussions and assistance regarding HS-AFM measurement.

I greatly thank Emeritus Prof. Dr. Haruma Kawaguchi (Keio Univ.), Prof. Dr. L. A. Lyon (Georgia Institute of Technology), Prof. Dr. Kenji Urayama (Kyoto Institute of Technology Univ.), Prof. Dr. Ryo Yoshida (Tokyo Univ.), Prof. Dr. Syuji Fujii (Osaka Institute of Technology), Prof. Dr. Takashi Miyata (Kansai Univ.), Prof. Dr. Michinari Kohri (Chiba Univ.), Prof. Dr. Akifumi Kawamura (Kansai Univ.), Prof. Dr. Takaaki Sato (Shinshu Univ.), and Prof. Dr. Kosuke Okeyoshi (Japan Advanced Institute of Science and Technology) for useful discussions about gel and colloid science.

My study was financially supported by fellowship (17J05706) from the Japan Society for the Promotion of Science (JSPS), and a Sasakawa Scientific Research Grant from the Japan Science Society (28-318). I am thankful for all the supports.

I greatly acknowledge the Suzuki lab members. They always influenced me positively and gave me a great working atmosphere in the lab and daily life. I wish the Suzuki lab members many more successful years.

Finally, I would like to express my gratitude to my family, Hidenobu, Sonomi, and Yoshiki.
Thank you for everything you have done for me. I can never thank you enough.

Shusuke Matsui
松井秀介